HIGH OCTANE AND OXYGENATED TEST SETUP FOR CFR OCTANE ENGINE

by
Johannes Gysbertus Bergenthuin

Thesis presented in partial fulfilment of the requirements for the degree of Master of Engineering (Mechanical) in the Faculty of Engineering at Stellenbosch University

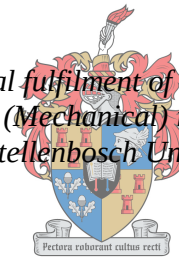

UNIVERSITEIT
iYUNIVESITHI
STELLENBOSCH
UNIVERSITY

Supervisor: Mr. Richard Walter Haines

Co-supervisor: Dr. Gareth Floweday

March 2018

DECLARATION

By submitting this thesis electronically, I declare that the entirety of the work contained therein is my own, original work, that I am the sole author thereof (save to the extent explicitly otherwise stated), that reproduction and publication thereof by Stellenbosch University will not infringe any third party rights and that I have not previously in its entirety or in part submitted it for obtaining any qualification.

Date: March 2018

UNIVERSITEIT·STELLENBOSCH·UNIVERSITY
jou kennisvennoot • your knowledge partner

Plagiaatverklaring / Plagiarism *Declaration*

1. Plagiaat is die oorneem en gebruik van die idees, materiaal en ander intellektuele eiendom van ander persone asof dit jou eie werk is.
   Plagiarism is the use of ideas, material and other intellectual property of another's work and to present is as my own.

2. Ek erken dat die pleeg van plagiaat 'n strafbare oortreding is aangesien dit 'n vorm van diefstal is.
   I agree that plagiarism is a punishable offence because it constitutes theft.

3. Ek verstaan ook dat direkte vertalings plagiaat is.
   I also understand that direct translations are plagiarism.

4. Dienooreenkomstig is alle aanhalings en bydraes vanuit enige bron (ingesluit die internet) volledig verwys (erken). Ek erken dat die woordelikse aanhaal van teks sonder aanhalingstekens (selfs al word die bron volledig erken) plagiaat is.
   Accordingly all quotations and contributions from any source whatsoever (including the internet) have been cited fully. I understand that the reproduction of text without quotation marks (even when the source is cited) is plagiarism.

5. Ek verklaar dat die werk in hierdie skryfstuk vervat, behalwe waar anders aangedui, my eie oorspronklike werk is en dat ek dit nie vantevore in die geheel of gedeeltelik ingehandig het vir bepunting in hierdie module/werkstuk of 'n ander module/werkstuk nie.
   I declare that the work contained in this assignment, except where otherwise stated, is my original work and that I have not previously (in its entirety or in part) submitted it for grading in this module/assignment or another module/assignment.

Studentenommer / Student number	Handtekening / Signature
Voorletters en van / Initials and surname	Datum / Date

ABSTRACT

Petrol blending involves mixing of several refinery fuel streams, each with different properties that contribute to the usability of the final product. The octane rating of a fuel stream is the measure to which auto-ignition can be resisted. Octane properties of fuel streams are measured on a Cooperative Fuels Research (CFR) engine. The typical operating range of a CFR engine does not allow for high octane (Research Octane Number > 100) and oxygenated (Vol % > 25) fuels. While the 100 RON CFR test limit may generally suffice for routine petrol product certification, it results in difficulty characterising the octane properties of the high octane blending components, leading to difficulty in octane prediction and plant planning. Additionally, the impending clean fuels 2 (CF2) legislation gives rise to the significance of research and development of environmentally friendlier fuels, which includes high volume content oxygenated fuels. There are currently no test laboratories in South Africa that are able to provide octane test results above the 100 RON, and 25 % Vol oxygenate limit.

In this study, a conventional CFR engine setup at Stellenbosch University was disassembled, inspected, upgraded and modified to allow for research on high octane and oxygenated fuels. The modified setup was calibrated and declared “fit for use”, based on toluene standardised fuels (TSF), and high volume content oxygenated sample tests. The octane properties of previously uncharacterised Sasol refinery stream components, such as TAME, C5 raffinate, and fuel ethanol blends were successfully investigated. TSF test results demonstrated excellent octane continuity, eliminating the need to resort to the American Society for Testing and Materials (ASTM) standard method of using tetraethyl lead (TEL) for bracketing high octane samples. Blending octane number (BON) determinations were investigated, and it was found that, in some cases, similar molecular construction of the base fuel and blending component reduces synergistic intermolecular effects, improving BON results. The modified CFR setup incorporated a chilled fuel float chamber in order to prevent light component evaporation, enabling research on previously untestable highly volatile streams. It was proven that liquid chilling of test samples does not invalidate octane results. A primary reference fuel (PRF) round robin test showed that the modified CFR engine setup at Stellenbosch University produces accurate and repeatable results, on a comparative level with modern, professional and certified octane test laboratories.

OPSOMMING

Petrolvermenging behels die vermenging van verskeie raffinaderykomponente met verskillende eienskappe wat bydra tot die bruikbaarheid van die finale produk. Die oktaangetal van ’n brandstofkomponent is die mate waartoe selfontbranding weerstaan kan word. Die oktaangetal van ’n brandstofkomponent word op ‘n “Cooperative Fuels Research”-enjin (CFR Engine) gemeet. Die tipiese bedryfsgrense van ’n CFR-enjin maak nie voorsiening vir hoëoktaanbrandstowwe (Research Octane Number > 100) en hoëkonsentrasie alkoholgebaseerde toetsmonsters (Vol % > 25) nie. Hoewel die 100 RON toetsgrens oor die algemeen voldoende is vir sertifisering van petrolprodukte, veroorsaak dit probleme met die tipering van die oktaaneienskappe van hoëoktaan-mengselkomponente wat weer probleme met oktaanvooruitskatting en aanlegbeplanning tot gevolg het. Die belang van hoë suurstofkonsentrasie brandstoftoetse neem tans toe met die oog op die toekomstige skoon brandstowwe 2 wetgewing (CF2). Daar is tans geen oktaantoetslaboratoria in Suid-Afrika wat oktaantoetsresultate bó die 100 RON- en 25 % perk kan lewer nie.

In hierdie studie is ‘n konvensionele CFR-enjinopstelling by die Stellenbosch Universiteit uitmekaargehaal, nagegaan, gerestoureer en aangepas ten einde navorsing op hoëoktaan- en alkoholgebaseerde brandstowwe moontlik te maak. Die aangepaste opstelling is gekalibreer en as geskik vir die bepaalde doel verklaar op grond van tolueen-gestandaardiseerde brandstof toetse, en toetse wat gedoen is op monsters met ’n hoë suurstofkonsentrasie. Die oktaaneienskappe van voorheen ongetipeerde Sasol-raffinaderykomponente, soos TAME, C_5-raffinaat en etanolbrandstofmengsels is suksesvol ondersoek. Die TSF-toetsresultate toon uitstekende oktaankontinuïteit wat die behoefte om die American Society for Testing and Materials (ASTM)-standaardmetode van tetraethyl lood (TEL) vir die tipering van hoëoktaanmonsters uitskakel. Vermengde oktaangetalle (BON) is bestudeer en daar is bevind dat soortgelyke molekulêre samestellings van ‘n basisbrandstof en mengselkomponente die sinergistiese uitwerking verminder wat in sekere gevalle BON-uitslae verbeter. Die aangepaste CFR-enjinopstelling het ’n verkoelde brandstoftenk ingesluit wat die verdamping van ligte komponente voorkom en sodoende navorsing op hoogs vlugtige, voorheen ontoetsbare komponente moontlik maak. Daar is bewys dat verkoelde vloeistof-toetsmonsters nie oktaanresultate ongeldig maak nie. ’n “Round robin”-primary reference fuel (PRF)-toets dui daarop dat die gewysigde CFR-enjinopstelling by Stellenbosch Universiteit akkurate en herhaalbare resultate lewer wat kan meeding met moderne, professionele en gesertifiseerde oktaantoets-laboratoria.

ACKNOWLEDGEMENTS

The author wishes to extend the sincerest gratitude to the following individuals. Without their tireless efforts, the successful completion of this project would not be possible.

- Mr. Richard Haines for sharing his knowledge and experience in the CFR test cell, and his guidance through the course of this project.
- Dr. Gareth Floweday for the Friday afternoon Skype sessions and research mentorship.
- Sasol Fuels Application Centre for their support with test fuels, and making this study possible.
- Mr. Reynaldo Rodriguez for the long hours in the CFR test cell.
- Mr. Juliun Stanfliet for always being available and eager to help.
- The M&M workshop staff for their professional and friendly assistance.

TABLE OF CONTENTS

LIST OF FIGURES

LIST OF TABLES

NOMENCLATURE

Symbol	Description	Unit
c_v	Specific heat (Constant volume)	kJ/kg·K
c_p	Specific heat (Constant pressure)	kJ/kg·K
dT	Change in temperature	K
dt	Change in time	s
h_v	Latent heat of vaporization	kJ/kg
k	Specific heat ratio	-
Q	Heat transfer rate	W
q	Heat transfer	J/kg
r	Compression ratio	-
P	Power	W
T	Temperature	K
u	Internal energy	kJ/kg
V	Volume	m^3
v	Velocity	m/s
W	Work	J
X	Position	m

Greek letters

α	Thermal diffusivity	m^2/s
β	Thermal expansion coefficient	1/T
η_{th}	Thermal efficiency	-
τ	Cycle period	s
μ	Friction coefficient	-

Subscripts

μ	Includes Friction
in	In to system
out	Out of system
otto	Otto cycle
th	Thermal

v	Volume
p	Pressure

Abbreviations

AC	Alternating current
A/F	Air/fuel
ASTM	American Society for Testing Materials
BDC	Bottom dead center
BTDC	Before top dead center
CFR	Cooperative Fuel Research
CCR	Critical compression ratio
CR	Compression ratio
DC	Direct current
DI	Direct injection
FCC	Fuel catalytic cracking
GTDI	Gasoline turbocharged direct injection
SI	Spark ignition
IC	Internal combustion
ID	Internal diameter
I.A.T	Inlet air temperature
KI	Knock intensity
MEP	Mean effective pressure
MON	Motor octane number
O.N.	Octane number
PRF	Primary reference fuel
PFI	Port fuel injection
RON	Research octane number
ULP	Unleaded petrol
SFA	Sasol fuel alcohol
SFC	Specific fuel consumption
TDC	Top dead center
TSF	Toluene standardization fuel

GLOSSARY

Term	Description
Auto-ignition	Uncontrolled combustion
Bottom-dead-centre (BDC)	Lowest piston position
Carbon dioxide	CO_2
Compression ratio (CR)	Ratio of combustion volume at TDC vs. BDC
Constant-volume heat addition	Temperature increase
Constant-volume heat rejection	Temperature decrease
EGR	Exhaust Gas Re-circulation
Spark ignition (SI)	Combustion controlled with a spark plug
Internal combustion (IC)	Combustion inside a combustion chamber
Isentropic compression	Compression with constant entropy
Isentropic expansion	Expansion with constant entropy
Knock intensity (KI)	Severity of knock
Mean effective pressure (MEP)	Pressure experienced by piston
Oxygenates	Contains hydroxyl group (-OH)
Thermal efficiency	Ratio of work to thermal energy supplied
Top-dead-centre (TDC)	Highest piston position

1. INTRODUCTION

1.1 BACKGROUND

Climate change, and the ever-increasing scarcity of oil and gas reserves, are the driving forces behind the efforts of the automotive industry to reduce fuel consumption and emission gasses (Nakada, 1994: 3-8).

Up to 30 % of the energy supplied to a spark ignition (SI) internal combustion (IC) engine is dissipated through friction losses (Hoshi, 1948:185-189). These losses can be limited by reducing the capacity and, typically, the number of cylinders of an engine (Nozawa, Morita & Shimizu,1994: 31-37). Downsizing of IC engines is recognized as a very suitable method for the concurrent enhancement of thermal efficiency, and reducing carbon dioxide (CO_2) emissions (Clerk, 1907: 121-152).

Customer requirements of power, torque, and increased thermal efficiency of downsized IC engines are satisfied by increasing the mean effective pressure (MEP) by means of intake densification, and increased compression ratios (CR). This leads to uncontrolled auto-ignition during the combustion process, commonly referred to as engine knock (Nakada, 1994: 3-8; De Bellis, 2016: 162-174).

Research octane number (RON) and motor octane number (MON) are measured fuel properties indicating the fuel's resistance to auto-ignition. Fuels with higher octane numbers are able to resist knock in IC engines operating at a higher mean effective pressure (MEP) (ASTM, 2016). Oxygenates, as an additive to conventional fuel, improves fuel volatility. This enhances combustion, and decreases carbon monoxide (CO) emissions (Assi, 2008). The significance of high octane and oxygenated fuels is therefore on the rise, along with the modern trend of downsizing IC engines.

There are currently no test laboratories in South Africa that are able to provide octane test results above the 100 RON, and 25 % Vol oxygenate limit. The aim of this project is to adapt and modify an existing Cooperative Fuel Research (CFR) engine setup at Stellenbosch University, in order to enable research on high octane (RON > 100) and oxygenated (Vol % > 25) fuels.

This document serves as a project report for a master's thesis. Available literature on the subjects involving high octane and oxygenated fuel testing are examined. Modifications and development of the test facility are listed and motivated, before test results of high octane and oxygenated fuels are presented. This document concludes with recommendations on improving the setup and test procedure for future projects.

1.2 PROJECT OBJECTIVES

1. Modify a CFR engine for testing high octane (RON > 100), and oxygenated (Vol % > 25) fuels. This required non-standard TSF bracket fuels, and oxygenate volume fractions that are outside the ASTM test method validity range.
2. Research and testing of previously uncharacterised Sasol refinery stream components, with high octane and oxygenated properties, using the upgraded and modified CFR engine test setup.

1.3 MOTIVATION

The significance of high octane and oxygenated fuels is on the rise with the modern trend of downsizing IC engines in the pursuit of improved fuel economy and reduced harmful exhaust emissions. Refineries characterise the octane properties of their petrol pool components in order to be able to numerically model and optimise refinery operation. The inability to test the octane of certain streams undermines this effort, resulting in operational and planning challenges and costly "octane give-away" because of overly conservative octane property margins, above the legally required octane specification values. This research project is a collaborative effort between Stellenbosch University and Sasol Technology (Pty) Ltd., hereafter referred to as Sasol. Successful execution of this project will allow for accurate and credible high octane and oxygenated fuels research at Stellenbosch University.

1.4 PLANNED ACTIVITIES

1. Literature review

Compile a report on CFR engines and octane research, specifically testing of high octane numbers (RON > 100) and oxygenated (Vol % > 25) fuels.

2. Engine setup

2.1. System specification and design work to define the project requirement details

Identify upgrades required for testing high octane and oxygenated fuels: hardware, measuring equipment and software.

2.2. Assessment of the engine condition

By means of disassembly and rigorous inspection. Compile an engine condition assessment report, as well as a modification specifications report, detailing the specifications of all modifications required for the intended test work.

2.3. Replacement or restoration of parts

As required proceeding 2.2.

2.4. Upgrading of control systems

Includes proportional–integral–derivative (PID) controller, cables and transducers for inlet air, coolant and oil temperatures; dynamometer speed control and additional heating element for inlet air.

2.5. Modification of fuel metering system

Modify fuel metering system to allow for higher fuelling requirements by replacing the existing fixed jet carburettor with a needle jet with larger bore.

3. Octane testing

3.1. Setup calibration

Calibration of thermocouples, pressure transducer, knock meter.

3.2. Fit for use tests

By means of toluene standardised fuels (TSF) test, replicating published octane data to prove validity of test results.

3.3. High octane and oxygenated fuels testing

Using special refinery component streams, fuel alcohols.

2. LITERATURE REVIEW

The Otto cycle is used to thermodynamically describe and quantify the efficiency of a petrol engine. The effects of downsizing and forced induction on combustion properties are investigated in section 2.1 and 2.2. Engine knock is an undesirable effect of high combustion temperatures and pressures. The causes, effects and prevention efforts of this phenomenon are explored in section 2.3. CFR engines are used as the industry standard equipment to measure the octane properties of fuels. In section 2.4, the standard CFR engine setup and knock measuring capabilities are shown. Octane test procedures, as accepted by the American Society for Testing and Materials (ASTM) are investigated in section 2.5.

2.1 THE OTTO CYCLE

The reciprocating engine has proved to be a versatile invention with a wide range of applications. Petrol and diesel IC engines are the foundation of personalised transport. Most petrol engine motor vehicles operate on a four-stroke spark-ignition cycle, known as the Otto cycle.

2.1.1 Description and history

The Otto cycle is named after Nikolaus A. Otto who, in 1876, built a successful four-stroke spark-ignition engine, using an ideal thermodynamic cycle proposed by Beau de Rochas in 1862. A schematic of the four-stroke mechanical cycle of a spark-ignition engine is shown in Figure 1.

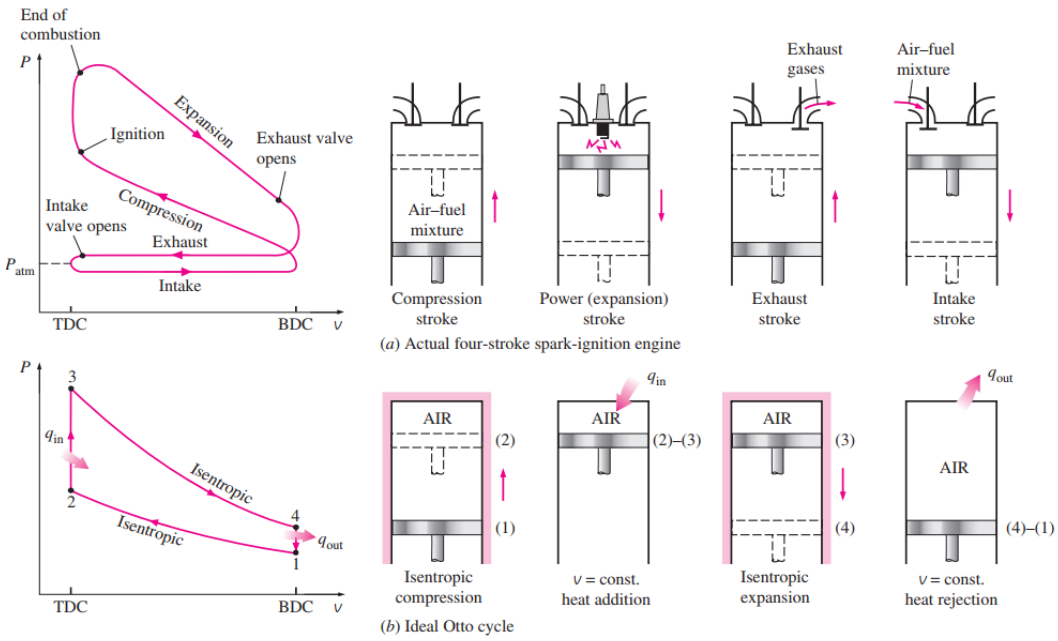

Figure 1: Actual and ideal cycles in spark-ignition engines and their P-v diagrams (Çengel and Boles, 2011: 483-496)

In most spark-ignition engines, the piston executes four complete strokes within the cylinder, and the crankshaft completes two revolutions to complete one thermodynamic cycle. During the first stroke, only the intake valve is open, and the low pressure created by the expanding volume inside the combustion chamber draws in a mixture of air and fuel, depending on engine design. This is known as the “intake stroke”. A valve spring shuts the intake valve, and the crankshaft forces the piston from its lowest position, bottom-dead-centre (BDC), to its highest position, top-dead-centre (TDC). This motion reduces the volume inside the cylinder, and compresses the air-fuel mixture, hence known as the “compression stroke”. Shortly before the piston reaches the TDC position, a spark plug fires, igniting the air-fuel mixture, creating a high pressure and temperature inside the cylinder. The expanding high-pressure gasses force the piston downwards, which in turn forces the crankshaft to rotate. This produces useful work output, and is known as the “expansion” or “power stroke”. During the “exhaust stroke”, the outlet valve is opened, and the piston moves upwards from the BDC to the TDC position, purging exhaust gasses out of the combustion chamber. These four strokes complete one reciprocating cycle, and are repeated to produce useable power and torque (Çengel & Boles, 2011: 483-496).

2.1.2 Ideal cycle analysis

According to Çengel and Boles (2011, 483-496), the thermodynamic analysis of an actual four-stroke spark ignition (SI) cycle, shown on a P-V diagram in Figure 3, is challenging due to irreversibilities. Therefore, when analysing a four-stroke engine, the ideal Otto cycle, shown on a P-V diagram in Figure 2, is used. The Otto cycle utilizes air-standard assumptions, and closely resembles the actual operating conditions of a four-stroke SI engine.

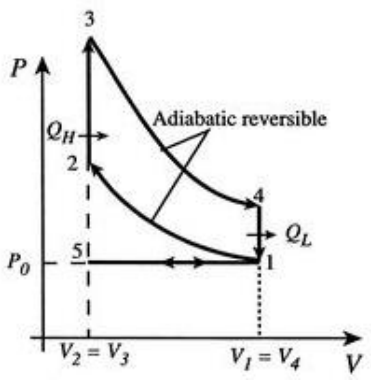

Figure 2: Ideal Otto cycle (3.5 The Internal Combustion Engine (Otto Cycle))

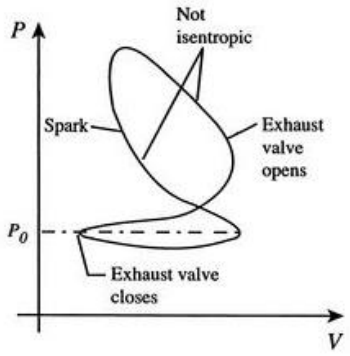

Figure 3: Actual Otto cycle (3.5 The Internal Combustion Engine (Otto Cycle))

The ideal cycle is derived from the actual cycle by what is commonly known as the air-standard assumptions:

1. The working fluid is air, which continuously circulates in a loop and always behaves as an ideal gas.
2. All the processes that make up the cycle are internally reversible.
3. The combustion process is replaced by a heat addition process from an external source.
4. The exhaust process is replaced by a heat-rejection process that restores the working fluid to its original state.

Friction is not considered in the ideal cycle. Therefore, the working fluid does not experience any pressure drop as it flows in pipes or devices such as heat exchangers. All expansion and compression processes are assumed to take

place in a quasi-equilibrium manner, and heat transfer through pipes and other components are assumed to be negligible. The ideal cycle is described by the following processes, related in the actual four stroke cycle shown in Figure 1:

1- 2 Isentropic compression
2-3 Constant-volume heat addition
3-4 Isentropic expansion
4-1 Constant-volume heat rejection

The ideal Otto cycle operates in a closed system, and disregarding changes in kinetic and potential energies, the energy balance for any of the processes is expressed, on a unit-mass basis, as:

$$(q_{in} - q_{out}) + (w_{in} - w_{out}) = \Delta u \quad (1)$$

Where q is heat transfer, w is system work and u is internal energy. No work is involved during the two heat transfer processes, since both take place at constant volume. Therefore, heat transfer to and from the working fluid can be expressed as:

$$q_{in} = u_3 - u_2 = c_v(T_3 - T_2) \quad (2)$$

And

$$q_{out} = u_4 - u_1 = c_v(T_4 - T_1) \quad (3)$$

With c_v the specific heat capacity of air at constant volume. The thermal efficiency of the ideal Otto cycle, under cold air standard assumptions, becomes:

$$\eta_{th,Otto} = \frac{w_{net}}{q_{in}} = 1 - \frac{q_{out}}{q_{in}} = 1 - \frac{T_4 - T_1}{T_3 - T_2} = 1 - \frac{T_1(\frac{T_4}{T_1} - 1)}{T_2(\frac{T_3}{T_2} - 1)} \quad (4)$$

Processes 1-2 and 3-4 are isentropic, and $V_2 = V_3$ and $V_4 = V_1$. Thus:

$$\frac{T_1}{T_2} = (\frac{V_2}{V_1})^{k-1} = (\frac{V_3}{V_4})^{k-1} = \frac{T_4}{T_3} \quad (5)$$

Substituting these equations into the thermal efficiency relation, and simplifying, gives the following:

$$\eta_{th,Otto} = 1 - \frac{1}{r^{k-1}} \tag{6}$$

Where r is the compression ratio of the system, shown in equation 7

$$r = \frac{V_{max}}{V_{min}} = \frac{V_1}{V_2} = \frac{V_{BDC}}{V_{TDC}} \tag{7}$$

And k is the specific heat ratio of the working fluid, shown in equation 8.

$$k = \frac{c_p}{c_v} \tag{8}$$

It can be seen from equation 6 that under cold-air-standard assumptions, the thermal efficiency of the ideal Otto cycle is dependent on the compression ratio of the engine, and the specific heat ratio of the working fluid. Figure 4 shows a plot of the thermal efficiency vs. compression ratio for k = 1.4, the specific heat ratio of air at room temperature.

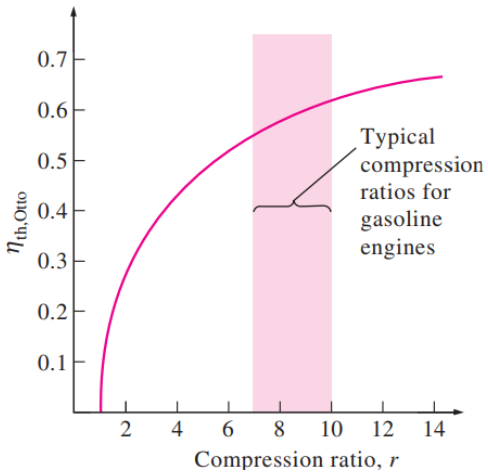

Figure 4: Thermal efficiency of the ideal Otto cycle as a function of compression ratio (k = 1.4) (Çengel and Boles, 2011: 483-496)

The range of typical compression ratios for a spark-ignition engine is highlighted in Figure 4. It can be seen that the efficiency of the ideal Otto cycle can be significantly improved above the upper limit of the indicated range. Engine knock, due to auto-ignition, becomes more likely when compression ratios above the limit shown in Figure 4 are used. It can therefore be said that the capability of the working fluid to resist auto-ignition is the upper limit of the thermal efficiency of a four-stroke spark-ignition engine. The thermal efficiency of spark-ignition engines used in vehicles typically ranges from 25 to 30 % (Çengel & Boles, 2011: 483-496).

2.1.3 Actual cycle analysis

The efficiency and power delivery of the actual four-stroke spark-ignition cycle includes the effects of heat transfer and friction (Hou, 2007: 1683-1690; Chen *et al*. 2003: 195-200). This is therefore a more accurate approach for the calculation of the efficiency of an SI IC engine, as it eliminates many of the assumptions and idealisations made in section 2.1.2.

The isochoric heating and cooling processes (2-3 and 4-1) are assumed to proceed according to constant temperature rates, i.e.:

$$\frac{dT}{dt} = \frac{1}{k_1} \text{ (for } 2-3) \text{ and } \frac{dT}{dt} = \frac{1}{k_2} \text{ (for } 4-1) \quad (9)$$

Where T is the absolute temperature, and t is absolute time, k_1 and k_2 are constants. Equation 9 describes average temperature rates, integrating this equation yields:

$$t_{v1} = k_1(T_3 - T_2),\ t_{v2} = k_2(T_4 - T_1) \quad (10)$$

Where t_{v1} and t_{v2} are the heating and cooling times, respectively. The cycle period can be described as:

$$\tau = t_{v1} + t_{v2} = k_1(T_3 - T_2) + k(T_4 - T_1) \quad (11)$$

And the work output is:

$$W = c_v(T_3 - T_2) - c_v(T_4 - T_1) \tag{12}$$

The power output of the cycle is described as:

$$P = \frac{W}{\tau} = \frac{c_v(T_3 - T_2) - c_v(T_4 - T_1)}{k_1(T_3 - T_2) + k_2(T_4 - T_1)} \tag{13}$$

When heat transfer through the cylinder walls is considered, the heat added to the working fluid through combustion becomes:

$$Q_{in} = c_v(T_3 - T_2) = \alpha - \beta(T_2 + T_3) \tag{14}$$

Where α and β are constants related to combustion and heat transfer respectively. From equation 14 we find:

$$T_3 = \frac{\alpha + (c_v - \beta)T_2}{(c_v + \beta)} \tag{15}$$

For processes 1-2 and 3-4, the end temperatures are obtained from:

$$T_2 = T_1 r^{k-1} \tag{16}$$

$$T_4 = T_3 r^{1-k} \tag{17}$$

Substituting (15) to (17) into (13) yields:

$$P = \frac{W}{\tau} = \frac{c_v[\alpha(1 - r^{1-k}) + 2\beta(1 - r^{k-1})T_1]}{(k_1 + kr^{1-k})(\alpha - 2\beta r^{k-1}T_1)} \tag{18}$$

Engine power is a parabola function of the compression ratio of the cycle. When considering the friction loss of the piston, a friction force, which is a linear function of velocity, is given by:

$$f_\mu = -\mu v = -\mu \frac{dx}{dt} \tag{19}$$

Where μ is a coefficient of friction, which takes into account global losses, and x is the position displacement of the piston. The power lost due to friction is:

$$P_\mu = \frac{dW_\mu}{dt} = -\mu \frac{dx}{dt}\frac{dx}{dt} = -\mu v^2 \tag{20}$$

The piston mean velocity is:

$$\tilde{v} = \frac{x_1 - x_2}{\Delta t_{12}} = \frac{x_2(r-1)}{\Delta t_{12}} \tag{21}$$

Where x_2 is the TDC position of the piston inside the cylinder, and Δt_{12} is the duration of the "power stroke". The resulting power output of the actual cycle is therefore:

$$P_{actual} = P - P_\mu = \frac{c_v[\alpha(1-r^{1-k})+2\beta(1-r^{k-1})T_1]}{(k_1+k_2 r^{1-k})(\alpha-2\beta r^{k-1}T_1)} - b(r-1)^2 \tag{22}$$

Where

$$b = \frac{\mu x_2^2}{(\Delta t_{12})^2} \tag{23}$$

The thermal efficiency of the actual Otto cycle is shown in equation 24.

$$\eta_{th,Actual} = \frac{P_{actual}}{Q_{in}/\tau} = \frac{c_v[\alpha(1-r^{1-k})+2\beta(1-r^{k-1})T_1] - b(r-1)^2(k_1+k_2 r^{1-k})(\alpha-2\beta r^{k-1}T_1)}{c_v(\alpha-2\beta r^{k-1}T_1)} \tag{24}$$

It is shown in Figure 4 that the thermal efficiency of the ideal Otto cycle increases with both compression ratio, and the specific heat of the working fluid. This is also true for an actual four-stroke spark-ignition IC engine, see equation 24. Shuhn-Shyurng Hou of Kun Shan University, Tainan, did a study in 2006 on the

effects of heat transfer on the power output and thermal efficiency of the Otto and Atkinson cycles. Figures 5 and 6 show the results for both the thermal efficiency of the cycle, and heat transfer in the cylinder vs. power output. The results for the Otto cycle are shown as a dotted line.

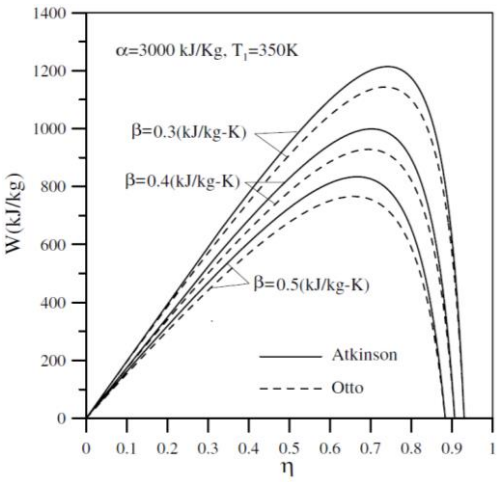

Figure 5: Effect of heat transfer on work output and thermal efficiency (Hou, 2007: 1683-1690)

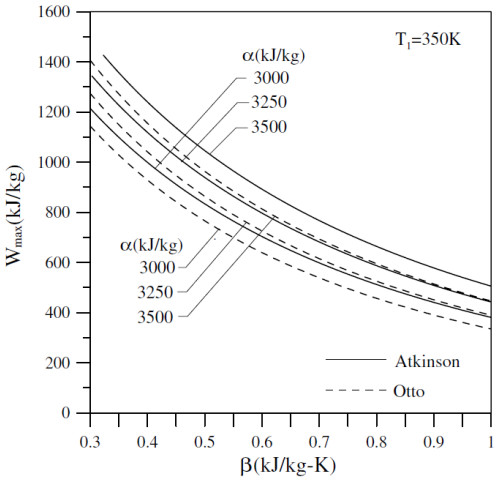

Figure 6: Effect of combustion on heat transfer and work output (Hou, 2007: 1683-1690)

It can be seen from Figures 5 and 6 that the maximum work output, and the corresponding efficiency at maximum work output decrease as the heat transfer constant β increases. In other words, higher heat transfer to the combustion chamber walls will lower the peak temperature and pressure, reducing the likelihood of auto-ignition, but also reducing the work per cycle, and the engine efficiency. It is also shown that the maximum work output and the corresponding efficiency at maximum work output increase as the combustion constant α increases (Hou, 2007: 1683-1690).

Chen et al. (2003) investigated the performance of an air-standard Otto cycle with heat transfer and friction-like term losses using finite-time thermodynamics. Figures 7 and 8 show the compression ratio vs. power, and compression ratio vs. efficiency characteristics of the irreversible Otto cycle, with heat transfer and friction effects.

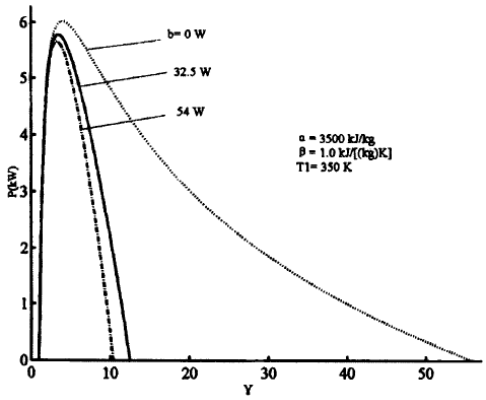

Figure 7: Effect of heat transfer on the compression ratio / power characteristic (Chen *et al*. 2003: 195-200)

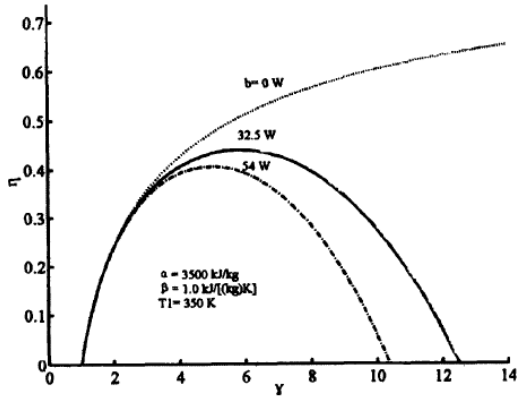

Figure 8: Effect of heat transfer on the compression ratio / efficiency characteristic (Chen *et al*. 2003: 195-200)

It is shown in Figure 7 that the power output of the actual Otto cycle reaches a peak value at a certain compression ratio. Figure 8 shows that the thermal efficiency of the cycle also reaches a peak value at the corresponding compression ratio. Higher compression ratios will increase the likelihood of engine knock, which dissipates the power produced by the cycle. It can also be seen from both Figures 7 and 8 that an increase in heat transfer through the cylinder wall reduces the efficiency and power output of the cycle (Chen *et al.* 2003: 195-200).

According to Heywood (1988: 161-197), a considerable portion of the gross indicated work per cycle of an IC engine is dissipated during the intake and exhaust strokes. Reducing the engine capacity will also reduce the power required to “pump” air through the combustion cycle, increasing the net thermal efficiency.

These studies show that the efficiency of the actual Otto cycle is largely dependent on compression ratio, heat transfer from the combustion chamber, and friction.

2.2 Mean effective pressure (MEP) and downsizing

A modern trend in the automotive industry is to “downsize” IC engines. The term, downsizing, refers to the general reduction of engine capacity, and typically, the number of cylinders, in the pursuit of improved efficiency, lower fuel consumption and reduced emission gasses. The European Car Manufacturer Association (ACEA) has committed to an average fleet target of 125 g/km CO_2 in 2015. In the year 2000, ACEA recorded an average of 169 g/km CO_2 for new vehicles (Silva et al. 2009: 215-222). It is shown in section 2.1.3 that the thermal efficiency of a four-stroke spark-ignition engine is largely dependent on compression ratio, and power output is dissipated through friction and heat transfer. Reducing the size (capacity) of an engine decreases mass and friction, which leads to greater efficiency and lower emissions.

Consumer requirements for modern vehicles are typically: lower fuel consumption, and increased performance (power and torque). The Jaguar/ Land Rover Powertrain Research group took on the challenge of the “Ultraboost” project in 2014. The aim of this project was to create a highly boosted (turbo- or supercharged), heavily downsized engine to provide the torque curve and power output of the naturally aspirated Jaguar Land Rover AJ133 5.0 litre V8 engine. They met their targets of 515 Nm at 3500 rpm; 283 kW / 380 bhp at 6500 rpm, and a 35% improvement in vehicle-level fuel economy using a 2.0 L turbocharged 4 cylinder petrol engineg with a compression ratio of 9.0:1, turbo boost pressure of 3.5 bar, and 130-135 bar maximum mean peak cylinder pressure (Turner, 2014).

It is shown in Figure 9, and equations (25) and (26) that, assuming constant engine speed, MEP has to increase in order for net work rate to remain constant, if the capacity of an IC engine is reduced. This is typically achieved by increasing the compression ratio, and adding forced induction (turbo- or supercharging) to an IC engine (De Bellis, 2016: 162-174; Clerk, 1907: 121-152).

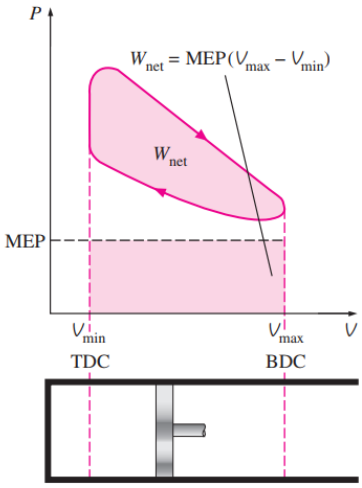

Figure 9: Piston-cylinder cycle P-v diagram (Çengel and Boles, 2011: 483-496)

$$\mathrm{MEP} = \frac{\mathrm{W_{net}}}{\mathrm{V_{max} - V_{min}}} \tag{25}$$

The net work output of the Otto cycle is shown in Figure 9 as the area enclosed by the cycle on a P-v diagram, and is expressed as:

$$\mathrm{W_{net}} = \mathrm{MEP} \cdot (\Delta \mathrm{V}) \tag{26}$$

Increased MEP, and the increased flow of oxygen due to forced induction, leads to higher combustion temperatures. This increases the possibility of auto-ignition, and ultimately, the likelihood of undesirable engine knock.

2.3 ENGINE KNOCK

It is shown in Figure 4, section 2.1.2, that the thermal efficiency of an IC engine can be increased by increasing the compression ratio. Section 2.2 shows that the MEP on which modern petrol engines operate is ever-increasing, along with the modern trend of downsizing. High compression ratios and high pressures increase the temperature of the air-fuel mixture (charge) inside the combustion chamber. In favourable conditions, the charge temperature can rise above a critical temperature level. This causes early and rapid burning of the fuel at some point, or points, ahead of the flame front, followed by almost instantaneous and

extremely rapid inflammation of the end gas, see Figure 10. The premature ignition of fuel, called auto-ignition, produces an audible noise, commonly referred to as engine knock (Çengel & Boles, 2011: 483-496).

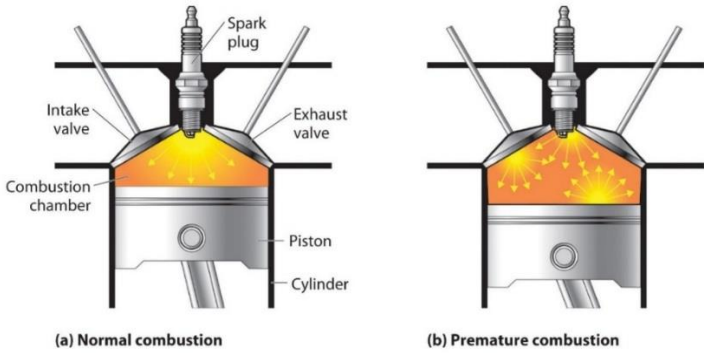

Figure 10: Knock visualisation ("3.8 Gasoline: A Deeper Look - chemwiki")

2.3.1 Causes and effects

According to Heywood (1988), knock is the name given to the noise which is transmitted through the engine structure when spontaneous ignition of a portion of the end-gas mixture ahead of the propagating flame occurs. When this abnormal combustion process takes place, there is an extremely rapid release of much of the chemical energy in the end-gas, causing very high local pressures and the propagation of pressure waves of substantial amplitude across the combustion chamber. Surface ignition is ignition of the A/F mixture by a hot spot on the combustion chamber walls such as an overheated valve or spark plug, or glowing combustion chamber deposit: i.e., by any means other than the normal spark discharge. It can occur before the occurrence of the spark (pre-ignition) or after (post-ignition). Following surface ignition, a turbulent flame develops at each surface-ignition location and starts to propagate across the chamber in an analogous manner to what occurs with normal spark ignition.

According to Çengel & Boles (2011: 483-496), high knock intensity (KI) in spark-ignition engines cannot be tolerated. Irregular combustion phasing dissipates performance, and the resulting shock waves cause serious engine damage. It is generally accepted that engine knock is the result of auto-ignition in the end-gas, before it is reached by the flame front emanating from the spark plug. Auto-

ignition is seldom homogeneous and usually occurs in randomly localized centres, as shown in Figure 10. When it occurs, auto-ignition generates pressure and detonation waves to propagate across, and excite the acoustic modes of the combustion chamber creating a distinct metallic ringing sound, and cause pitting in the cylinder head, shown in Figure 11. Figure 12 is a Laser-induced fluorescence (LIF) image showing auto-ignition centres ahead of the original propagating flame front.

Figure 11: Long-term effects of knock (Combustion Modeling [online], 2017)

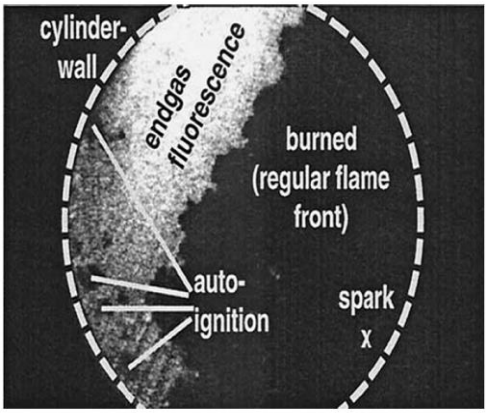

Figure 12: Auto-ignition visualization (Zhen *et al*., 2012: 628-636)

According to Zhen *et al.* (2012), the most common negative effects of engine knock are:

- Breakage of piston rings
- Cylinder head erosion
- Piston crown and top land erosion
- Piston melting
- Limits engine compression ratio or vehicle acceleration performance
- Air pollution
- Decrease in engine efficiency
- Considerable rise in engine specific fuel consumption (SFC)
- Possibility of structural harms to engine in a long-term period

Knock is most critical at WOT (Wide Open Throttle) and at low speed because of its persistence and potential for damage. Part-throttle knock is a transient phenomenon, and is a nuisance to the driver. (Stone, 1992).

2.3.2 Measurement and visualization

According to Heywood (1988) knock is a complex phenomenon. The likelihood of knock is dependent on engine, fuel, vehicle factors and ambient conditions (temperature and humidity). The methods of detecting knock can be classified in two broad categories, namely: direct and indirect methods. Direct methods are based on the measurement and study of parameters inside the combustion chamber, e.g. measuring in-cylinder pressures vs. crank angle. Figures 13 and 14 show the in-cylinder pressure vs. crank angle curves of a knock free, and a knocking SI IC engine respectively. It can be seen that much higher pressures and, oscillating pressure spikes, are measured when knock occurs. Indirect methods detect the effects of engine knock, e.g. cylinder block vibration.

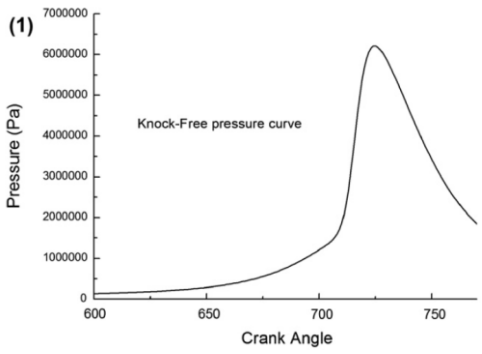

Figure 13: Knock free pressure curve (Zhen *et al*., 2012: 628-636)

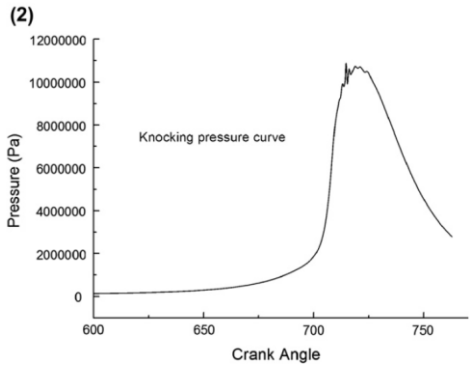

Figure 14: Knocking pressure curve (Zhen *et al*., 2012: 628-636)

Figure 15 shows a series of high-speed images of in-cylinder pressure, related to crank angle, for a non-knocking (1), and a knocking (2) SI IC engine. These images can be sequentially related to the pressure traces shown in Figures 14 and 15. Images A to E show the propagation of a normal flame front in a non-knocking engine. In the knocking engine cycle, frame F represents the normal flame front propagation. It shows the location of the combustion flame with the dark crescent-shaped end-gas region ahead of it, prior to any auto-ignition. In

frame G, the hot-spots arise at the upper left of the frame, which generates the auto-ignition region in the end-gas. The auto-ignition region moves upward, and it is brighter and hotter. The auto-ignition region propagates to the right, and in frame J, the end-gas is burned completely. The rapid burning of the end gas creates shock waves that result in the “spikes” shown on the pressure trace in Figure 14.

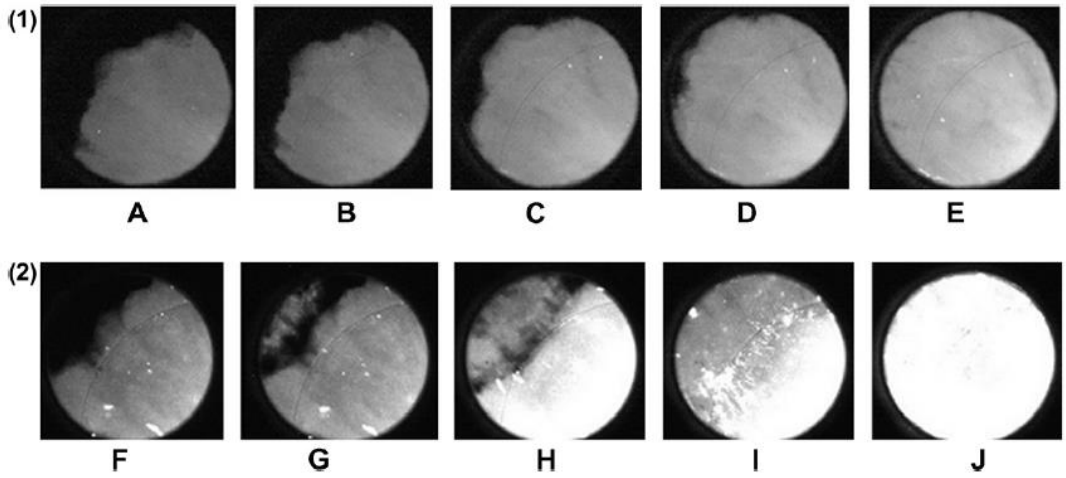

Figure 15: (1) Non-knocking engine cycle. (2) Knocking engine cycle. (Zhen *et al*., 2012: 628-636)

Knock sensors are used in modern petrol engine vehicles to form part of a feedback control system. Electronic control units (ECU) control spark timing and air/fuel (A/F) ratio, to ensure the SI engine can operate close to its knock limit, without inducing auto-ignition (Zhen et al., 2012: 628-636).

According to Kalghatgi *et al*. (2009), non-downsized engines in motor vehicles run clear of dangerous knock, by design and the use of knock sensors. Extremely high knock intensities (>100 bar) and high peak pressures (>200 bar) are observed occasionally during the testing of prototype, downsized, turbocharged engines; such events have been informally described as “Superknock”. Usually they are associated with pre-ignition.

2.3.3 Avoiding knock

According to Zhen *et al*. (2012), controllable circumstances which influence the likelihood of auto-ignition are commonly referred to as “machine and molecule”. This refers to engine design (machine), and fuel molecular structure (molecule). Engineers aim to design engines and fuels to resist auto-ignition by manipulating the architecture and operating conditions inside the combustion chamber, and increasing the octane rating of fuels.

- **Machine (Engine design)**

Conditions that are favourable to induce auto-ignition and engine knock are: high temperatures and high pressures. High inlet temperatures and pressures are caused by turbocharging or supercharging, without fitting an intercooler. The inlet and outlet manifold design also influences back pressure and heat release.

The use of cooled exhaust gas re-circulation (EGR) can suppress end-gas auto-ignition. Hot residual gas, however, can increase the inlet gas temperature and promote engine knock.

Turbulence inside the cylinder requires a more energetic spark to initiate combustion, and may delay ignition of the flame front. Once combustion has started, it proceeds more quickly with increased turbulence, reducing combustion duration and the tendency to knock.

The use of direct injection (DI) of a second fuel, ethanol or methanol (or their concurrent blends), is a means of avoiding knock. The dynamics of alcohol vaporization has a substantial impact on the temperature of the unburned gas in which auto-ignition occurs. With DI, thermal energy, used to evaporate the fuel, is drawn out of the A/F mixture and combustion chamber walls, rather than the inlet port, as is the case with port fuel injected and carburettor engines.

It is shown in section 2.1.2 that the thermal efficiency of SI engines is related to the compression ratio. High compression ratios, however, result in high in-cylinder pressures and temperatures, and therefore promote auto-ignition and knock.

Over-advanced ignition timing causes cylinder pressures to rise too rapidly. Knock can be mitigated by retarding ignition timing.

- **Molecule (Fuel structure)**

According to Heywood (1988: 62-69), conventional fuels are blends of many different hydrocarbon compounds obtained by refining crude oil, or synthetic and bio fuel raw materials such as coal, natural gas and bio-mass. These fuels are predominantly carbon and hydrogen (typically around 86 % carbon and 14 % hydrogen by weight). Other fuels of interest are alcohols (oxygenates), gaseous fuels (natural gas and liquid petroleum gas), and single hydrocarbon compounds. Some knowledge of the different classes of organic compounds and their molecular structure is necessary in order to understand combustion mechanisms.

Straight chain paraffins (alkanes) consist of single-bonded open-chain saturated hydrocarbon molecules. Saturated implies that no hydrogen can be added to the molecule. Molecules, larger than methane exist in straight chain, and branched chain configurations. These are called normal (n-) and iso- compounds, respectively. Examples of paraffins are: methane (CH_4), ethane (C_2H_6), propane (C_3H_8), n-octane (C_8H_{18}) and iso-octane (2,2,4-trimethylpentane).

Cycloparaffins (also termed napthenes or cycloalkanes), consist of single bond (no double bond) ring hydrocarbons. These molecules are unsaturated, since the ring can be broken, providing space for an additional hydrogen atom to be added. Relevant examples of cyclanes are: cyclopropane (C_3H_6), cyclobutane (C_4H_8) and cyclopentane (C_5H_{10}).

Olefins (alkenes) are unsaturated open chain hydrocarbon compounds containing a double bond. Relevant examples of olefins are: ethene (or ethylene) (C_2H_4), propene (or propylene) (C_3H_6), and butene (or butylene) (C_4H_8). From butene upwards, several structural isomers are possible, depending on the location of the double bond in the basic carbon chain. Straight- and branched chain structures exist. Di-olefins contain two double bonds.

Acetylenes (alkynes) are open chain unsaturated hydrocarbon compounds with one carbon-carbon triple bond. The first member is acetylene. Additional members of the alkyne series comprise of open chain molecules, similar to higher alkenes, but with each double bond replaced by a triple bond.

Benzene (C_6H_6) is the building block for aromatic hydrocarbons. This ring structure is very stable and accommodates additional $–CH_2$ groups in side chains, and not by expansion. Relevant examples of aromatics are: toluene (C_7H_8) and xylene (several structural arrangements). More complex hydrocarbons incorporate ethyl, propyl and heavier alkyl side chains in a variety of structural arrangements.

In monohydric alcohols, one hydroxyl (-OH) group is substituted for one hydrogen atom. Thus methane becomes methyl alcohol (CH_3OH), or methanol; ethane becomes ethyl alcohol (C_2H_5OH), also called ethanol, etc.

According to Heywood (1988), Individual hydrocarbon compounds vary enormously in their ability to resist knock, depending on their molecular size and structure Knocking tendency is related to molecular structure as follows:

Paraffins:

- Increasing the length of the carbon chain increases the knocking tendency.
- Compacting the carbon atoms by incorporating side chains (thereby shortening the length of the basic chain) decreases the tendency to knock.
- Adding methyl groups (CH,) to the side of the basic carbon chain, in the second from the end or center position, decreases the knocking tendency.

Olefins:

- The introduction of one double bond has little antiknock effect; two or three double bonds generally result in appreciably less knocking tendency.

- Exceptions to this rule are acetylene (C_2H_2), ethylene (C_2H_4), and propylene (C_3H_6), which knock much more readily than the corresponding saturated hydrocarbons.

Napthenes and aromatics:

- Napthenes have significantly greater knocking tendency than have the corresponding size aromatics.
- Introducing one double bond has little antiknock effect; two and three double bonds generally reduce knocking tendency appreciably.
- Lengthening the side chain attached to the basic ring structure increases the knocking tendency in both groups of fuels, whereas branching of the side chain decreases the knocking tendency.

According to Ronney (2013), the molecular structure of a fuel dictates the likelihood of knock. The rate of auto-ignition is dependent on the rate of removal of hydrogen atoms (H) during the combustion reaction, and therefore depends on the strength of C-H bonds in the molecule. The strength of C-H bonds in hydrocarbon molecules are dependent on the number of C-C bonds. Figure 16 shows that C-H bonds in hydrocarbons are stronger with fewer C-C bonds.

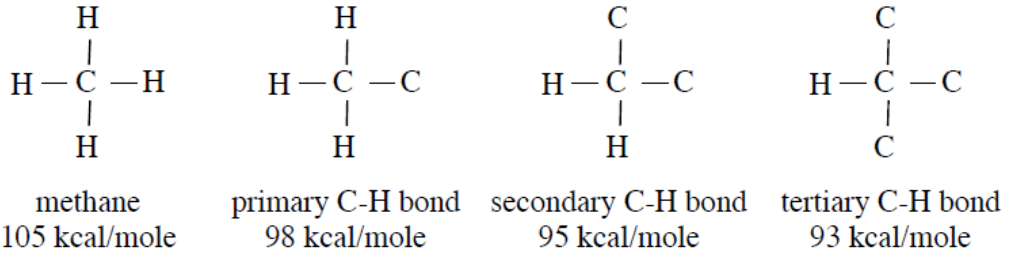

Figure 16: Hydrocarbon bond strength (Ronney, 2013)

Stronger C-H bonds result in slower reaction rates, and therefore reduces the likelihood of auto-ignition. The molecular construction of primary reference fuels (PRF), n-heptane and iso-octane are shown in Figures 17 and 18. n-Heptane has a Research Octane Number (RON) of 0. It is an unbranched, straight chain paraffin with seven Carbon, and sixteen Hydrogen atoms. 2,2,4 trimethylpentane,

commonly referred to as iso-octane, has a RON of 100. It is a branched paraffin with 15 primary, 2 secondary and 1 tertiary C-H bonds.

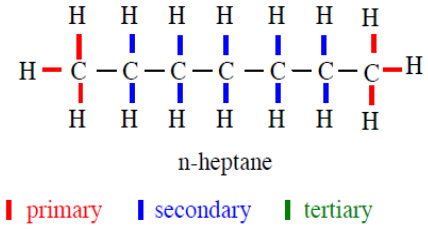

Figure 17: n-Heptane bond strength (Ronney, 2013)

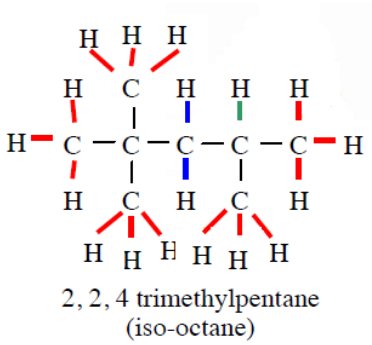

Figure 18: Iso-octane bond strength (Ronney, 2013)

Linear blends of iso-octane and n-heptane are used in CFR engines to bracket test samples, and measure octane ratings. The relationship between octane number (RON), and the number of carbon atoms per molecule is shown in Figure 71, Appendix B. According to Blackmoore (1977), the octane rating of a hydrocarbon molecule is shown to decrease with an increase in carbon atoms. A branched molecule, however, is shown to have a higher knock resistance than a straight chain molecule with an equal number of carbon atoms.

2.3.4 Fuel physical properties and knock

According to Gersen *et al.* (2016), auto-ignition of the end-gas is critically sensitive to the pressures and temperatures inside the combustion chamber during the combustion period. Changes in the heat capacity of the A/F mixture, variations in the initial pressure, and changes in the phasing of the combustion process can all affect the likelihood of engine knock. Auto-ignition is a time-dependant phenomenon. The reactivity of the fuel, the A/F ratio, and temperatures and pressures inside the combustion chamber will all affect the required time for the end-gas to spontaneously combust. If this reaction time is slow, the propagating flame front (regular combustion) will completely consume the end-gas before auto-ignition can occur. Fuel components with an inhibiting effect on the rate of reaction and heat release will therefore reduce the likeliness of knock.

Richards *et al.* (2014) states that pre-ignition can be influenced by the fuel's ability to heat up a potential hot spot in the combustion volume. This was found to be partially correlated to flame speed. Increased burn rate in the early phase of combustion increases the ultimate pressure in the cylinder, which in turn increases the temperature of the end gas. Therefore, hot spot temperatures rise with a higher flame speed.

According to Leone et al. (2015), the latent heat of vaporization (H_v), and volatility of a fuel affects the in-cylinder combustion temperatures. After injection, an evaporative cooling effect decreases the A/F mixture temperature in relation to the H_v of the fuel. This has a significant influence on the likelihood of knock. The ignition delay time (reaction time) for hydrocarbon fuels is generally modelled as decreasing exponentially with increasing temperature. The fuel $H_{v,}$ per unit mass, combined with the mass ratio of fuel required for a stoichiometric A/F mixture, determines the upper limit of charge cooling. The H_v of a stoichiometric mixture of ethanol is approximately 4-fold greater than that of gasoline. The H_v of hydrocarbon gasoline has been reported to contribute 4 octane numbers (O.N.) of knock resistance in a direct injection (DI) engine relative to a port fuel injection (PFI) engine. In a gasoline turbocharged direct injection (GTDI) engine, gasoline contributed 5 O.N. of cooling-related knock resistance while E85 contributed 18 O.N.

Stein et al. (2013) states that although increased CR and engine downsizing / downspeeding provide improved thermal efficiency and CO_2 emissions in the vehicle, they will cause degraded vehicle performance if the engine is not supplied with fuel having at least the intended ethanol content and RON as per original design.

The mass fraction of oxygen in a fuel molecule affects the required stoichiometric A/F ratio. The more fuel required for stoichiometric combustion, the higher the effect of evaporative cooling on combustion temperatures and knock resistance Heywood (1988).

2.4 CFR ENGINES

The Cooperative Fuel Research (CFR) committee was founded in the 1920's as the increasing popularity of personalised transport gave rise to the need for engine manufacturers and fuel producers to quantify the knock resistance properties of fuels. In 1928, a single cylinder research engine, designed by the Waukesha Motor Company, was chosen to be the standardised platform for knock and octane research. The CFR engine is used to this day as the industry standard equipment. Figure 19 shows the original CFR engine test cell at Stellenbosch University.

Figure 19: Original CFR engine setup at Stellenbosch University

2.4.1 Engine characteristics

The CFR research engine is a standardised single cylinder, four stroke, spark-ignition engine with a variable compression ratio. Engine knock is induced by adjusting the compression ratio within the range of 4:1 to 18:1, using a cranked worm shaft and worm wheel drive assembly in the cylinder clamping sleeve. The

engine is fuelled by a carburettor with a single vertical jet and fuel flow control, to permit adjustment of the A/F ratio. A thermal syphon recirculating jacket coolant system is used to cool the engine. The test setup is fitted with a multiple fuel tank system with selector valves to deliver fuel through a single jet passage and carburettor venturi. The air intake system is fitted with controlling equipment for temperature and humidity. Even though the operating conditions for the octane tests are measured in SI units, the standardised CFR engine measurements are imperial, because of the extensive range of existing, expensive tooling that has been created for this equipment. Table 1 lists the basic characteristics of a modern CFR engine (ASTM, 2016).

Hunwartzen (1982) successfully adapted a standard CFR engine setup for testing of pure alcohol and gasoline alcohol blends by implementing a needle valve in the carburettor system to adjust A/F ratios, and by adding an external band heater to the intake manifold, to compensate for the high latent heat of vaporisation of oxygenates.

Table 1: Modern CFR engine characteristics (ASTM, 2016)

Item	Description
Test engine	CFR F-1 with cast iron, box type crankcase. Flywheel and power absorption electrical motor for constant speed operation
Cylinder type	Cast iron with flat combustion surface and integral coolant jacket
Compression ratio	Adjustable 4:1 to 18:1
Cylinder bore	82.55 mm
Stroke	114.30 mm
Displacement	37.33 inch^3. (611.73 cm^3)
Valve mechanism	Open rocker assembly with linkage for constant valve clearance as CR changes
Intake valve	Stellite faced, with180° shroud
Exhaust valve	Stellite faced, plain type without shroud
Piston	Cast iron, flat top
Camshaft overlap	5°
Fuel system	Single vertical jet carburettor with fuel flow control to permit adjustment of fuel-air ratio
Venturi throat	9/16 inch.
Ignition	Electronically triggered condenser discharge through coil spark plug
Ignition timing	13° btdc (RON) / 18-24° btdc (MON)
Intake air humidity	Controlled within specified limit range

2.4.2 Knock measurement

Figure 20 illustrates the operation of a knock measuring device used to detect and quantify knock in CFR engines. A contact pin is connected to a diaphragm, which deflects during knock as a result of the rate of pressure rise inside the combustion chamber. A knock event would therefore force the diaphragm to expand, and the bouncing pin would close an electrical circuit with a heating coil. The temperature of the heating coil is measured as an indication of the knock intensity. An ammeter is used to relate the temperature of the heating coil to knock intensity. The bouncing pin was specified as the standard instrumentation,

until it was supersede in 1970 by an electronic knock measuring system (Swarts, 2006) .

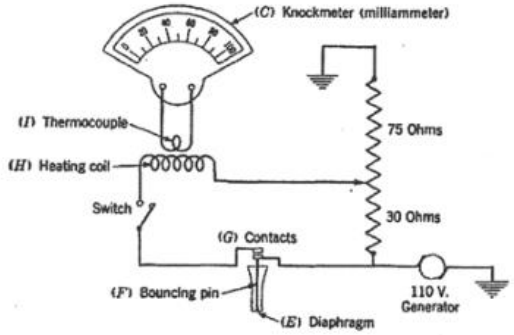

Figure 20: Early CFR knock meter system (Swarts, 2006)

2.5 OCTANE TESTING

The Octane number of a fuel is determined using a CFR engine in a test cell laboratory. A CFR engine is connected to a dynamometer, which is used as a resistance brake, to maintain engine speed. The compression ratio of a CFR engine is adjustable, and together with the knock meter, and temperature and pressure measuring equipment, the knock characteristics of a fuel can be examined.

There are two ASTM standard test methods for the octane number of a fuel. The Research Octane Number (RON), and Motor Octane Number (MON), are tested with specific engine and instrumentation settings and standard operating conditions. These tests are designed to simulate different driving conditions. The Anti-knock Index (AKI), commonly used in America and Canada, is the average of the RON and MON values.

According to Yang *et al.* (2013), .octane numbers have been conventionally used to provide quantitative measurement for fuel knock propensity. However, the standard octane test conditions in a CFR engine, e.g. naturally aspirated, carburettor fuelling, etc. are considerably different from that in modern SI engines. Modern SI engines often operate at conditions outside those used to determine the RON and MON octane numbers. The K-factor in the Octane Index, OI = RON – K(RON-MON), which by definition is 0 for RON test conditions and 1

for MON conditions, is often negative in turbocharged, direct injection engines, and it varies significantly with operating conditions. Octane numbers are therefore limited in their ability to predict fuel anti-knock performance in modern, downsized SI engines, although they are still good for indicative purposes. According to Yates et al. (2009) the high latent heat of the alcohols would introduce a physical cooling aspect to the octane method that would have a direct implication on the octane rating (RON) measured on a CFR engine. The cooling effect of alcohols does not effect MON results since the mixture temperature is controlled using electric heaters.

2.5.1 RON - ASTM D2699

The Research Octane Number (RON) of a fuel is measured under mild operating conditions with regard to inlet temperature and engine RPM, simulating normal driving conditions. The octane number (O.N.) scale covers a range of 0 to 120, but the research method has a working range of 40 to 120 RON, with typical fuels produced for SI engines in the range of 88 to 101 (ASTM D2699, 2016). Linear blends of iso-octane and n-heptane are used as primary reference fuels to bracket test samples, which limits octane tests to <100 O.N. The D2699 Standard test method for Research Octane Number of spark-ignition engine fuel is a laboratory test method that covers the standard test procedure, and a defined set of operating conditions. Table 2 lists a summary of the standard operating conditions of the RON test (ASTM D2699, 2016).

Table 2: Summary of operating conditions (RON) (ASTM D2699, 2016)

Condition	Research method value and range
Engine speed (RPM)	600 ± 6
Oil pressure @ operating temp (kPa)	172 to 207
Intake humidity (kg H_20/ kg dry air)	0.00356 to 0.00712
Intake air temperature	52 ± 1°C
Mixture temperature	52°C
A/F ratio	Adjusted for maximum knock
Ignition timing	13° btdc

Basic engine and instrument settings that are specified in the ASTM D2699 test method include: Installation of engine equipment and instrumentation, operating conditions based on component specifications, and assembly settings and operating conditions. The accepted test procedures are described in chapter 2.5.4 of this report, and reference fuel blending tables and guide tables of constant knock intensity are included in the appendices of the test standard. RON is used as the standard octane rating for fuel in South Africa, Australia, New Zealand and most of Europe.

2.5.2 MON - ASTM D2700

The Motor Octane Number (MON) of a fuel is tested under more challenging operating conditions with regard to inlet temperature and engine RPM. The O.N. scale covers a range of 0 to 120, but the MON method has a working range of 40 to 120, with typical fuels produced for SI engines in the range of 80 to 90 MON. The D2700 Standard test method for MON of spark-ignition engine fuel, is a laboratory test method that covers the standard test procedure, and a defined set of operating conditions. Table 3 lists a summary of the operating conditions of the MON test (ASTM D2700, 2016).

Table 3: Summary of operating conditions (MON) (ASTM D2700, 2016)

Condition	Motor method value and range
Engine speed (RPM)	900 $\pm$ 9
Oil pressure @ operating temp (kPa)	172 to 207
Intake humidity (kg H_20/ kg dry air)	0.00356 to 0.00712
Mixture temperature	149 $\pm$ 1°C
A/F ratio	Adjusted for maximum knock
Ignition timing	14 - 26° btdc (Adjusted with compression ratio)

The difference between the operating conditions listed in Tables 2 and 3 show that the MON test utilises pre-heated A/F mixture and variable ignition timing in order to simulate operation under more different conditions. Ignition timing

remains constant during the RON test, and only the intake air temperature is controlled. As a result, the RON rating of a fuel is likely to be 10 or 12 O.N. higher than the MON rating for the same amount of knock resistance.

2.5.3 Anti-knock Index (AKI) and Octane Sensitivity

The Pump Octane Number (PON) or Anti-knock Index (AKI) is calculated as the arithmetic average of a sample's RON and MON values, and is often used as the standard octane rating in the USA and Canada. The Octane Sensitivity of a fuel, or the sensitivity of the knock characteristics of a fuel to changes in the operating conditions of an SI engine, is indicated by the difference between the RON and MON ratings. The larger the difference between RON and MON, the more sensitive the fuel is to operating conditions (Blackmore, 1977: 44-66).

2.5.4 Octane test procedures

The ASTM standards list four accepted test procedures for RON and MON, using a CFR test facility. The methods described in this chapter require that the operating conditions of the engine and equipment comply with the ASTM standards. A fit-for-use test (eg. toluene standardised fuels test, section 4.2) has to be completed to ensure reliable test results (ASTM D2699, 2016). Note that in the following descriptions the A/F ratio of the engine is adjusted by the original setup, utilising the fuel level, and fuel reservoir height. This system was improved by modifications described in section 3.3.8. The modification simplifies fine tuning of the A/F ratio, and the test procedure followed by the author utilized this function.

- **Bracketing – Equilibrium Fuel Level**

A fuel sample, with unknown octane characteristics is introduced to the CFR engine. The engine is operated under RON or MON conditions as listed in section 2.5.1 and 2.5.2. The compression ratio of the CFR engine is adjusted, such that mid-range knock intensity (KI) is displayed on the analogue knock meter. The A/F ratio is adjusted for maximum knock intensity, and the compression ratio (CR) of the engine is adjusted such that maximum KI is displayed as 50 ± 2 divisions on the analogue knock meter. An estimated octane value for the sample can be calculated using CR reference tables in the ASTM

methods. Two PRF blends, with octane ratings lower, and higher than the estimated rating of the sample are tested on the same CR and operating conditions, with A/F ratio adjusted for maximum KI. The KI and known octane ratings for both PRF's are used to interpolate linearly for the sample octane number. The accuracy of the results when using this method relies on PRF blending accuracy, and KI reading accuracy.

- **Bracketing – Dynamic Fuel Level**

A fuel sample is introduced to the CFR engine. The engine is operated under RON or MON conditions as listed in section 2.5.1 and 2.5.2. The compression ratio of the CFR engine is adjusted, such that mid-range knock intensity is displayed on the analogue knock meter, with approx. mid-range fuel level. An estimated octane value for the sample can be calculated using CR reference tables in the ASTM methods. Two PRF bracketing fuels, one higher and one lower than the estimated sample O.N. are blended. For the sample fuel, and both PRF bracketing fuels, the fuel reservoir is filled to the top. As the engine operates on the mid-range KI CR, the fuel level drops due to fuel consumption. This affects the A/F ratio of the engine since fuel pressure in the carburettor decreases with the fuel level in the reservoir. The operator notes the maximum KI on the analogue meter, which occurs at a certain fuel level. The octane rating of the sample is interpolated linearly between the maximum KI and known octane ratings of the PRF bracketing fuels. This method eliminates possible errors in establishing the fuel level at which maximum KI occurs, but requires more time and fuel. This method is only applicable for ratings within the range of 80 to 100 O.N.

- **Critical Compression Ratio**

If a characteristic curve for the CFR engine is calibrated, a Critical Compression Ratio (CCR) method can be used to determine the octane rating of a fuel sample. The characteristic curve of a CFR engine describes the relationship between knock intensity; compression ratio and octane rating (see Figure 47, section 4.1). The cylinder height of the CFR engine is related to compression ratio, and the analogue knock meter is used to measure knock intensity. A fuel sample is introduced to the CFR engine, operating under RON or MON conditions as listed

in section 2.5.1 and 2.5.2. The CR of the engine is adjusted such that mid range knock intensity, 50 ± 2 divisions on the analogue knock meter, is displayed. The octane rating of the fuel sample is calculated by linearly interpolating CCR and octane data points on the characteristic curve of the CFR engine. This is the most time, and fuel efficient method, since it does not require PRF blending and bracket testing for each sample.

- **Bracketing - OA**

This method requires a modern CFR engine setup with automated A/F ratio and CR control. The methodology of the equilibrium fuel level method is applied for the test sample, and PRF bracket fuels. The system is automated, and KI data is captured and interpolated by software. This method is not applicable to the CFR setup at Stellenbosch University.

2.6 LITERATURE SUMMARY

The automotive industry aims to reduce fuel consumption and harmful emission gasses by downsizing IC engines. Customer requirements for modern vehicles are improved power delivery and fuel economy. These objectives are achieved by increasing MEP via forced induction of downsized engines, thereby increasing thermal efficiency of the thermodynamic cycle.

High temperatures and pressures in the combustion chamber, caused by high CR or forced induction, can lead to auto-ignition and engine knock. Knock is undesirable, and can cause long-term damage, dissipate power output and increase fuel consumption. The octane rating of a fuel is a measure to which it can resist auto-ignition. High octane fuels enable automotive manufacturers to produce downsized engines with high compression ratios, and forced induction. The octane rating of a fuel is determined on a CFR engine through ASTM standard tests for RON and MON. The standard operating range for a CFR engine does not allow for high octane (RON > 100) and oxygenated fuels.

Disassembly, inspection, restoration and modifications to the CFR engine at Stellenbosch University, required for high octane and oxygenated fuels testing, are discussed in section 3 of this report.

3. DEVELOPMENT OF TEST FACILITY

The original setup of CFR engine at Stellenbosch University is shown in Figure 19, section 2.4.1. The standard specification engine was suited to octane testing of conventional fuels (O.N. < 100). The testing phase of the final year project of Mr. CJN Jooste in October 2016, presented an opportunity to assess the running condition of the engine and testing equipment before disassembly and upgrades (Jooste, 2016). It was found during preliminary testing that the engine was in a reasonably good condition, and produced repeatable results. It was noted that the A/F ratio, measured with a lambda sensor and scanner, was unstable, and that the exhaust setup did not adhere to ASTM standards. Details of the preliminary testing phase are included in this report in Appendix E. In this section, the condition assessment process of the CFR engine is discussed. Modifications required for high octane and oxygenated fuels testing are described, and the final setup of the test facility is explored.

3.1 DISSASSEMBLY AND CONDITION ASSESSMENT

The CFR engine was disassembled in order to individually assess the condition of critical components. Figures 21 and 22 show the disassembled crankcase and cylinder head. All components were thoroughly cleaned prior to inspection.

.

Figure 21: Disassembled cylinder head

Figure 22: Disassembled crankcase

It was noted that the cylinder, and connecting-rod shell bearings showed scuff marks (scratches and particle tracking) typically caused by contaminated engine

oil. The connecting-rod shell bearings were found to be in usable condition, but can be considered for replacement in future projects. This model CFR engine did not have an oil filtration system as standard.

Light damage on the piston crown, and top land of the piston, was caused by an inspection sleeve protruding into the combustion chamber (see Figure 33 in section 3.2.6). The compression rings were undamaged, and the piston and ring set was therefore in a usable condition. The protruding inspection sleeve was modified as discussed in section 3.2.6

The CFR engine at Stellenbosch University is a donation from the Department of Mechanical Engineering at the University of Cape Town, where it was used for research by A. Swarts (Swarts, 2006).The engine was substantially rebuilt prior to the commencement of his research to include a new head, piston and rings.

With the knowledge that the CFR engine was comprehensively rebuilt fairly recently, and with the confidence inspired by preliminary tests, and visual condition assessment, only the most crucial components of the CFR engine were measured. The ASTM Manual for Rating Motor, Diesel and Aviation Fuels (1973-74) provides the original manufacturing tolerances for critical components of the CFR engine. These measurements include lower, upper and replacement limits for certain components in the cylinder head and crankcase. It was found that all measured components fall within the tolerances prescribed by ASTM.

3.2 UPGRADES AND MODIFICATION

A thorough inspection of the disassembled components of the CFR engine was followed by cleaning, sanding and painting, in order to restore the CFR engine to an aesthetic and functional condition. All gaskets, seals and thermocouple fittings were replaced to reduce leaks and safety hazards. Figures 23 and 24 show the restored and re-painted CFR engine and components before reassembly and modifications.

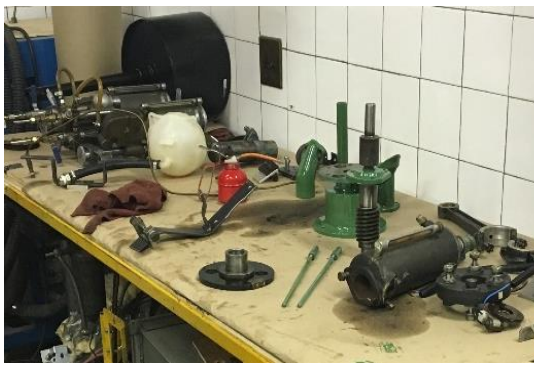

Figure 23: Cleaned, restored and painted components

Figure 24: Restored and painted CFR engine

3.2.1 Exhaust setup

The exhaust system of the CFR engine in its original condition did not adhere to the specifications prescribed in the ASTM Manual for Rating Motor, Diesel and Aviation Fuels (1973-74). Figure 25 shows the original exhaust setup compared to the required specification.

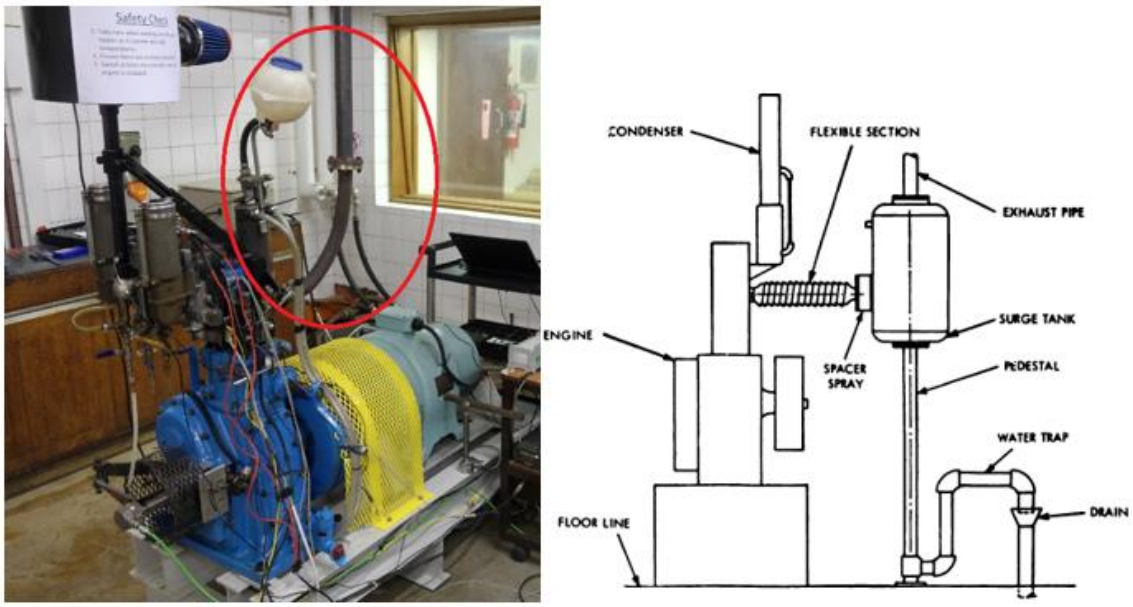

Figure 25: Original exhaust setup vs. ASTM specification (ASTM, 1973-74)

Figure 26 shows a flexible hose, in the original setup, bending upwards, directly from the engine outlet towards a roof mounted exhaust system. The bend in the original setup increases exhaust backpressure. The ASTM specification states that a surge tank must be mounted on the same level as the engine exhaust outlet. A flexible hose, at least 18 inch long and with a 4 inch internal diameter, must connect the surge tank to the exhaust outlet on the cylinder head. The surge tank must be connected to a roof mounted exhaust system via a flexible hose, with no more than three bends. (ASTM D2699, 2016).

A steel frame, shown in Figure 74 in Appendix D, was designed to bolt onto the base frame of the CFR engine, and support a surge tank cylinder above the DC dynamometer. Stainless steel braided flexible hoses were used to connect the exhaust system in accordance with the ASTM specifications. Figure 26 shows the position of the surge tank cylinder, mounted on the steel frame. The complete setup is shown in the final assembly, as seen in Figures 43 and 44 in section 3.2.9.

Figure 26: Mounted exhaust frame

3.2.2 Shaft encoder

The original AVL shaft encoder was replaced with a Kubler optic unit with a resolution of 0.1° crank angle. This device was used for accurate pressure to crank angle synchronisation, and engine speed measurement. A sleeve on the output shaft of the CFR engine was modified to accommodate the new unit. A technical drawing of the modified sleeve is included in this report in Figure 76, Appendix D.

An adjustable and fully floating mounting bracket was designed to accommodate the Kubler shaft encoder. A rod-end spherical bearing connects the mounting bracket to the shaft encoder. This enables three degrees of freedom, and a “floating end’ to accommodate vibrations, oscillations and shaft run out or alignment issues. A technical drawing of the mounting bracket is included in this report in Appendix D, Figures 77 and 78. Figure 27 shows the Kubler shaft encoder, modified output shaft and mounting bracket on the CFR engine.

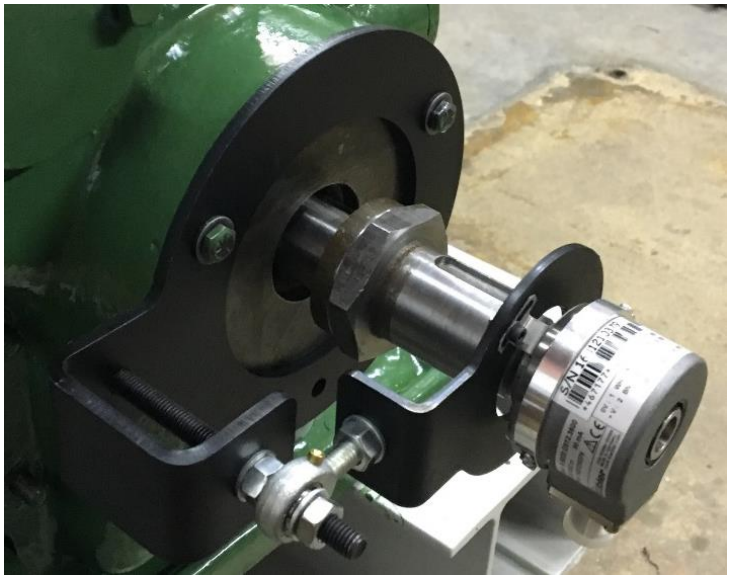

Figure 27: Mounted shaft encoder and bracket

3.2.3 Fuel reservoir chiller system

The blending ratio of fuel samples is crucial to the accuracy and credibility of octane test results. Components such as C_5 raffinate are highly volatile, and can

evaporate at low temperatures. C_5 raffinate has a boiling point of -5 to 5°C (PCS, 2014). The blending ratio of a test sample or bracketing fuel, and ultimately test results, can be influenced if one or more of its components evaporate after blending. Fuel blends are made using a digital balance scale and blending software, described in Appendix A of this report.

A simple chilling system was implemented to ensure test samples remain at a low temperature for the duration of an octane test. A 130 L Defy chest freezer was purchased. Test samples were placed in the freezer promptly after blending, and left overnight. Sample fuels were tested the following day, with fuel temperatures of ± -20°C prior to testing. Octane tests lasted approximately 5 minutes per fuel sample.

A 3/8 inch copper tube was selected based on availability, and wound around the cylindrical fuel float chamber of the CFR engine, Figure 28. The copper tube acts as a cooling coil around the fuel float chamber.

Figure 28: 3/8 inch Copper tube wound flat around fuel reservoir

A square plastic tub was placed inside the chest freezer, and filled with a 50 % (Vol %) blend of summer coolant and water. A submersible pond pump was placed inside the tub. The pump circulates chilled coolant through the copper

coil, creating a cooling effect on the surface of the fuel float chamber, and shielding the outer surface of the fuel reservoir against heat radiating from the CFR engine. Figure 29 shows the coolant tub inside the chest freezer, and the thermally insulated cooling coil.

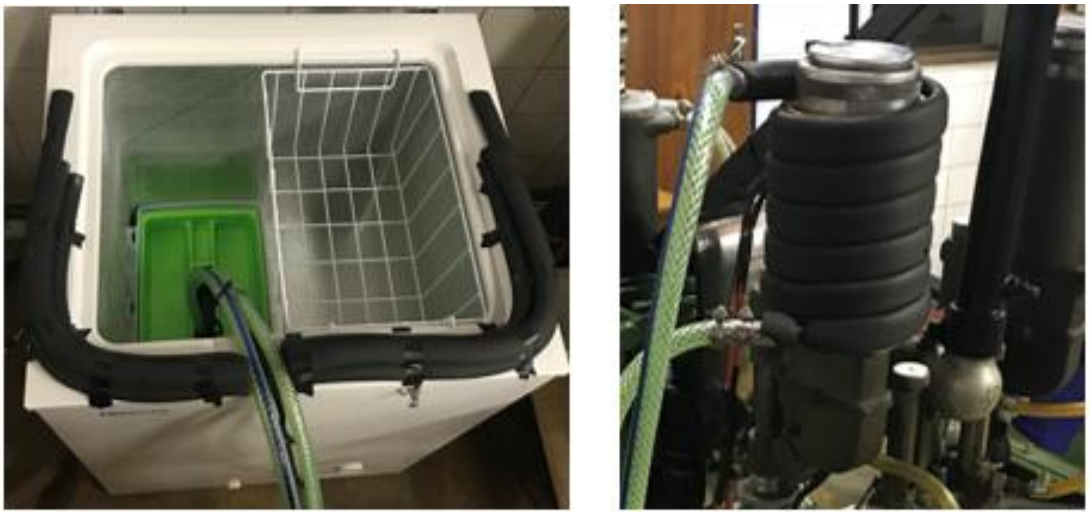

Figure 29: Submersible pump and chest freezer (Left); Insulated cooling coil (Right)

3.2.4 Ignition system

The original CFR engine setup utilised a points and distributer system to control ignition timing. Ignition timing has a substantial influence on engine knock intensity (see Table 5, section 4.3). The ASTM RON and MON tests require different ignition timing settings, and ignition timing is adjusted in relation to CR during MON test (see Table 3, section 2.5.2). A Perfect Power XMS5B – 8A ECU was purchased to control ignition timing. This module is capable of controlling ignition as well as fuel injection of a multi cylinder engine. This creates the possibility of converting the fuelling system of the CFR engine to electronic fuel injection in future projects.

A 60-2 trigger wheel, shown in Figure 30, was designed to supply crack angle, and piston position feedback to the ECU. The trigger wheel was laser cut from mild steel, with slots for fastening bolts, to allow for angle adjustment of the trigger wheel in relation to the TDC position of the engine.

Figure 30: Machined trigger wheel and fitment

A magnetic sensor was mounted on an adjustable bracket underneath the trigger wheel. The sensor produces a voltage signal to the ECU, which is used to relate crank angle and the piston of the position to ignition timing.

The Perfect Power ECU was delivered with a factory fault, and was returned for repairs. It was decided to continue with the project, and start the testing phase using the original ignition system. The ECU was only returned after a significant portion of testing had already been conducted. It was decided to complete the testing for this project with the original ignition system, so as not to change the test setup and compromise the credibility of results.

3.2.5 Oil filtration system

It was noted during disassembly and inspection of the CFR engine that the oil system was contaminated with dust and dirt. This can potentially damage critical components such as bearings, camshafts and gears. The original setup of the CFR engine did not have an oil filtration system. Modern CFR engines are designed with an external oil filter as standard.

The oil galleries of the CFR engine were flushed with paraffin. A small fuel pump and oil filter was used to circulate paraffin through the oil galleries of the CFR engine. A small phosphor bronze plug, Figure 31, was designed to block one of

the oil galleries in the CFR crankcase, in order to re-route the flow of oil through an externally mounted oil filter.

Figure 31: Oil gallery plug

Figure 32 shows the externally mounted oil filtration system of the CFR engine. Note the oil gallery plug, rerouting oil flow through the filtration system.

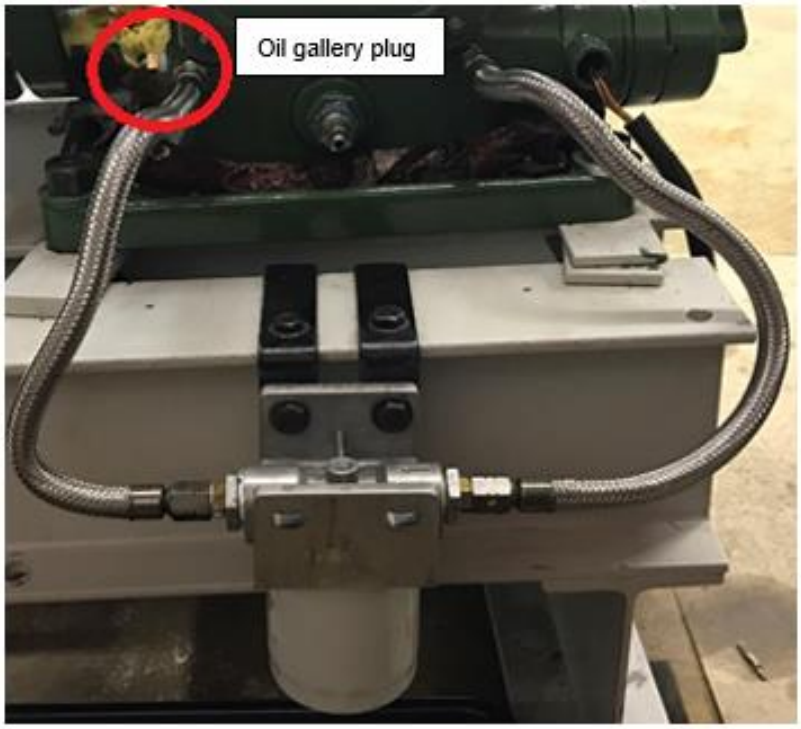

Figure 32: Oil filtration system

3.2.6 Inspection sleeve and spark plug

Upon disassembly, it was found that an inspection sleeve protruded into the combustion chamber, causing slight damage to the top land of the piston. Figure 33 shows that the protruding sleeve bent as it was contacted by the piston, minimising damage to the piston crown and top land.

Figure 33: Damaged piston and protruding inspection sleeve

The piston was de-carbonated using Scotch-bright, and thoroughly cleaned with compressed air and a paraffin cleaning gun. It can be seen from Figure 33 that the protruding sleeve did not seriously damage the piston, and all the compression rings were still in good condition. The piston and ring set could therefore be re-used.

Two inspection sleeves were manufactured to fit inside the cylinder head. One is used for fitting a pressure transducer, and a dummy is made for the damaged sleeve shown in Figure 33. The dummy sleeve is shown in Figure 34.

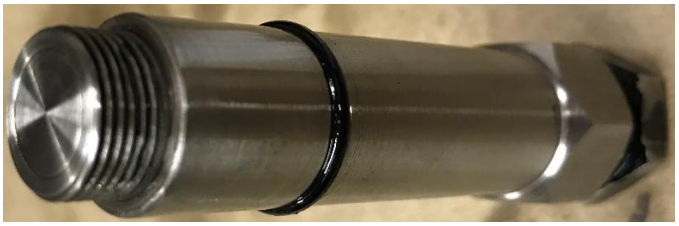

Figure 34: Re-machined dummy sleeve

It was noted upon inspection of the combustion chamber with a bore scope, that the spark plug left an undesirable additional clearance volume in the combustion chamber, see Figure 35. It was found that the original specification spark plug (Champion D16) was replaced by a smaller, more modern unit and a brass insert. The brass insert was removed and replaced with the original specification spark plug. No leaks past the thread were observed once the change was made. Figure 36 shows the combustion chamber with the new inspection sleeve, and replaced spark plug, as specified by ASTM (ASTM D2700, 2016).

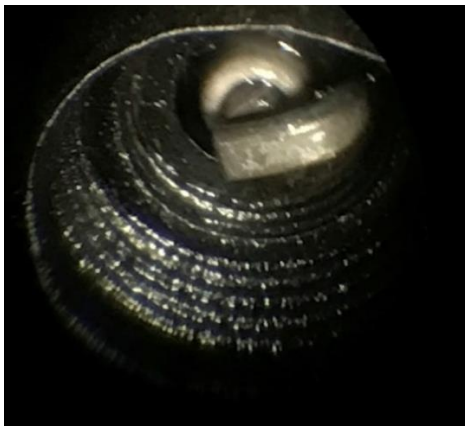

Figure 35: Smaller spark plug and insert

Figure 36: Original specification spark plug and inspection sleeve dummy

Removing the excess air pockets inside the combustion chamber, shown in Figures 35 and 36, allows for higher achievable compression ratios, and improves combustion quality by eliminating cold spots, and low-pressure areas. It was suspected that the unusual shape of the combustion chamber (resulting from

the damaged inspection sleeve and spark plug gap) might have been responsible for the instability in lambda readings, noted during preliminary testing.

A compression test was conducted on the CFR engine before and after disassembly and modification. Figure 37 shows that the upgrade and modification process improved the compression of the CFR engine. The compression tester was calibrated using a Fluke P5514-70M Hydraulic compression test pump (serial number: 71343). Calibration data is included in this report in Appendix C.

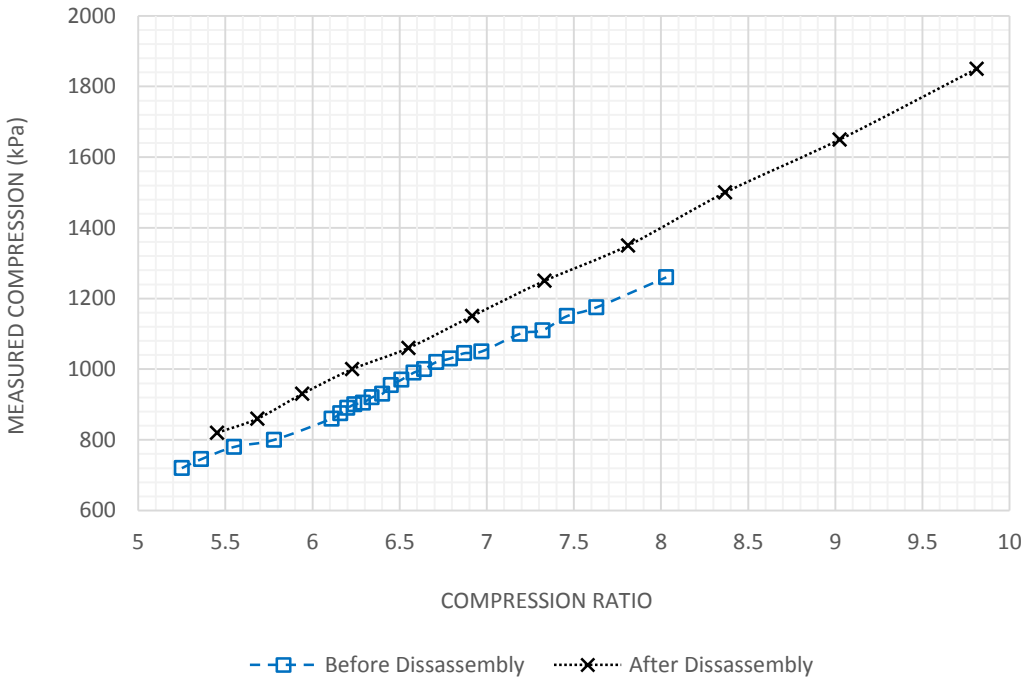

Figure 37: Improved Compression after upgrades and modification

The improved compression shown in Figure 37 is a result of minimizing any leaks in the cylinder, and the smaller diameter spark plug and insert.

3.2.7 Heating elements

The ASTM 2700 standard test procedure for MON specifies that the A/F mixture temperature must be 149 $\pm$ 1 °C. Alcohols, such as ethanol, have a high latent heat of vaporisation, 846 kJ/kg, compared to other chemicals used in octane testing such as n-heptane (318 kJ/kg) and toluene (351 kJ/kg) (Green, 2008).

Oxygenated fuel samples with a high volume percentage alcohol will therefore reduce the mixture temperature upon vaporisation.

The standard CFR engine test setup utilises two internal heating elements, controlled by PID controllers and thermocouples, to control inlet and mixture temperature. The first internal heater is mounted inside the air intake of the engine, Figure 38. A thermocouple downstream of the heater, and a PID controller, regulates the inlet air temperature to a constant 52 ± 1 °C.

A second internal heater, shown in Figure 39, was fitted in the inlet manifold, commonly referred to as the “MON pipe”. This element was placed downstream of the carburettor, and therefore controls the A/F mixture temperature. In order to achieve a mixture temperature of 149 ± 1°C while testing oxygenated fuel samples, a third external band heater was fitted around the inlet manifold. The band heater works in conjunction with the internal heater in the MON pipe to control mixture temperature.

Figure 38: Inlet air heater

Figure 39: MON intake manifold with external band heater and internal heater

3.2.8 Fuel metering system

The molecular structure of ethanol contains a hydroxyl group (-OH). This affects the required A/F ratio for stoichiometric combustion, as shown in the calculation below. The balanced chemical equation for the stoichiometric combustion process of ethanol is shown in equation 27.

$$C_2H_6O + 3(O_2 + 3.76 \cdot N_2) = 2 \cdot CO_2 + 3 \cdot H_2O + 11.28 \cdot N_2 \quad (27)$$

The respective mass of air and fuel (ethanol) required for the stoichiometric combustion process shown in 27, is calculated in equations 28 and 29.

$$m_{air} = (3 \times 4.76\ kmol) \cdot \left(29 \frac{kg}{kmol}\right) = 414.12\ kg \quad (28)$$

$$m_{fuel} = (1\ kmol) \cdot \left(46 \frac{kg}{kmol}\right) = 46\ kg \quad (29)$$

The A/F ratio, required for stoichiometric combustion is calculated in equation 30.

$$AF = \frac{m_{air}}{m_{fuel}} = 9 \quad (30)$$

It is shown that the A/F ratio required for stoichiometric combustion, when running the CFR engine on ethanol, is significantly lower than that of conventional petrol (A/F = 14.7). This requires a much larger fuel flow rate through the carburettor. A new jet, with a larger diameter bore, was designed and manufactured from phosphor bronze. A micrometre was modified to act as an adjustable needle valve for the newly designed carburettor jet. The spindle of the micrometre was machined to form a sharp needle, as per DIN 51 756 Standard, to fit inside the bore of the jet, see Figure 40.

Figure 40: Variable fuel metering device

Figure 41 shows the micrometre needle valve as fitted in the carburettor of the CFR engine.

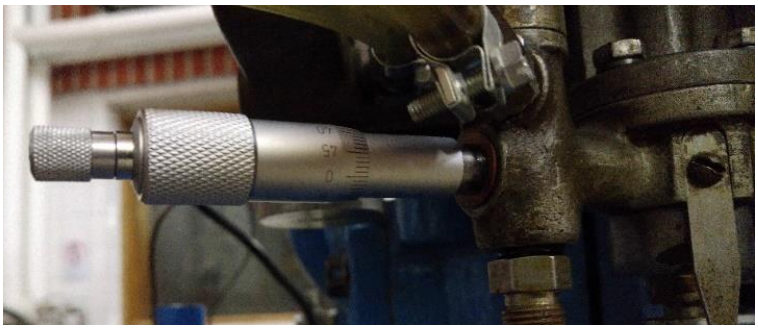

Figure 41: Carburettor with adjustable needle

A lamda sensor, and ETAS lamda scanner, was used to measure the A/F ratio of the engine. This allows the user to adjust the A/F ratio to achieve maximum knock intensity during octane tests, see Figure 42.

Figure 42: Lamda sensor and lamda scanner

3.2.9 Final assembly

Figure 43 shows the final assembly of the CFR engine setup, modified for research on high octane and oxygenated fuels. All instrumentation, used for octane research, can be seen behind the CFR engine test bench. The PC and digital scale, used for fuel blending, can be seen to the right of the instrumentation bench. A schematic layout of the CFR engine is shown in Figure92 in Appendix J.

Figure 43: Final setup, Instrumentation and PC

Figure 44 shows the final CFR engine setup from a different angle. The chest freezer, used to chill fuel samples, and the fuel reservoir cooling system, can be seen to the left of the instrumentation bench. The redesigned exhaust system and external oil filtration system can be seen in Figures 43 and 44. A condensate

well was installed in the overhead exhaust system. A valve and hose was used to drain condensate regularly after testing.

Figure 44: Final setup, instrumentation and cooling system

Calibration of the modified test setup, and high octane and oxygenated fuels testing and results are discussed in section 4 of this report.

4. TESTING AND RESULTS

Modifications, as described in section 3, to the CFR engine at Stellenbosch University enables researchers to investigate high octane and oxygenated fuels. A CCR method, described in section 2.5.4, was used to measure the O.N. of fuel samples to an accuracy of ± 0.5 O.N. The bracketing (equilibrium fuel level) method, described in section 2.5.4, was used to refine the accuracy of O.N. measurements for the Sasol round robin sample test (section 4.7). An adjustable fuel metering system, discussed in section 3.2.8, was used to control the A/F ratio of the CFR engine during all tests. ASTM standard octane test procedures were adapted to incorporate the micrometre needle jet. Fuel samples were blended using digital balance scale and software, and left overnight in a chest freezer. The fuel blending procedure is described in Appendix A of this report. The fuel reservoir cooling system, described in section 3.2.3, was used during all tests. Safety precautions for the test setup are included in Appendix I. Engine speed and temperature measurements were constantly monitored during testing, to ensure the test environment adhered to the ASTM specifications, and safety requirements.

The KI / CR, and dial gauge / CR relationships of the engine were re-calibrated after upgrades and modifications. A toluene standardization fuels test was performed as a “fit for use” test, proceeding calibration of the engine and measuring equipment. Sections 4.1 and 4.2 show the calibration test results that prove that the CFR engine produces accurate results.

The sensitivity of the CFR engine to produce accurate octane results when operating with the fuel reservoir chilling system was investigated using regular ULP pump fuel. Pump fuel was also used for baseline tests on the sensitivity of the engine to changes in inlet air temperature and ignition timing. Section 4.3 shows pump fuel test results.

The unique capabilities of the octane laboratory at Stellenbosch University, after modifications to the CFR engine, allowed for octane tests of previously uncharacterised Sasol fuel streams. Section 4.4 shows the test results for C_5 raffinate.

One of the original project objectives was to modify the CFR setup to enable octane tests of oxygenates. Section 4.5 shows a comparison of octane test result of oxygenates, compared to data from literature. This section proves the capability of the CFR setup for accurate octane research on oxygenates. Blending number determinations and the octane properties of refinery grade Sasol fuel alcohol were also investigated in this section.

The octane properties of TAME are investigated in section 4.6 by means of direct measurement, and two different approaches to blending number determinations.

Section 4.7 shows the results of a round robin octane test involving professional octane laboratories.

4.1 VERIFICATION OF COMPRESSION RATIO CURVE

A dial gauge was used to monitor the adjustable CR of the CFR engine. The dial gauge was mounted between the cylinder head and crankcase. Adjustment of the cylinder height was shown as a distance reading on the dial gauge, and could be related to a reference value for CR. A liquid fill method, as described in the ASTM manual for rating motor, diesel and aviation fuels, was used to establish a reference value for cylinder height and CR (ASTM, 1971).

The knock pickup sensor, mounted in the roof of the combustion chamber, was removed. A calibrated burette was used to fill the combustion chamber with 140 mL distilled water. With the piston at TDC, the CR of the CFR engine was increased, such that the meniscus of the water reached the flat top of the cylinder head. This process was repeated three times, and the dial gauge reading at this cylinder height was monitored. According to the ASTM manual for rating motor, diesel and aviation fuels, the dial gauge reading measured in this position, correlates to a CR of 5.496 (ASTM, 1971).

This measured relationship between cylinder height and CR was used as a reference point. The change in combustion volume correlating to a change in cylinder height was calculated using measurements for the bore and stroke of the CFR engine in Table 1. Figure 45 shows the calculated relationship between

cylinder height, measured with the dial gauge, and combustion volume, filled with distilled water. The liquid fill method was used to verify the measured relationship at various points.

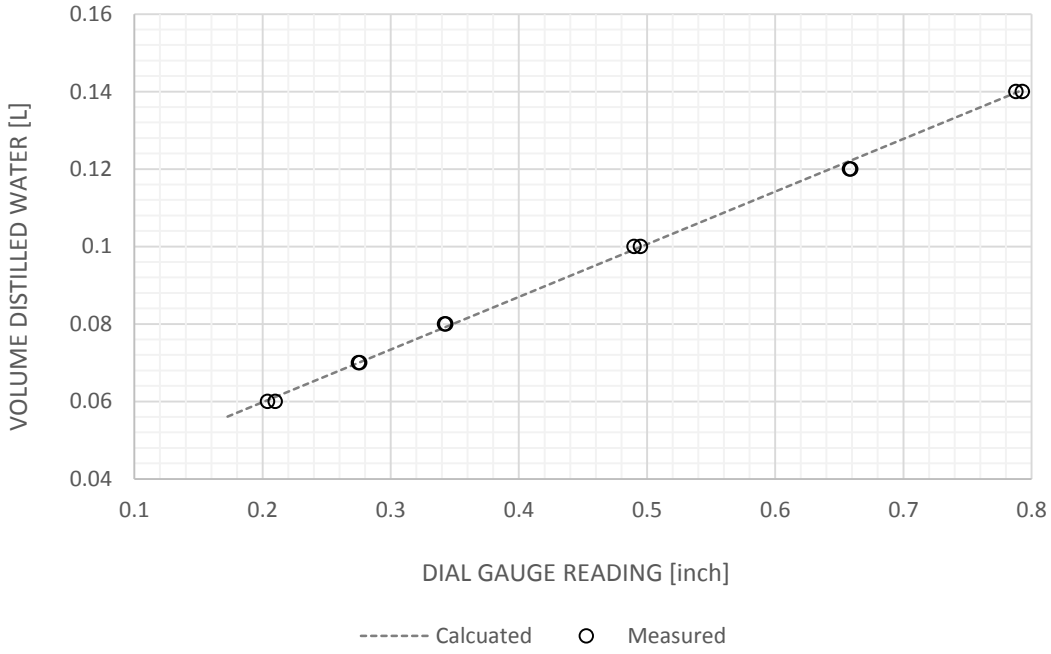

Figure 45: Liquid fill method results

CR was calculated from combustion volume using the swept volume of the CFR engine (bore and stroke measurements). Figure 46 shows the relationship between CR and dial gauge reading.

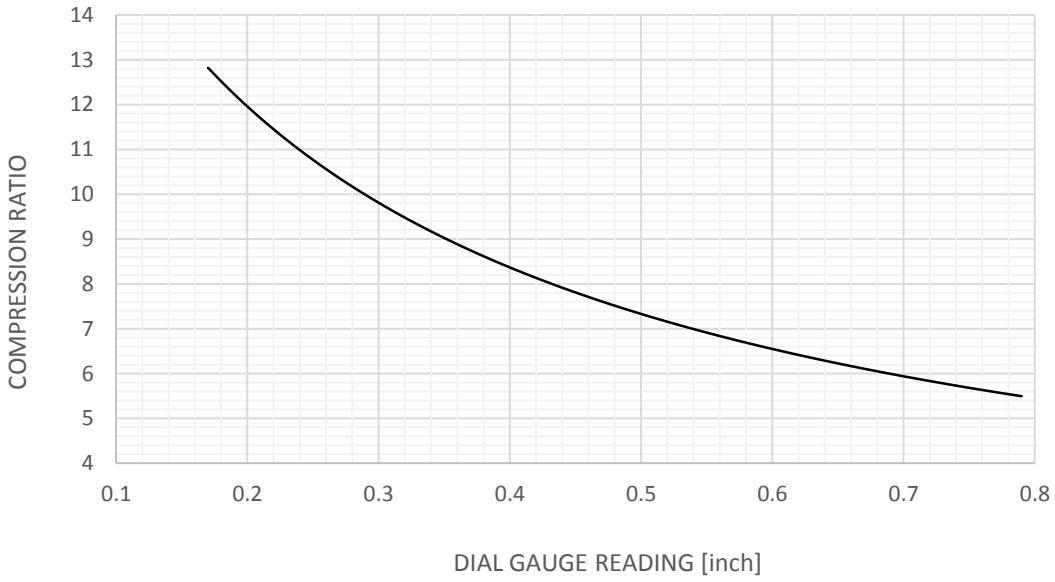

Figure 46: CR / Dial gauge relationship

The curve in Figure 46 was used during octane measurement to determine the CCR at which a fuel sample reaches a certain knock intensity. KI was measured using a detonation meter and displayed on an analogue KI gauge. The KI/CCR relationship was calibrated using iso-octane. Under RON standard ASTM operating conditions, the gauge was adjusted to reach mid-scale knock intensity, 50 ± 2 divisions, at a dial gauge reading of 0.454 inch, correlating to a CCR of 7.770 (ASTM D2699, 2016). This calibration was verified regularly during the testing phase of this project, and calibration data and test dates are included in this report in Appendix C. The characteristic curve of the CFR engine was used to relate CCR to the octane number of a sample fuel (CCR method, section 2.5.4.). This curve was calibrated following upgrades and modifications to the engine setup. Figure 47 shows the characteristic curve calibration. PRF blends (iso-octane and n-heptane), ranging in O.N. from 50 to 100, were tested under RON standard operating conditions.

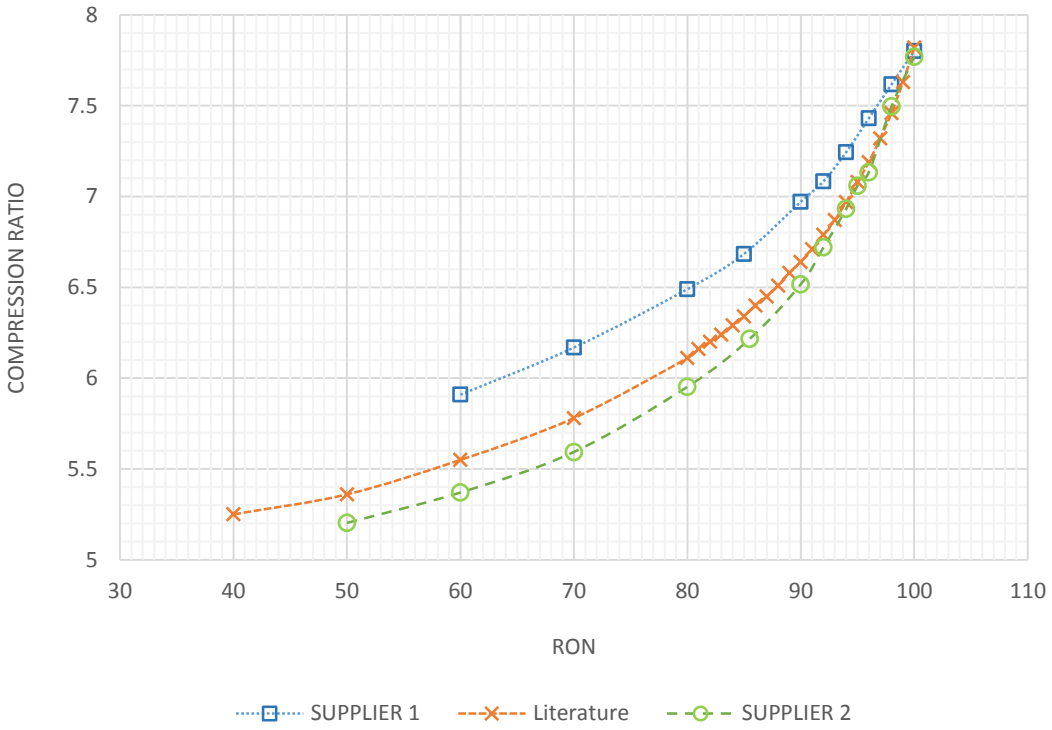

Figure 47: Re-calibrated CR curve

It was noted that the re-calibrated characteristic curve (Supplier 1) was not consistent with the curve used by Swarts (Swarts, 2006), before upgrades and modification of the engine. The curve used by Swarts (Swarts, 2006) is referred to as “Literature” in Figure 47. It was suspected that the primary reference fuels used for this calibration were contaminated. PRF’s from a different supplier were purchased, and the calibration test was repeated (Supplier 2). Figure 47 shows that the characteristic curve produced by PRF’s from Supplier 2 followed the original curve from literature more closely. It can be seen that the curve is lower, verifying the improved compression of the engine after upgrades and modification, shown in Figure 37. With increased compression, it is expected that a fuel sample with a certain O.N. will reach mid-scale KI at a lower CR. A sample of n-heptane from supplier 1 was analysed at the department of Process Engineering at Stellenbosch University. The sample was found to be 33 % pure, in contrast to the supplier specified purity of 99.7 %. A chemical analysis report is included in Appendix H. The characteristic curve produced by PRF’s from

Supplier 1 was therefore discarded, and the characteristic curve produced with PRF's from Supplier 2 was used for octane measurement in this project.

The effect of different chemicals, and their respective combustion properties, on measured KI and octane results was investigated. Figures 48 and 49 show the measured CCR related to defined O.N. for a variety of fuel samples used in this project. The RON and MON values in Figures 48 and 49 respectively are by PRF blending definition, TSF blending definition or carefully scrutinised literature values from ASTM appendices (ASTM D2699, 2016; ASTM D2700, 2016).

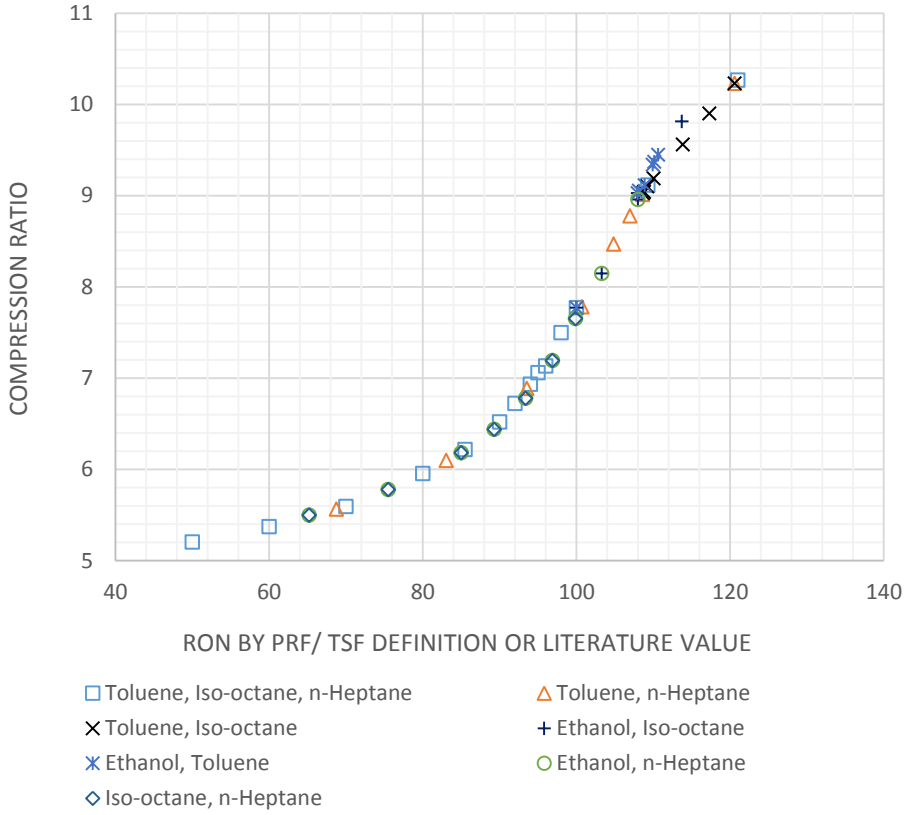

Figure 48: RON - PRF and TSF characteristic curve

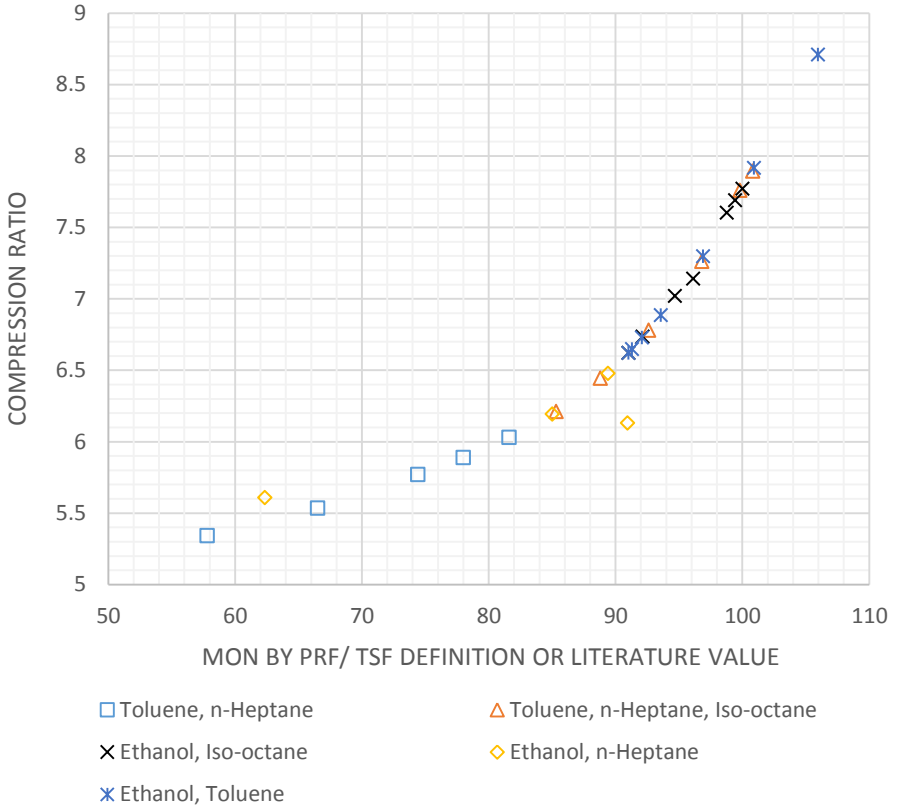

Figure 49: MON - PRF and TSF characteristic curve

One data point in Figure 49, at approximately 91 MON, is considered an erroneous outlier. It is shown in Figures 48 and 49 that data points overlap, and the characteristic curve, calibrated with PRF's in Figure 47, is followed regardless of chemical composition.

4.2 TOLUENE STANDARDIZATION FUEL TEST

The toluene standardization fuel test is a "fit for use test", prescribed by the ASTM manual for rating motor, diesel and aviation fuels, to verify the CFR engine and measuring equipment condition and calibration. Fuel samples used for the test are a series of toluene, n-heptane and iso-octane mixtures, blended on a volumetric ratio basis. According to ASTM (1971), these calibrated blends are highly sensitive to component purity and blending accuracy, and octane results are greatly affected by any variations or irregularities in engine, measuring equipment or the condition of the combustion chamber (ASTM, 1971).

Blending data on the TSF blends are listed in Appendix F, Tables 23 and 24 for RON and MON respectively. According to ASTM (1971), TSF samples and their octane properties have been calibrated by the National Exchange Group laboratories in the 1950's. A tolerance band is specified for each TSF blend. A CFR engine setup must produce octane results within the tolerance band, for each TSF blend, to be declared "fit for use".

4.2.1 Research Method

Figure 50 shows TSF octane results, and the tolerance band as specified by ASTM (1971), for the Research method.

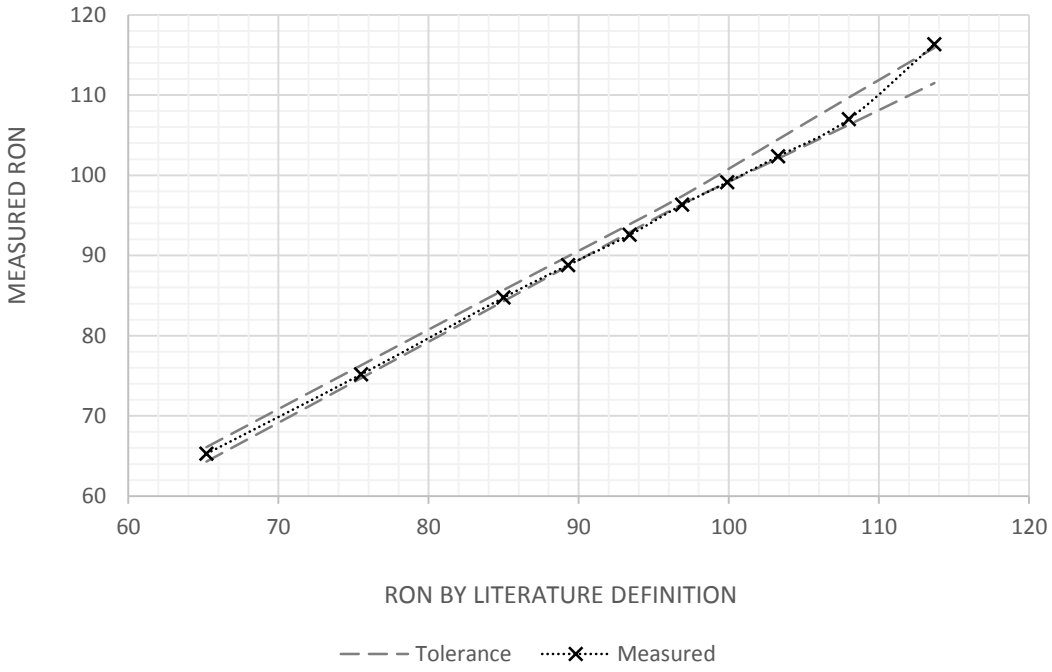

Figure 50: Toluene test RON results

It is shown in Figure 50 that TSF RON measurements are on the lower limit of the tolerance band specified by ASTM (1971) as “fit for use”. Adjustment of the inlet air temperature (I.A.T) is permitted to bring TSF results within the tolerance band. The effect of I.A.T on RON results was investigated, and is discussed in section 4.3. It was decided that the result shown in Figure 50 was satisfactory for the purposes of this project, and that the I.A.T would not be adjusted.

A large measurement error was recorded for the 113.7 RON TSF blend. It was noted during testing that KI and A/F ratio became more unstable as the CR of the CFR engine increased. With a CR of 9.811, required to induce mid-range KI for this high octane TSF blend, unstable KI readings were recorded. Implementing a digital reading for KI, or using a pressure transducer and band filter to identify knock, and quantify KI, will improve the accuracy of octane results at high compression ratios.

It was concluded that the results presented in Figure 50 indicate that the CFR engine and measuring equipment are in an acceptable condition. Figure 50

shows that RON measurements, with the CCR procedure, were approximately 0.5 O.N. low. It is advised that the equilibrium fuel level bracketing method, described in section 2.5.4, be used in conjunction with the CCR method if refined accuracy is required.

4.2.2 Motor Method

During MON tests, ignition timing is automatically and continuously adjusted in relation to CR (see Table 3, section 2.5.2). Ignition timing, on the older model CFR engine at Stellenbosch University, was adjusted manually. The process of manually adjusting ignition timing in relation to CR, while simultaneously adjusting compression ratio in relation to KI proved to be a challenge in obtaining maximum KI.

Figure 51 shows the relationship between ignition timing and MON, calculated from Tables 3 and A4.3 in the ASTM 2700 document. Table 3 in the ASTM method provides the relationship between ignition timing and cylinder height, used to calibrate the automated adjustment mechanism on modern CFR engines. Table A4.3 shows the relationship between cylinder height and MON (ASTM D2700, 2016: 9; 34).

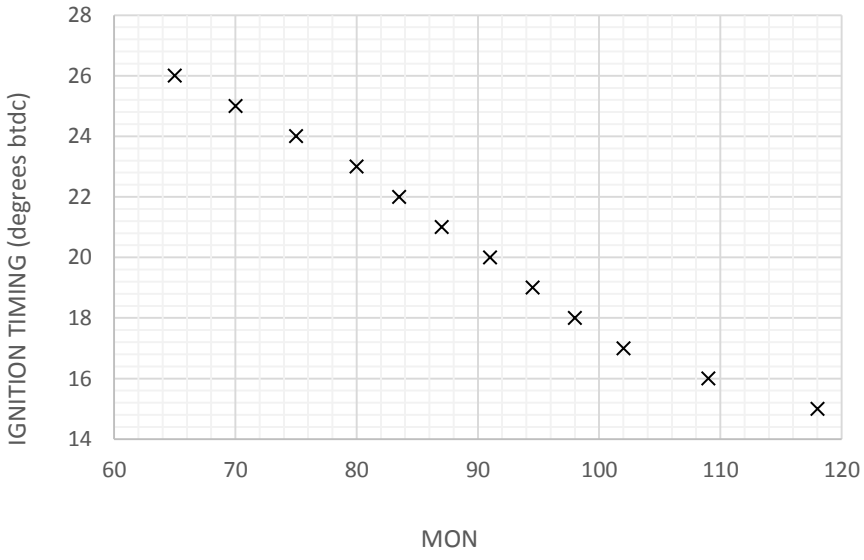

Figure 51: Ignition timing adjustment for motor method

TSF blending octane numbers, shown in Table 24 in Appendix F, were known from literature. Ignition timing was set prior to testing, according to the theoretical blending O.N., and using the relationship shown in Figure 51. This methodology was followed for all MON tests with a known blending O.N. from literature. Without automated CR / ignition timing adjustment, the adjustment of CR and ignition timing became an iterative process that used up unnecessary testing time and fuel volumes. Recommendations for future work on improving this issue are discussed in section 5.2.

According to the ASTM 2700 document, mixture temperature must be controlled to 149 ± 1°C. ASTM (1971) states that the mixture temperature can be adjusted within a range of 285°F to 325°F (141 °C to 163 °C). It was found during the TSF test, using the CCR method, that the CFR engine produced the most accurate MON results when operating with a mixture temperature of 155°C, which is within the allowable range. Figure 52 shows the TSF test results for MON, and the specified tolerance band.

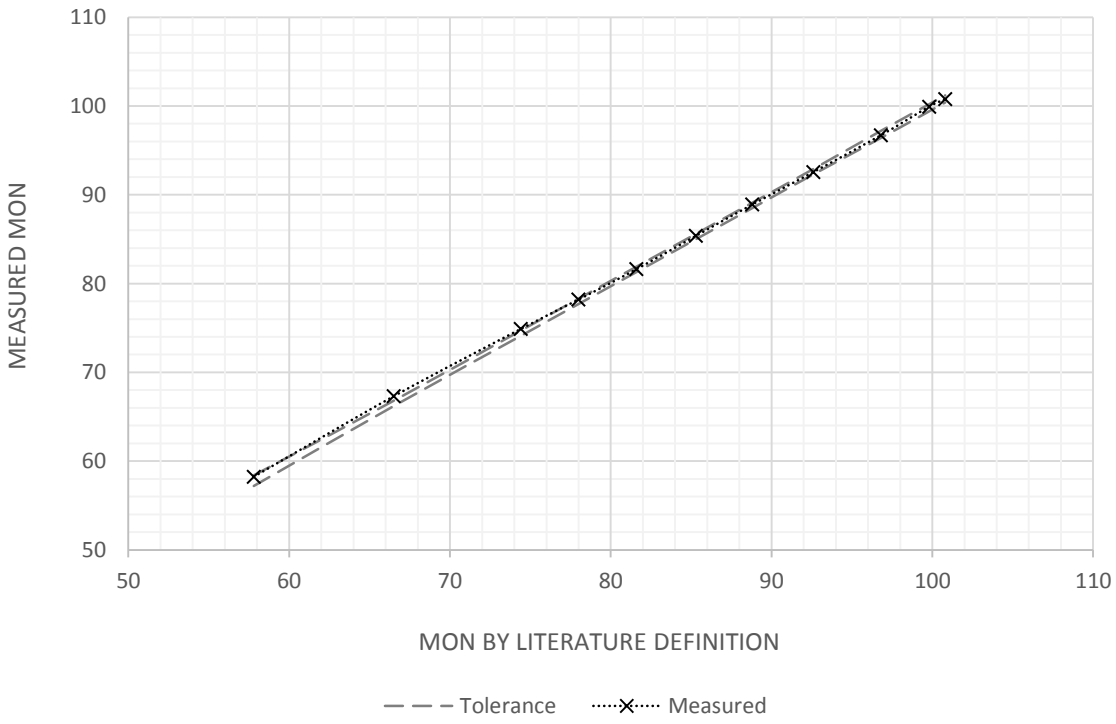

Figure 52: Toluene test MON results

It was concluded from the result in Figure 52 that acceptable octane measurement results were obtained from the modified CFR engine, when using the critical compression ratio method, but that the equilibrium fuel level bracketing method, described in section 2.5.4 must be used in conjunction with the CCR method if refined accuracy is required.

4.3 PUMP FUEL TESTS

In order to avoid evaporation of volatile blending components during octane testing, fuel samples were placed in a household chest freezer, promptly after blending, and left overnight to chill to a low temperature (± -20°C). Evaporation of volatile components will alter blending ratios and influence octane results. The chest freezer was also used to chill a coolant mixture, which was circulated around the fuel float chamber during testing (see section 3.2.3).

The effect of chilling fuel samples on octane results was investigated using 95 RON unleaded petrol (ULP). One sample was left in the chest freezer overnight, while another was tested at room temperature. Table 4 shows the sensitivity of octane measurements (RON) to fuel temperature.

Table 4: Sensitivity of RON measurement to fuel temperature

	Room temperature			Chilled		
	Test 1	**Test 2**	**Test 3**	**Test 1**	**Test 2**	**Test 3**
Fuel temperature (°C)	14.80	15.10	15.00	-21.80	-20.30	-19.20
Mixture temp (°C)	34.30	34.10	34.40	33.70	34.30	35.10
Dial gauge reading	0.532	0.535	0.534	0.533	0.534	0.531
Measured RON	95.00	94.81	94.87	94.93	94.87	95.06
Average RON	94.89			94.95		
Delta	0.06					

Table 4 shows similar mixture temperatures for chilled and room temperature test samples. During RON tests, inlet air temperature (I.A.T) was controlled to 52 ± 1 °C. Maximum KI (calibrated to 50 ± 2 divisions on the knock meter) was recorded at an A/F ratio of approximately 0.94 Lambda. This relates to 13.818 units air to one unit of fuel. The thermal energy required to heat 1 gram of liquid fuel by 35

°C (the temperature difference between chilled and room temperature samples) is shown in equation 31. With Q, thermal energy; m, mass; c, specific heat of gasoline according to Green (2008), and ΔT the change in temperature.

$$Q = m \cdot c_p \cdot \Delta T = (0.001\ kg) \cdot (2.11\ k\mathrm{J/kgK}) \cdot (35\ K) = 0.074\ kJ \qquad (31)$$

The thermal energy required to evaporate 1 gram of liquid fuel is shown in equation 32. With H_v, the latent heat of vaporization of gasoline according to Green (2008).

$$Q = m \cdot h_v = (0.001\ kg) \cdot (348.9\ kJ/kg) = 0.348\ kJ \qquad (32)$$

It is shown in equations 31 and 32 that the latent heat of vaporization dominates. The high A/F ratio and high inlet air temperature result in the fuel temperature not having a significant influence on mixture temperature. It is therefore shown in Table 4 that chilling fuel samples in the chest freezer does not have a significant influence on RON results. During MON testing, the mixture temperature of the CFR engine is controlled, and the fuel temperature will therefore not affect the combustion process.

The I.A.T of the CFR engine can be adjusted during the Research method, such that octane measurements meet specified tolerances prescribed for TSF blends, section 4.2. The standard I.A.T setting for RON is 52 ± 1°C. According to ASTM (1971), the I.A.T can be adjusted in a range of 30 °C to 74 °C. It is stated that octane results can be adjusted at typically 0.1 RON / 1 °F. The effect of inlet air temperature on octane measurement was investigated using 95 ULP at room temperature. Figure 53 shows the measured RON vs. I.A.T.

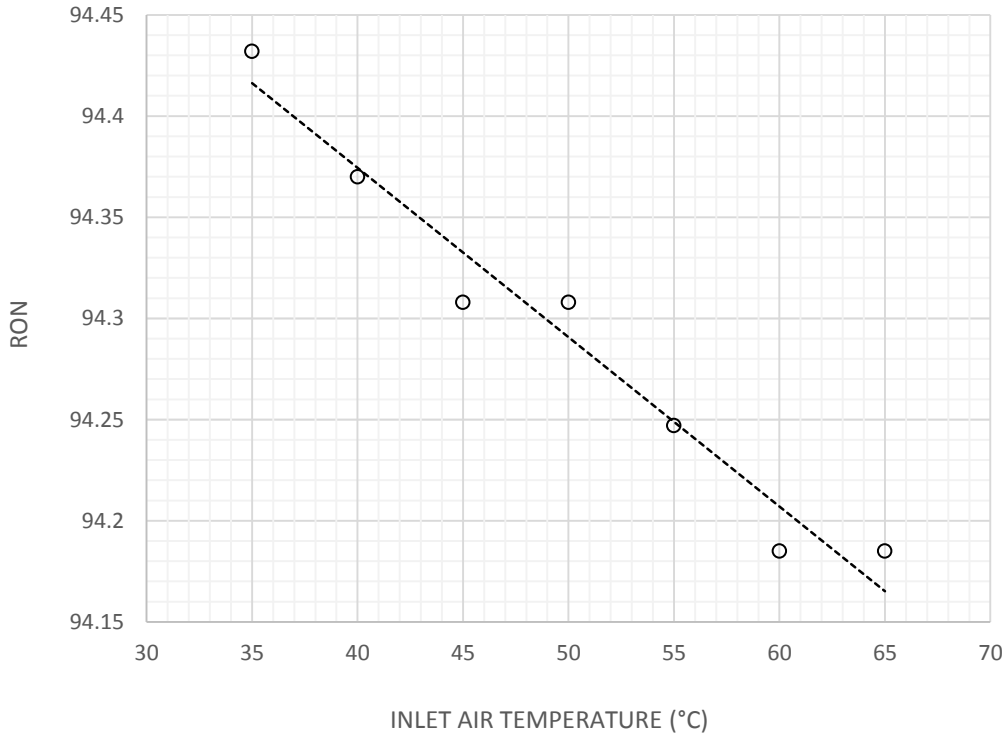

Figure 53: Sensitivity to inlet air temperature

Note the scale on the Y-axis of the graph in Figure 53. It is shown that by adjusting the air intake temperature within the specified range, RON measurements can be adjusted by approximately 0.2 O.N.

The sensitivity of MON results on ignition timing was investigated using 95 ULP. The CR of the CFR engine was set to 7.0591, and a dial gauge reading of 0.532, to induce mid scale KI. Ignition timing was adjusted using a timing light, and a degree board on the outlet shaft of the CFR engine. Table 5 shows the KI, measured on the knock meter for a range of ignition timing settings.

Table 5: Sensitivity to ignition timing (MON)

95 ULP	
Ignition timing (Degrees crank angle before TDC)	**Measured KI**
19	0
20	5
21	32
22	46
23	93
24	100

It is shown that KI, and MON results are very sensitive to ignition timing. It is therefore recommended that the ECU ignition system be used for future octane research projects to ensure accurate settings.

4.4 SPECIAL COMPONENT STREAMS

According to J. Lee *et. al.* (2013), light olefins, such as ethylene and propylene, are important materials of the petrochemical industry. The catalytic cracking of various feed stocks, including naphtha, heavy oil, and C_4/C_5 hydrocarbons, has been shown to produce light olefins. Among them, C_5 raffinate has attracted much attention as a promising source, since C_5 raffinate is sufficiently produced as a by-product in the naphtha cracking centre and fuel catalytic cracking (FCC) refinery stream.

C_5 raffinate is a highly volatile liquid at room temperature, with a boiling point of -5 to 5°C (PCS, 2014). Typically, such volatile fuels cannot be tested in a CFR engine, since the sample would boil out of the fuel float chamber, thereby invalidating the test result. It was decided to test the fuel sample chilling system, and fuel reservoir refrigeration system of the modified CFR test setup, discussed in section 3.2.3, by measuring the octane properties of neat C_5 raffinate.

A sample of C_5 raffinate was chilled overnight in the chest freezer, and tested according to the ASTM RON and MON specifications. Table 6 shows the octane properties of C_5 raffinate.

Table 6: C_5 raffinate octane properties

	Dial	CCR	Measured ON	A/F (ʎ)	Temperature (°C)
RON	0.603	6.530	90.133	0.95	-21.2
MON	0.681	6.046	81.966	0.94	-20.9
AKI	86.049				

The results shown in Table 6 correlate well with data published in the petroleum processing handbook (Mcketta, 1992) of RON = 90 and MON = 80. Literature data values for C_5 raffinate's RON and MON will vary due to refinery configuration. This result proves that highly volatile samples can be tested with minimized evaporation. Blending ratios will not be affected by evaporation of volatile components.

4.5 OXYGENATED SAMPLES

4.5.1 Fit for use test

The modifications to the CFR engine setup described in section 3.2.7 and 3.2.8, enables octane research on oxygenated fuels (Vol % > 25). Results from literature were replicated to serve as a “fit for use” test of the CFR engine setup for oxygenates. Foong *et al.* (2013) studied the octane numbers of ethanol, blended with gasoline and its surrogates. The graph in Figure 54 shows the measured RON’s of ethanol blends with toluene, iso-octane and n-heptane, compared to the results published by Foong *et al.*

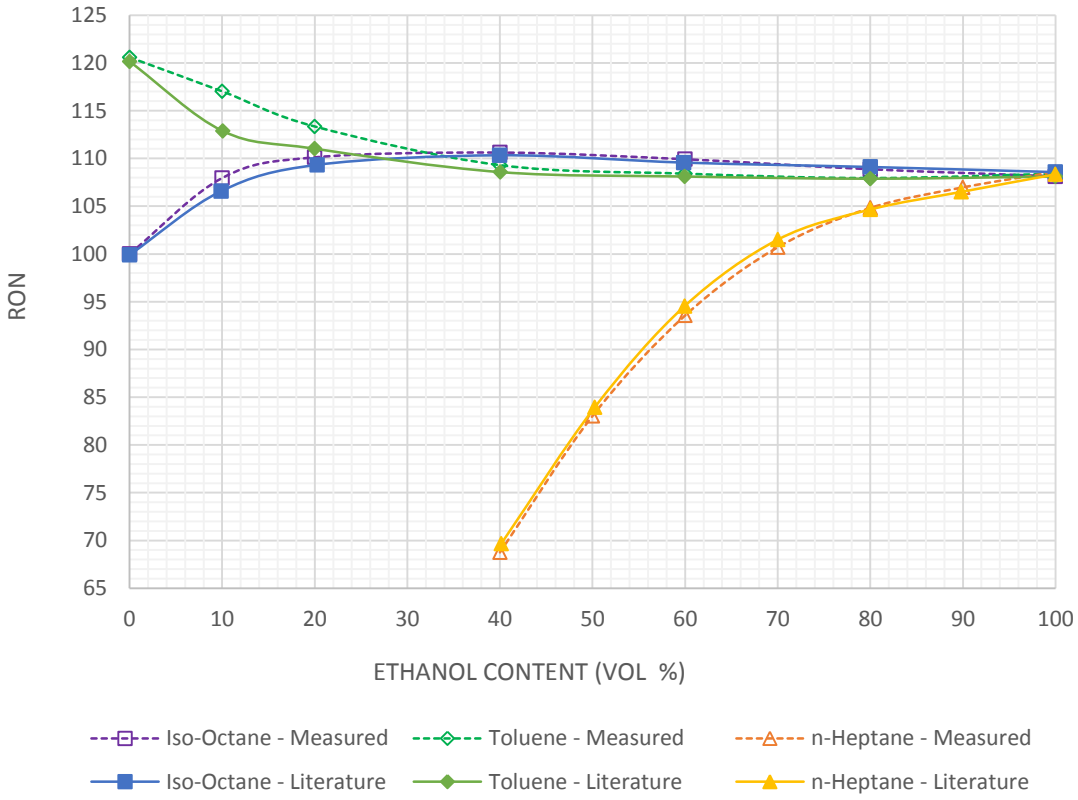

Figure 54: Ethanol RON results compared to literature (Foong *et al.* 2013)

Figure 54 shows a very good correlation between measured results and data from literature. As discovered previously in the TSF test in section 4.2, it was noted that KI measurements became unstable at very high CR's. Difficulty was experienced in measuring octane numbers higher than 110 RON, due to unstable KI readings. This can be seen in the large delta between E10 and E20 toluene blends, compared to literature values. The overall result shown in Figure 54 inspires confidence in the suitability of the CFR setup for oxygenated fuels research for RON ≤ 110.

The graph in Figure 55 shows the measured MON results of ethanol blends with toluene, iso-octane and n-heptane, compared to the results published by Foong *et al.* Ignition timing was set prior to testing, using the literature defined blending O.N., and the ignition timing/ MON relationship shown in Figure 51 in section 4.2.2.

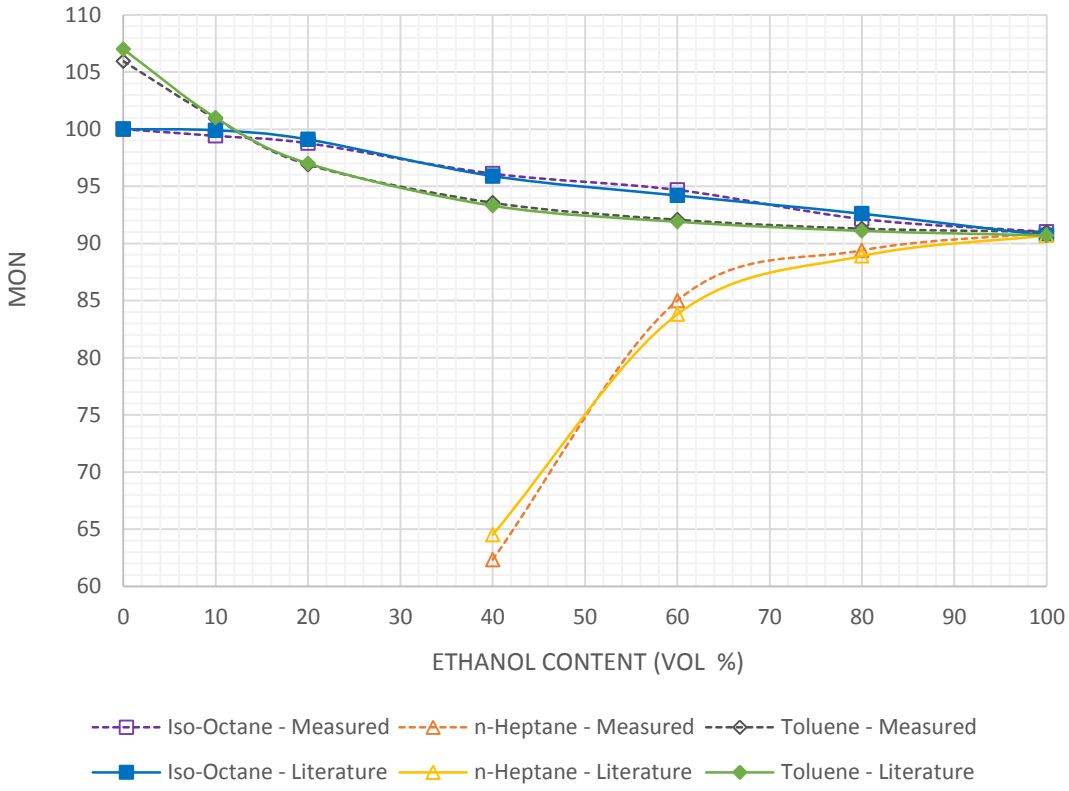

Figure 55: Ethanol MON results compared to literature (Foong *et al*. 2013)

Figure 55 shows a very good correlation between measured results, and data from literature. It was concluded from the results shown in Figures 54 and 55 that the modified CFR setup was suitable for producing accurate RON and MON results for oxygenated fuels, using ethanol.

4.5.2 Blending octane number (BON)

Octane research on ethanol, using a standard CFR engine, is difficult because of the high octane, and oxygen content of fuel alcohols. Little data is therefore available in literature. Because of the challenges involved with octane testing at high CRs, a method of diluting a high octane/oxygenated base fuel with a suitable blending component, in order to lower the octane number of the blend, and extrapolating the results is commonly used in industry. According to V. H. Rapp *et al*. (2014), the blending octane number (BON) represents the potential

octane number of a base fuel in its pure form. The blending octane number of a base fuel can be calculated as:

$$\mathrm{BON} = ON_{Ref} + \frac{1}{f}(ON_{bl} - ON_{Ref}) \quad (33)$$

Where ON_{Ref} is the octane number of the base fuel, ON_{bl} is the measured octane number of the base fuel / blending component mixture, and f is the fraction of the blending component used to lower the mixture octane number. This method calculates a theoretical O.N. of the base fuel, based on a single octane measurement of the blend, and the volume fraction of the blending component.

In addition to the single-point extrapolation method shown in equation 33, a multi-point extrapolation method was investigated. If the measured O.N. of the base fuel/ blending component mixture produces linear results with respect to volume fraction, a linear trend line can be fitted through the data points, and extrapolated to show the theoretical BON of the base fuel in its pure form.

1. RON

The suitability of the blending component, used to calculate BON's, was investigated by comparing BRON results of 99.9 % pure ethanol blended with n-heptane (Table 7), and 99.9 % pure ethanol blended with 1-pentanol (Table 8). 1-Pentanol was selected as a prospective blending component for ethanol, based on literature defined octane properties, and its relatively low boiling point. It was expected from the data published by Wallner *et. al.* (2012), RON = 86; MON = 76, and the similarities in molecular structure between 1-pentanol and ethanol, that the addition of 1-pentanol would sufficiently decrease the O.N. of pure ethanol to be measured at a lower CR, and BON's would respond linearly to blending ratios (Wallner *et. al.*, 2012).

Table 7: 99.9 % pure ethanol / n-heptane BRON values

Ethanol (99.9 %)		
n-Heptane (Vol %)	**Measured RON**	**BRON (Ethanol)**
60	68.75	107.93
50	83.03	108.08
40	93.56	108.22
30	100.70	108.33
20	104.82	108.41
10	106.97	108.43
0	108.60	NA
Average BRON		**108.23**

Table 8: 99.9 % pure ethanol / 1-pentanol BRON values

Ethanol (99.9 %)		
1 - Pentanol (Vol %)	**Measured RON**	**BRON (Ethanol)**
60	98.69	108.43
50	100.46	108.43
40	102.24	108.44
30	103.41	108.42
20	104.80	108.41
10	106.11	108.35
0	108.60	NA
Average BRON		**108.41**

The calculated BRON values for pure ethanol in Tables 7 and 8 show excellent consistency with the RON value of 108.6 published by Yates et al. (2010). Table 7 shows that BRON results, calculated for ethanol, are most accurate with the least amount of n-heptane in the blend. The low O.N. of n-heptane, compared to ethanol, is effective in lowering the O.N. of the mixture, but compromises the accuracy of the extrapolation process. It is shown in Table 8 that the similarities in the molecular structures of ethanol as base fuel, and 1-pentanol as blending component, yielded more accurate and stable extrapolated results for the BRON of pure ethanol. According to Mirabella (2015) BON's typically depend on the base stock composition, due to the synergistic intermolecular interactions with hydrocarbons. It can therefore be recommended that BON results are relatively accurate, provided the correct blending component for the base fuel is used. No engine operating problems (e.g. rough running) were encountered while testing

1-pentanol samples. It is therefore concluded that 1-pentanol is a suitable and effective blending component for ethanol. A multi-point extrapolation method for calculating the O.N. of a base fuel, using measured blending octane numbers was investigated. The measured BON's for ethanol, using n-heptane and 1-pentanol as blending components, were plotted in relation to the blending ratio by volume. A linear trend line was fitted through suitable data points, and extrapolated to calculate the BRON of ethanol in pure form.

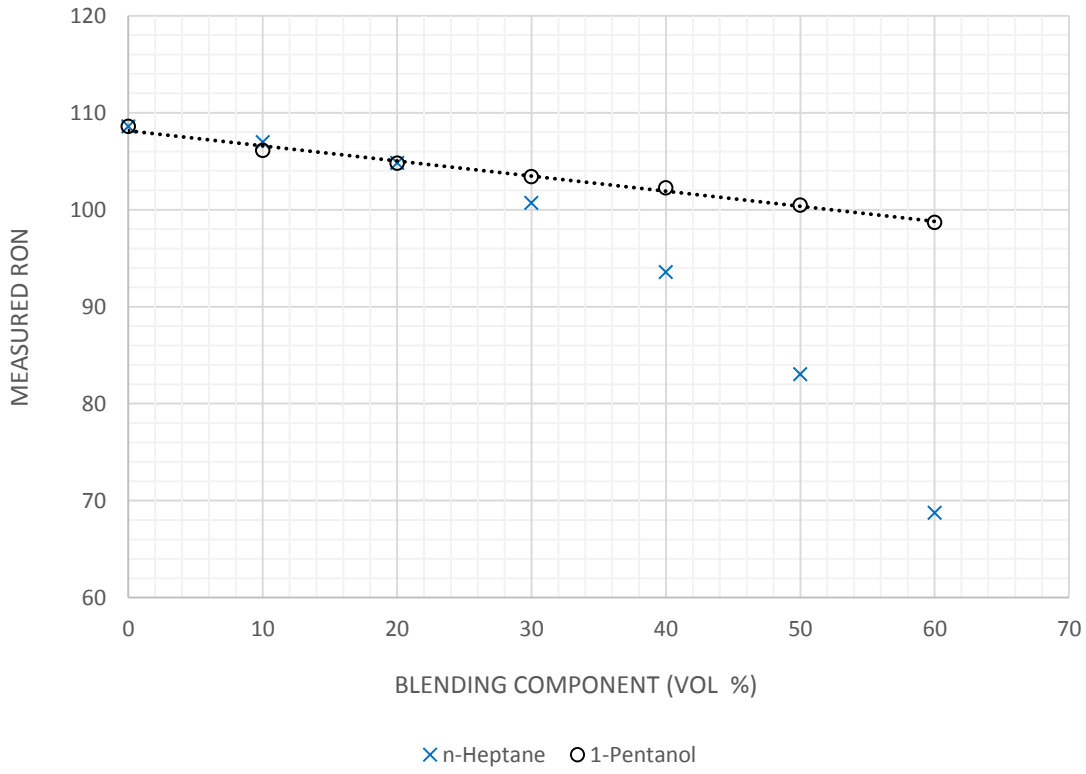

Figure 56: Comparison of n-heptane / 1-pentanol as ethanol BRON component

It is shown in Figure 56 that BRON results for ethanol, using n-heptane as blending component, are not linear in relation to blending ratio, and a linear trend line would not produce a credible extrapolation result. It can also be seen that ethanol and 1-pentanol blends produce linear BRON results in relation to blending ratio. A linear trend line was fitted through the data points, and the blending octane number of pure ethanol can be extrapolated to 108 RON, which

correlates very well with the single-point extrapolation method, and direct measurement of ethanol in Tables 7 and 8.

2. MON

Tables 9 and 10 show the BON results for ethanol, blended with n-heptane and 1-pentanol, for the Motor method. Ignition timing was initially set according to Figure 51, using the literature defined MON of pure ethanol, and subsequently adjusted for each blend as the measured O.N. decreased with an increase in the volume fraction of the blending component.

Table 9: 99.9 % pure ethanol / n-heptane BMON values

Ethanol (99.9 %)		
n - Heptane (Vol %)	**Measured MON**	**BMON (Ethanol)**
60	62.33	90.47
50	77.48	90.68
40	85.00	90.79
30	88.21	90.85
20	89.39	90.86
10	90.00	90.85
0	90.94	NA
Average BRON		**90.75**

Table 10: 99.9 % pure ethanol / 1-pentanol BMON values

Ethanol (99.9 %)		
1 - Pentanol (Vol %)	**Measured MON**	**BMON (Ethanol)**
60	87.25	90.48
50	88.02	90.48
40	88.50	90.48
30	89.19	90.49
20	89.69	90.49
10	90.20	90.50
0	90.53	NA
Average BMON		**90.49**

The calculated BRON values for pure ethanol in Tables 9 and 10 show good consistency with the MON value of 89.7 published by Yates et al. (2010). Note that the smaller change in O.N. with an increase in 1-pentanol, compared to n-

heptane, simplified the process of optimising the ignition timing / CR relationship. It is shown in Tables 9 and 10 that the similarities in the molecular structures of ethanol as base fuel, and 1-pentanol as blending component, yielded more accurate and stable extrapolated results for the BMON of pure ethanol. Figure 57 shows the multi-point extrapolation method for BMON of ethanol with n-heptane and 1-pentanol as blending components.

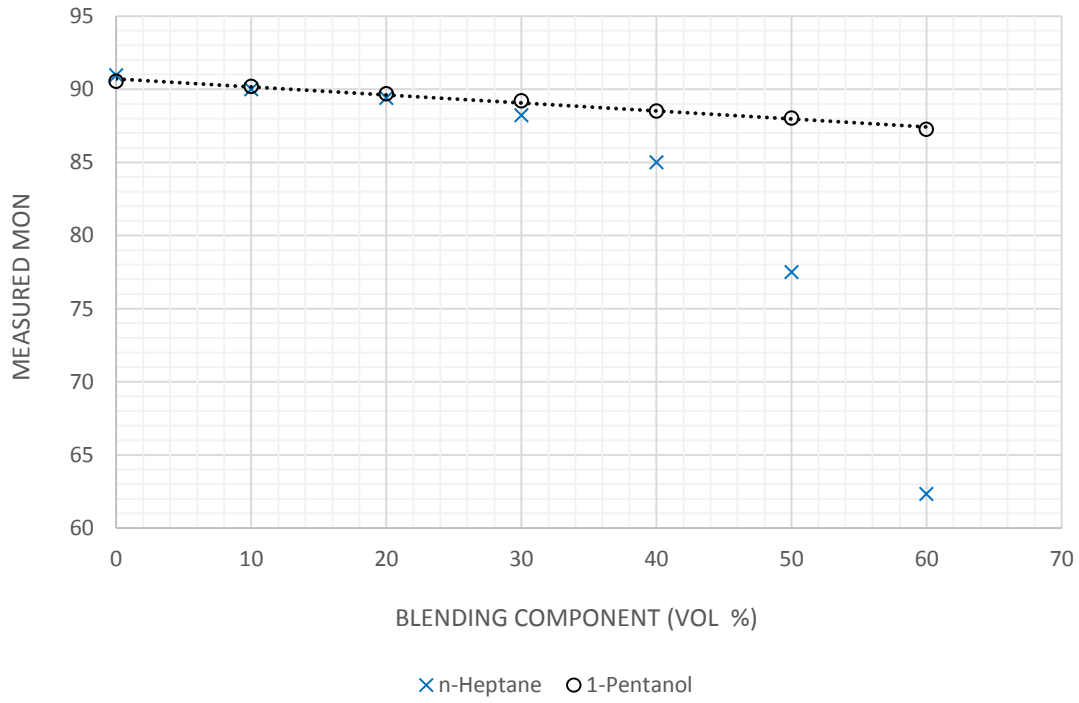

Figure 57: Comparison of n-heptane / 1-pentanol as ethanol BMON component

A linear relationship between the measured MON, and the volume fraction 1-pentanol in the blend is shown in Figure 57. The extrapolated BMON result for pure ethanol of 91 correlates well with the single-point extrapolation method, and direct measurement of ethanol in Tables 9 and 10. It can be seen that a non-linear relationship between measured MON and the volume fraction of n-heptane in the blend was recorded. It is therefore concluded that 1-pentanol is a suitable blending component for calculating BRON's and BMON's of ethanol, for both the single-point, and multi-point extrapolation methods discussed in this study.

4.5.3 Octane properties of refinery grade Sasol Fuel Alcohol (SFA)

SFA is an impure refinery grade ethanol product, and hence comparison of octane test results to literature values is dubious. It was therefore decided to test the octane properties of both SFA and high purity solvent ethanol, enabling both comparison to literature and delta characterization. Tables 11 and 12 show the BRON and BMON results for SFA, blended with 1-pentanol to reduce the O.N. of the mixture. The measured O.N. of the mixtures are extrapolated according to equation 33, to produce theoretical BON's for SFA in its pure form. It is shown in section 4.5.2 that 1-pentanol is a suitable blending component for calculating BON's for ethanol.

Table 11: Refinery grade SFA / 1-pentanol BRON values

SFA (~95 %)		
1 - Pentanol (Vol %)	**Measured RON**	**BRON (SFA)**
60	97.84	106.22
50	100.19	106.24
40	101.96	106.26
30	102.96	106.25
20	104.02	106.25
10	105.13	106.24
0	106.37	NA
Average BRON		**106.24**

Table 12: Refinery grade SFA / 1-pentanol BMON values

SFA (~95 %)		
1 - Pentanol (Vol %)	**Measured MON**	**BMON (SFA)**
60	88.94	91.32
50	89.22	91.32
40	89.63	91.32
30	90.06	91.32
20	90.67	91.32
10	91.08	91.33
0	91.36	NA
Average BMON		**91.32**

It can be seen from Table 11 that the direct RON measurement of pure SFA resulted in a lower octane rating, compared to high purity solvent ethanol in Table

7. BRON values calculated for SFA / 1-pentanol blends show excellent consistency. It is concluded from the results shown in Tables 7 and 11 that the RON of refinery grade fuel alcohol is approximately 2 O.N. lower than 99.9 % pure ethanol.

It was noted during MON testing that the mixture temperature of the CFR engine dropped more severely after refuelling with SFA, compared to high purity solvent ethanol. It can be concluded that SFA has a higher latent heat of vaporization, compared to 99.9 % pure ethanol. As a result, more time was required for the mixture heating elements to control the mixture temperature to the set point. Table 12 shows that the BMON of SFA is approximately 0.5 O.N. higher than high purity solvent ethanol. A larger octane sensitivity was calculated from the BRON and BMON results of ethanol (17.926), compared to SFA (14.923). It was therefore concluded that SFA, because of its higher latent heat of vaporization, has superior octane properties in harsh operating conditions. Figure 58 shows the linear response of measured O.N. in relation to the volume fraction of the blending component, and the multi-point extrapolated BRON and BMON results for SFA.

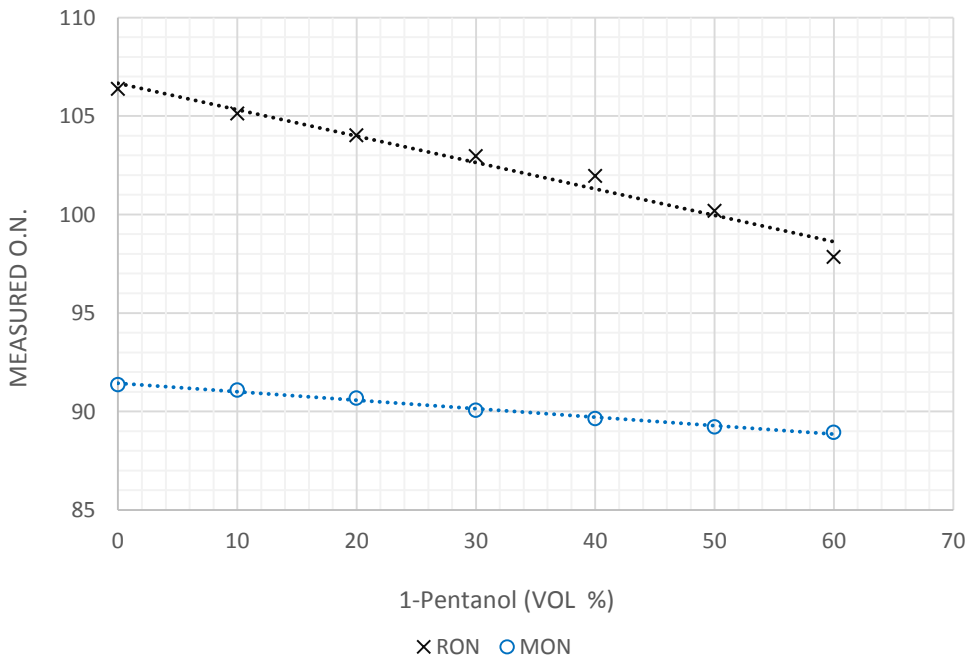

Figure 58: Refinery grade SFA octane properties

It is shown in Figure 58 that a BRON of 106.6, and BMON of 91.2 can be extrapolated for SFA according to the multi-point extrapolation method. This correlates well with data shown in Tables 11 and 12.

4.6 OCTANE PROPERTIES OF TAME

Tert-Amyl methyl ether (TAME) is used as an additive to raise the oxygen content, and increase the octane rating of conventional fuels. Little data is available in literature on the O.N. of TAME in its pure form. In the higher CR range, the precision of octane tests degenerate because of unstable KI measurement, as seen in Figure 56, section 4.5.1. These uncertainties can be mitigated via repeat measurements, but the results are still less certain than what is typically possible at lower octane levels. The high octane and oxygenated capabilities of the modified CFR engine at Stellenbosch University presented an opportunity to investigate the octane properties of TAME.

The RON and MON of TAME were tested directly through pure samples, utilizing the high octane capabilities of the modified CFR engine. BON's were also tested, in order to compare the results with direct measurement. The suitability of two blending components, n-heptane and 1,2 dimethoxyethane, for BON calculations were investigated through a single-point, and multi-point extrapolation method. 1,2 Dimethoxyethane was selected as a prospective blending component, based on the high cetane (low octane) property, and similar molecular structure to TAME.

4.6.1 Single-point extrapolation method

The method described in section 4.5.2, and equation 33 was used to calculate the BON's for TAME, using different components to lower the measured octane number. Tables 13 and 14 show the BRON results of TAME / n-heptane, and TAME / 1,2 dimethoxyethane blends.

Table 13: TAME / n-heptane BRON values

TAME		
n-Heptane (Vol %)	**Measured RON**	**BRON (TAME)**
60	80.11	107.66
40	90.60	107.69
30	95.32	107.70
20	100.52	107.75
10	104.56	107.77
0	108.13	N/A
Average BRON		**107.71**

Table 14: TAME / 1,2 dimethoxyethane BRON values

TAME		
1,2 Dimethoxyethane (Vol %)	**Measured RON**	**BRON (TAME)**
60	< 50	N/A
40	61.22	106.95
30	78.21	107.13
20	90.46	107.24
10	100.26	107.34
0	108.13	N/A
Average BRON		**107.17**

It is shown in Tables 13 and 14 that the direct measurement of pure TAME resulted in a RON of 108.31. This correlates well with data published in literature. A range of 104.0 – 117.0 RON was published in SAE (Mirabella, 2016). It can be seen that n-heptane, as a blending component, sufficiently lowered the measured mixture RON, and produced consistent extrapolation results for the BRON of pure TAME. Table 14 shows that the ultra-low octane properties of 1,2 dimethoxyethane resulted in very low measured RON's for the mixtures. As a result, extrapolated BRON calculations for pure TAME, for high volume fractions of the blending component, were not as accurate as seen in Table 13.

Tables 15 and 16 show the BMON results of TAME / n-heptane, and TAME / 1,2 dimethoxyethane blends.

Table 15: TAME / n-heptane BMON values

TAME		
n-Heptane (Vol %)	**Measured MON**	**BMON (TAME)**
60	87.63	99.07
40	94.49	99.14
30	96.12	99.16
20	97.24	99.16
10	97.79	99.12
0	97.26	N/A
Average BMON		**99.13**

Table 16: TAME / 1,2 dimethoxythane BMON values

TAME		
1,2 Dimethoxyethane (Vol %)	**Measured MON**	**BMON (TAME)**
60	54.07	98.44
40	70.02	98.46
30	88.40	98.83
20	94.24	98.94
10	97.64	99.04
0	99.19	N/A
Average BMON		**98.74**

It is shown in Tables 15 and 16 that direct measurements of pure TAME resulted in a MON of 99.195, and 97.267. A range of 95.0 – 106.0 MON was published in SAE (Mirabella, 2016). Ignition timing was initially set to a MON of 100, based on the values published by SAE, and adjusted for maximum KI with each subsequent blend. It can be seen from Table 15 that n-heptane is a suitable blending component for lowering the measured MON of TAME mixtures. An average BMON of 99.134 was calculated with n-heptane blends. Table 16 shows that the ultra-low octane properties of 1,2 dimethoxyethane resulted in very low measured MON's for the mixtures. The average BMON results for 1,2 dimethoxyethane blends is 98.746.

It is shown in section 4.5.2 that a blending component with a similar molecular structure to the base fuel reduces intermolecular synergistic effects when calculating an extrapolated BON. The ultra-low octane properties of 1,2 dimethoxyethane lowered the mixture O.N. drastically, and BON results with a

high volume fraction of this blending component were less accurate as a result. It is therefore concluded that both n-heptane and 1,2 dimethoxyethane are suitable blending components for the single-point extrapolation method, but that lower volume fractions of the high cetane ether is required.

4.6.2 Multi-point extrapolation method

The measured O.N.s for TAME, using n-heptane and 1,2 dimethoxyethane as blending components, were plotted in relation to the blending ratio by volume. A linear trend line was fitted through suitable data points, and extrapolated to calculate the BON of the TAME in pure form. Figure 59 shows the BRON result.

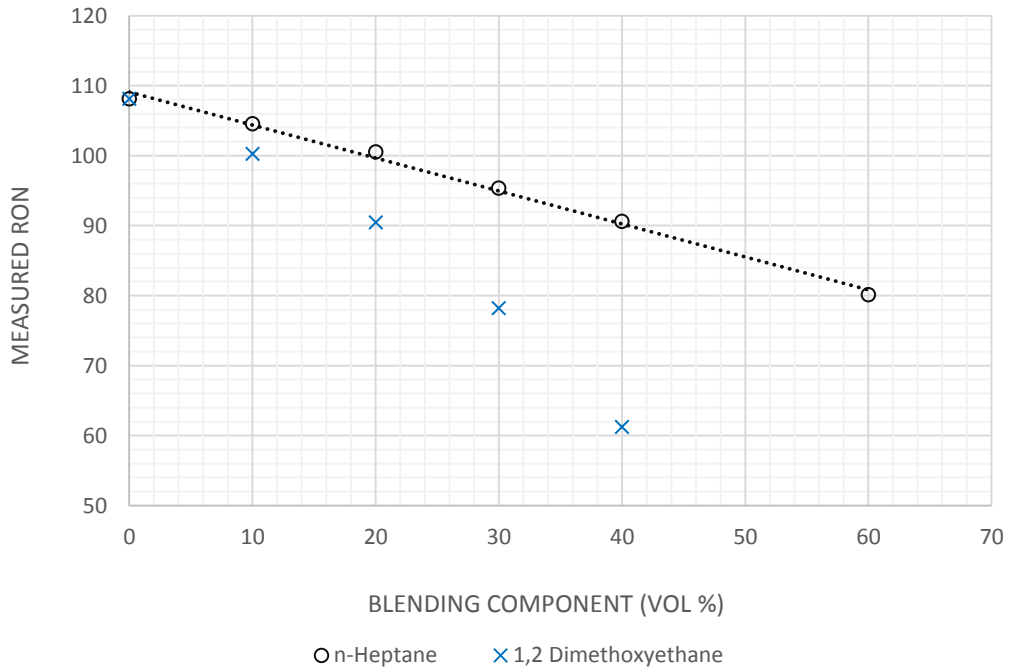

Figure 59: Comparison of n-heptane / 1,2 dimethoxyethane as TAME BRON component

It can be seen that measured results for TAME / n-heptane mixtures are linear with respect to blending ratio. A linear trend line was fitted through n-heptane data points, and extrapolated to calculate the BRON for TAME. Figure 59 shows a BRON of 109 can be calculated for TAME / n-heptane blends, which correlates well with the direct measurement, and single-point extrapolation in Table 13. The

ultra low octane properties of 1,2 dimethoxyethane yields non-linear octane results with respect to blending ratio. Figure 60 shows the BMON result.

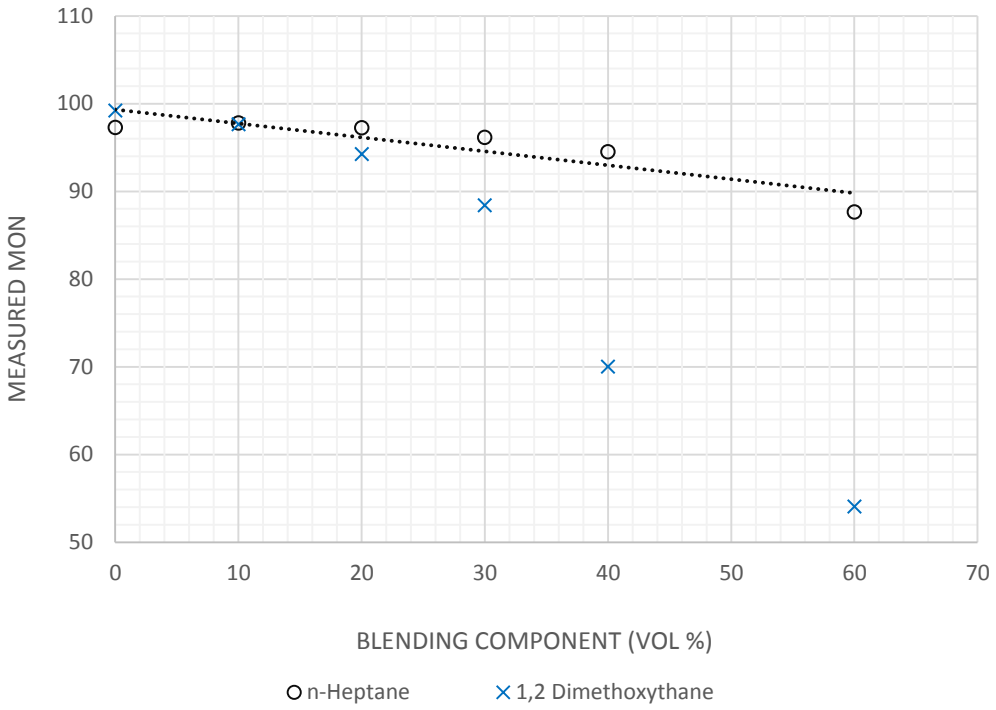

Figure 60: Comparison of n-heptane / 1,2 dimethoxyethane as TAME BMON component

Figure 60 shows that measured MON results of n-heptane are more linear with respect to blending ratio, compared to 1,2 dimethoxyethane. An extrapolated BMON of 99 is shown in Figure 60, which correlates well with direct measurement, and single-point extrapolation in Table 15. It is therefore concluded that the linear octane response of TAME / n-heptane blends, with respect to blending ratio, yields accurate BON results with a multi-point extrapolation method. The ultra-low octane properties of 1,2 dimethoxyethane compromises the linearity of octane results with respect to blending ratio.

4.7 ROUND ROBIN SET OF FUELS

A set of 16 PRF blend samples (8 x RON and 8 x MON) were prepared by the Sasol Fuels Research Centre. No information on these samples were supplied,

and five different laboratories were used to test their octane properties. Laboratories A to D in Tables 19 and 20 are professional octane test centres with the latest technology CFR engines and test equipment. Tables 17 and 18 show the RON and MON results, tested at Stellenbosch University. The measurement errors for the CCR procedure and equilibrium fuel level bracketing procedure are shown.

Table 17: RON – Round robin result

		Measured RON			
Sample	**O.N.**	**CCR - Procedure**	**Error**	**Bracket - Procedure**	**Error**
U-PRF-R1	99.1	98.41	-0.68	98.14	-0.95
U-PRF-R2	98.8	97.69	-1.10	97.83	-0.97
U-PRF-R3	96.1	95.00	-1.10	95.03	-1.06
U-PRF-R4	92.3	91.50	-0.79	91.57	-0.72
U-PRF-R5	92.0	91.15	-0.84	91.14	-0.85
U-PRF-R6	86.8	86.23	-0.63	86.91	0.04
U-PRF-R7	81.2	80.22	-0.97	80.11	-1.08
U-PRF-R8	80.9	79.69	-1.20	79.88	-1.02
		Average	**-0.91**	**Average**	**-0.82**

Table 18: MON – Round robin result

		Measured MON			
Sample	**O.N.**	**CCR - Procedure**	**Error**	**Bracket - Procedure**	**Error**
U-PRF-R1	99.2	98.16	-1.03	98.50	-0.70
U-PRF-R2	98.9	98.03	-0.86	98.09	-0.81
U-PRF-R3	95.9	96.65	0.75	94.88	-1.01
U-PRF-R4	92.2	92.53	0.33	91.33	-0.86
U-PRF-R5	91.9	93.20	1.30	90.83	-1.06
U-PRF-R6	87.2	90.45	3.18	86.92	-0.35
U-PRF-R7	81.1	80.23	-0.88	80.80	-0.30
U-PRF-R8	80.8	81.31	0.51	82.32	1.52
		Average	**1.02**	**Average**	**-0.44**

It is shown in Tables 17 and 18 that octane measurements on the CFR engine at Stellenbosch University tend to be slightly low. It can be seen that measurement errors can be significantly reduced by implementing the equilibrium fuel level bracketing test procedure. Tables 19 and 20 show the octane measurement

deltas, obtained from four professional laboratories, compared to the results from the modified CFR engine at Stellenbosch University. Octane measurements are included in Appendix G.

Table 19: Measurement delta (RON)

Sample	Actual RON	Lab A	Lab B	Lab C	Lab D	Stellenbosch University
PRF-R1	99.1	0.35	0.1	0.05	1.2	-0.958
PRF-R2	98.8	-0.1	-0.25	-0.15	0.2	-0.967
PRF-R3	96.1	0.3	0.1	0.4	1.7	-1.063
PRF-R4	92.3	0.1	0.5	0.5	2.1	-0.729
PRF-R5	92.0	0.1	0.05	0.05	1.9	-0.852
PRF-R6	86.8	0.78	0.83	0.48	1.93	0.046
PRF-R7	81.2	-1.35	-0.15	0.3	1.6	-1.089
PRF-R8	80.9	0.15	0.05	-0.25	1.5	-1.020
Average delta (abs)		0.403	0.254	0.273	1.516	0.841

Table 20: Measurement delta (MON)

Sample	Actual MON	Lab A	Lab B	Lab C	Lab D	Stellenbosch University
PRF-M1	99.2	0.7	0.6	-1.3	0.5	-0.700
PRF-M2	98.9	-0.15	-0.5	-0.65	-1.1	-0.810
PRF-M3	95.9	0.4	1.15	-0.6	0.4	-1.011
PRF-M4	92.2	-0.1	0.1	-0.1	1.4	-0.867
PRF-M5	91.9	0.05	0.2	-0.35	-1.3	-1.067
PRF-M6	87.2	-0.82	-0.92	-0.87	0.52	-0.350
PRF-M7	81.1	-1.7	-0.9	2.9	2.1	-0.300
PRF-M8	80.8	0.25	0.3	-0.75	-0.2	1.521
Average delta (abs)		0.589	0.634	1.025	0.890	0.795

It is shown in Tables 19 and 20 that, based on average measurement delta, the modified CFR setup at Stellenbosch University ranked fourth out of five laboratories with RON measurement, and third out of five laboratories with MON measurement. It is therefore concluded that the CFR engine setup at Stellenbosch University is capable of high octane and oxygenated fuels research, with accuracy on a comparative level with certified professional laboratories.

5. CONCLUSIONS AND RECOMENDATIONS

5.1 Conclusion

This document serves as a project report for a master's thesis. The author reviews available literature on the subjects involving high octane and oxygenated fuels testing. The modifications and development of the test facility are listed and motivated, before test results of high octane and oxygenated fuels are presented.

The CFR engine was disassembled, and found to be in good working condition. An inspection sleeve was found to protrude into the combustion chamber, hitting the piston. New sleeves were manufactured, and a modified spark plug / sleeve fitting arrangement was restored to the original specification. A compression test showed reduced leakage through the damaged sleeve, and spark plug fitting thread.

An external oil filtration system was added after noting particle drag marks on the connecting rod shell bearings. This modification will reduce wear, and improve component longevity. An adjustable needle jet was implemented in the carburettor, allowing for A/F ratio adjustment, and, in conjunction with added mixture temperature control, create the possibility of testing oxygenated fuel samples such as ethanol and SFA. A chiller system was designed for the fuel float chamber allowing for research on very volatile test samples, and was found not to compromise octane results.

The modified and upgraded CFR setup was calibrated using pure iso-octane, and data from literature. A variety of different fuel samples with different chemical compositions were tested. Data points for different fuel samples all fall on the calibrated CCR curve, giving credibility to the methodology of using TSFs for high octane bracketing.

High octane and oxygenated fuel samples such as toluene, TAME and ethanol were successfully measured, and results correlate well with published data from literature.

The differences between the octane properties of high purity solvent ethanol and refinery grade SFA were successfully characterised. Two methods of calculating BON's on a CFR engine without the high CR capabilities of the modified setup at Stellenbosch University were investigated with two different blending components. It was found that 1-pentanol was an effective in sufficiently reducing the measured O.N. of ethanol mixtures, and produced liner octane results with respect to blending ratios. 1-pentanol was found to be a superior blending component to n-heptane for calculating the BON's of ethanol

The octane properties of TAME were measured directly, using the high CR capabilities of the modified CFR engine. Two methods of calculating BON's were investigated with two blending components. It was found that the ultra-low octane properties of 1,2 dimethoxyethane was effective in lowering the O.N. of TAME blends, but did not produce linear octane results w.r.t blending ratios. n-Heptane was found to be a superior blending component to 1,2 dimethoxyethane for calculating the BON's of TAME.

A PRF round robin octane test showed that the modified CFR engine test setup at Stellenbosch University ranked fourth out of 5 state of the art, professional octane testing laboratories for RON measurement, and third out of five for MON tests.

5.2 CFR setup recommendations

Based on the challenges and difficulties faced in the testing phase of this study, the following recommendations to improve the efficiency and accuracy of octane research for future projects are made:

1. Improve the accuracy of KI quantification.
    a. Use a pressure transducer and band pass filter to identify knock and KI, rather than analogue KI dial meter.
    b. Implement a tuneable damping circuit on the knock meter, eliminating the fluctuation without changing the average reading.
    c. Reduce KI reading fluctuation by increasing the thermal inertia of the heating coil in the knock pickup sensor.

2. Convert the analogue KI signal to a digital reading that can be tracked and recorded on a PC. This will improve the accuracy of the equilibrium fuel level bracketing method.
3. Add a 3rd fuel reservoir to improve the efficiency of the bracketing method, i.e. the fuel sample, and two bracket fuels are used simultaneously, and the operator can select which one to test with the fuel selector.
4. Automate fuel-blending system in a vapour cabinet.
5. Automate CR adjustment with an electric motor / gearbox on the worm gear lever, and calibrate CR / cylinder height relationships with contact switches for reference positions.
6. Implement ECU for ignition timing; automatically adjust ignition timing in relation to CR using feedback from automated CR adjustment.
7. Replace out of date electric drive system and tacho generator to improve engine speed control.
8. Calibrate and “hard code” engine speeds for RON and MON into drive system, and control with two switches.
9. Ensure PRF purity before calibration or use by means of GC analysis at the Process Engineering Department at Stellenbosch University.
10. Replace connecting-rod shell bearings at next service.
11. Implement compressed air and crumbed walnut cleaning system for the combustion chamber.
12. Investigate engine modifications to allow testing of gaseous fuels, e.g. Butane used in petrol blending

5.3 Fuels testing recommendations

1. Characterise the delta between Sasol refinery stream TAME, and high purity solvent TAME.
2. Investigate the suitability of low octane aromatic blending components for BON calculations for toluene.
3. Develop and calibrate a non-linear octane prediction model in MS Excel to assist in prediction of BON’s to simplify reference fuel preparation.
4. Following point 12 in 5.2, characterisation of the effects of blending butane into different fuel compositions.

6. REFERENCES

Anon. 2015. 3.8 Gasoline: A Deeper Look - Chemwiki. [Online]
Available at: Chemwiki.ucdavis.edu.
[Accessed 11 July 2016]. Presentation.

Anon. 2016. 3.5 The Internal Combustion Engine (Otto Cycle). [Online]
Available at: Web.mit.edu.
[Accessed 21 June 2016]. Presentation.

Assi, R. 2008. The Relation Between Gasoline Quality, Octane Number and The Environment. Amman: Jordan National Workshop - Presentation.

ASTM. 1971. Manual for rating motor, diesel and aviation fuels. American Society for Testing and Materials.

ASTM. 2016. D2699 Standard Test Method for Research Octane Number of Spark-Ignition Engine Fuel.

ASTM. 2016. D2700 Standard Test Method for Motor Octane Number of Spark-Ignition Engine Fuel.

Blackmore, D. *et al.* 1977. Fuel economy of the gasoline engine. Fuel, Lubricant and other effects. Palgrave Macmillan.

Çengel, Y. & Boles. M.A., 2011. *Thermodynamics*. Singapore: McGraw-Hill.

Chen, L. *et al.* 2003. The Power and Efficiency Characteristics for an Irreversible Otto Cycle. *International Journal of Ambient Energy,* 24(4): 195-200.

Clerk, D. 1907. On the limits of thermal efficiency in internal combustion engines (including appendixes). Minutes of the Proceedings, 169: 121-152.

De Bellis, V. 2016. Performance Optimization Of A Spark-Ignition Turbocharged VVA Engine Under Knock Limited Operation. *Applied Energy,* 164: 162-174.

Foong. T.M. *et al*. 2013. The octane numbers of ethanol blended with gasoline and its surrogates. *Elsevier Fuel*, 115: 727-739.

Gersen, S. *et al*. 2016. Characterizing Gaseous Fuels for Their Knock Resistance based on the Chemical and Physical Properties of the Fuel. *SAE International Journal of Fuels and Lubricants*, 9(1): 1-13.

Ghosh, P. *et al.* 2006. Development of a Detailed Gasoline Composition-Based Octane Model. *Ind. Eng Chem. Res,* 45: 337-345.

Green, D. 2008. Perry's chemical engineers' handbook. New York. McGraw-Hill.

Heywood, J. B. 1988. *Internal Combustion Engine Fundamentals.* New York: McGraw-Hill.

Hou, S. 2007. Comparison of Performance of Air Standard Atkinson and Otto Cycles with Heat Transfer Considerations. *Energy Conversion and Management,* 48(5):1683-1690.

Hoshi, M. 1984. Reducing Friction Losses In Automobile Engines. *Tribology International,* 17(4): 185-189.

Hunwartzen, I. 1982. Modification of CFR test engine unit to determine octane numbers of pure alcohols and gasoline alcohol blends. SAE International Journal of Engines 820002.

Jooste, C. 2016. Upgrade of a single cylinder research engine used to measure the octane ratings of petrol/ethanol blends. Stellenbosch University.

Lee, J. *et al*. 2013. Production of light olefins through catalytic cracking of C5 raffinate over carbon-templated ZSM-5. *Fuel Processing Technology*, 108: 25-30.

Larsen, U. Johansen, T. & Schramm, J. 2009. Ethanol As A Fuel For Road Transportation. IEA Implementing Agreement on Advanced Motor Fuels, EFP06: 39-52.

Leone, T. *et al.* 2015. The effect of compression ratio, fuel octane rating, and ethanol content on spark-ignition engine efficiency. *Environ. Sci. Technol.,* 49: 10778-10789.

Kalghatgi, G. *et al.* 2009. The nature of “superknock” and its origins in SI engines. Shell Global Solutions (UK).

Mac Ketta, J. 1992. *Petroleum processing handbook*. New York: Marcel Dekker.

Mirabella. 2016. Blending Octane Evaluation of Fuel Ethers: a Literature Review. *SAE International*. SAE2016-01-0883.

Nakada, M., 1994. Trends In Engine Technology And Tribology. *Tribology International,* 27(1).

Nigro, F. & Szwarc, A. Ethanol As A Fuel. *Ethanol and Bioelectricity Sugarcane in the Future of the Energy Matrix*. 159-163.

Nozawa, R. Yoshiro, M. & Michinori, S., 1994. Effects Of Engine Downsizing On Friction Losses And Fuel Economy. *Tribology International,* 27(1): 31-37.

PCS. 2014. Safety Data Sheet (SDS) C_5 Raffinate.

Rapp. Vi. H. *et al.* 2014. Research Octane Numbers of Primary and Mixed Alcohols from Biomass-Based Syngas. *Energy and Fuels*, 28, 3185 – 3191.

Richards, P. et al. K. 2014. Automotive fuels reference book. Warrendale, Pa.: SAE International.

Ronney, Dr. P. 2013. "AME 436 - Lecture 10 - Cumbustion Engines". Presentation.

Silva, C., Ross, M. & Farias, T. 2009. Analysis And Simulation Of “Low-Cost” Strategies To Reduce Fuel Consumption And Emissions In Conventional Gasoline Light-Duty Vehicles. *Energy Conversion and Management,* 50(2): 215-222.

Stein, R., Anderson, J. & Wallington, T. 2013. An overview of the effects of ethanol-gasoline blends on SI engine performance, fuel efficiency and emmisions. SAE International Journal of Engines, 6(1): 470-487.

Stone, R. 1992. Introduction to internal combustion engines. Warrendale, Pa: SAE international.

Str.llnl.gov. 2017. Combustion Modeling. [online] Available at: https://str.llnl.gov/str/Westbrook.html [Accessed 27 Oct. 2017].

Swarts, A. 2006. Insights to octane rating and the underlying role of autoignition. Department of Mechanical Engineering, University of Cape Town.

The Environmental Protection Agency. 1995. Fuel Economy Impact Analysis Of RFG. EPA 420-F-95-003.

Turner, J. 2014. Ultraboost: Investigation into the limits of extreme engine downsizing. Presentation.

Wallner. T. *et al*. 2012. Analytical Assessment of C2-C8 alcohols as Spark-Ignition Engine Fuels. Proceedings of the FISITA 2012 World Automotive Congress, Lecture Notes in Electrical Engineering 191.

Yang, Y. et al. 2013. Understanding fuel anti-knock performances in modern SI engines using fundamental HCCI experiments. SAND2013-10628C.

Yates, A., Bell, A. & Swarts, A. 2010. Insights relating to the autoignition characteristics of alcohol fuels. Fuel, 89(1): 83-93.

Zhen, Xudong *et al.* 2012. The Engine Knock Analysis – An Overview. *Applied Energy,* 92: 628-636.

APPENDIX A – Blending software

A gravimetric system for accurately blending primary reference fuels was developed by a co-supervisor to this project, Dr. Gareth Floweday. The Microsoft Excel program was designed to read real time mass measurements from a digital scale, connected to a PC through communication ports. The crux VBA coding in this RS232 serial port tool is a set of coding called modCOMM, which uses Windows API to perform serial communications. David M. Hitchner originally wrote the code, and development of the gravimetric blending software was based on an article by Maurizio Di Paolo Emilio. The system, shown in Figure 61, allows the user to accurately blend fuels with up to three components by relating the gravimetric data of each component, in the order that they are added to the fuel mixture, to the total mass of the mixture. Figure 61 shows a PC, newly purchased digital scale and glassware used to blend test fuels for the CFR engine.

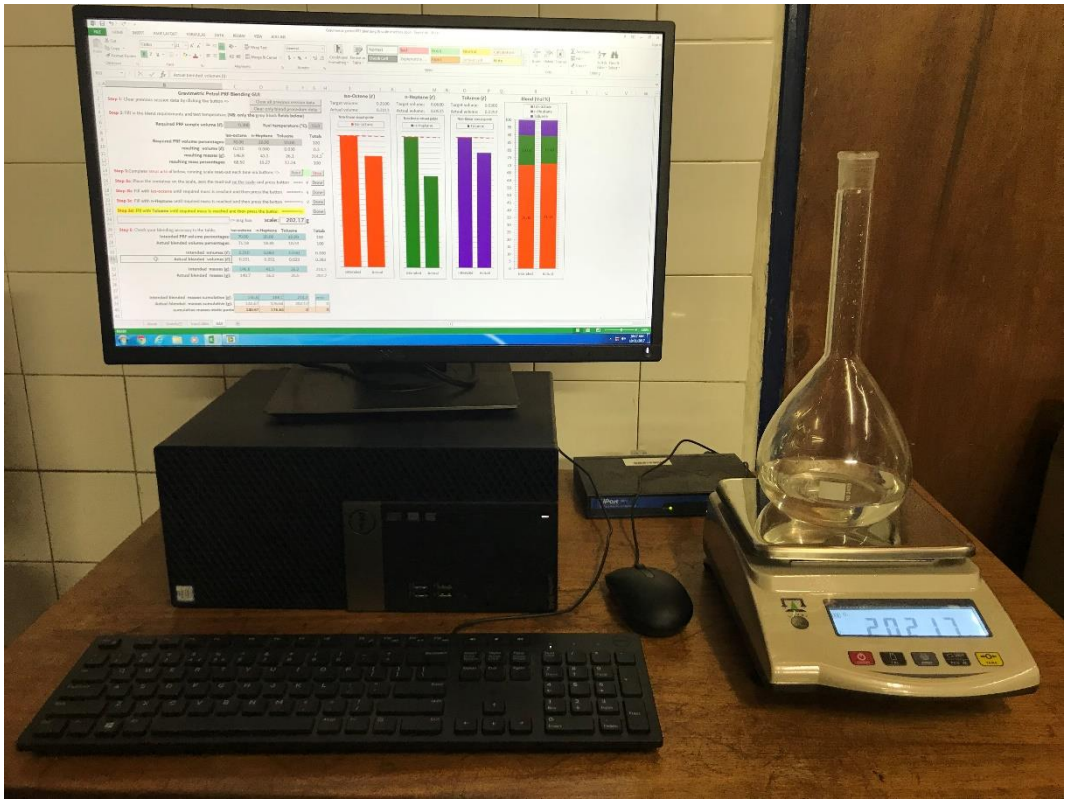

Figure 61: PRF blending station

The Microsoft Excel program consists of four tabs: an introductory page; a page with physical properties of the available PRF components; input data required for connection with a digital scale; and a graphic user interface for fuel blending. The introductory page, shown in Figure 62, provides the user with a background and instructions on how to use the software.

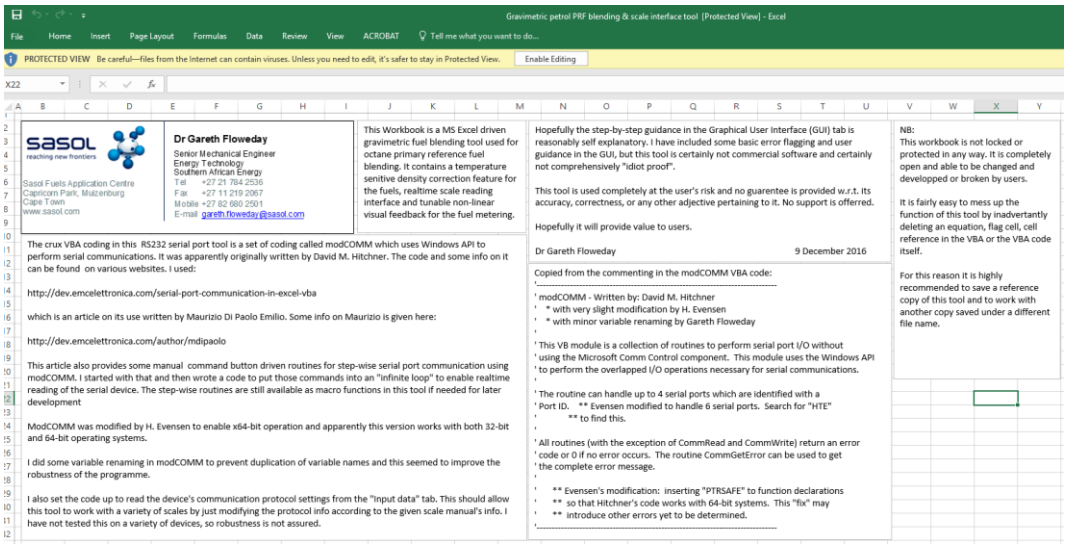

Figure 62: Introductory page and instructions

The gravimetric data of three blending components: iso-octane; n-heptane and toluene, are “hard coded” into the Excel software in the second tab. This includes the liquid density, expansion coefficient, and an algorithm to adjust density with temperature. See Figure 63.

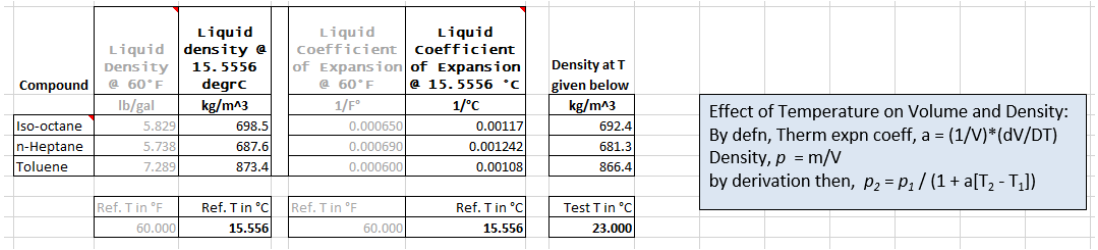

Compound	Liquid Density @ 60°F	Liquid density @ 15.5556 degrC	Liquid Coefficient of Expansion @ 60°F	Liquid coefficient of Expansion @ 15.5556 °C	Density at T given below
	lb/gal	kg/m^3	1/F°	1/°C	kg/m^3
Iso-octane	5.829	698.5	0.000650	0.00117	692.4
n-Heptane	5.738	687.6	0.000690	0.001242	681.3
Toluene	7.289	873.4	0.000600	0.00108	866.4
	Ref. T in °F	Ref. T in °C	Ref. T in °F	Ref. T in °C	Test T in °C
	60.000	15.556	60.000	15.556	23.000

Effect of Temperature on Volume and Density:
By defn, Therm expn coeff, a = (1/V)*(dV/DT)
Density, p = m/V
by derivation then, $p_2 = p_1 / (1 + a[T_2 - T_1])$

Figure 63: Physical properties of PRF components

The third tab, shown in Figure 64, contains information regarding the communication between a digital scale, and the PC, through a RS232 communication port. Any digital scale with RS232 connection can be used in conjunction with the Excel software, although the particular communications protocol settings must be configured appropriately on the scale and in the Excel programme.

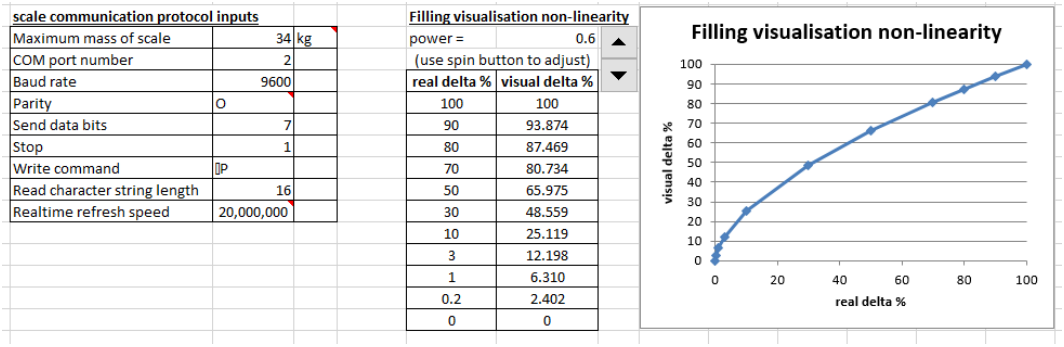

scale communication protocol inputs		
Maximum mass of scale	34	kg
COM port number	2	
Baud rate	9600	
Parity	O	
Send data bits	7	
Stop	1	
Write command	P	
Read character string length	16	
Realtime refresh speed	20,000,000	

Filling visualisation non-linearity	
power =	0.6
(use spin button to adjust)	
real delta %	visual delta %
100	100
90	93.874
80	87.469
70	80.734
50	65.975
30	48.559
10	25.119
3	12.198
1	6.310
0.2	2.402
0	0

Figure 64: Input data

A graphic user interface (GUI) is used during the actual blending process. This easy to use, stepwise process is clearly laid out with instructions, as shown in Figure 65. The user starts a blending process by clearing all previous data. The second step is to specify the components, and blending ratio of the required PRF. The software relates the fuel temperature to the physical properties shown in Figure 63, to calculate the required mass of each component of the PRF blend.

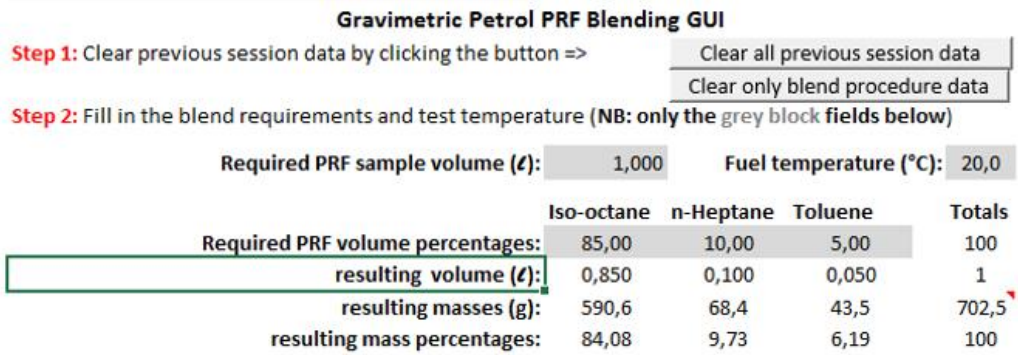

Gravimetric Petrol PRF Blending GUI

Step 1: Clear previous session data by clicking the button =>

Clear all previous session data

Clear only blend procedure data

Step 2: Fill in the blend requirements and test temperature (**NB: only the grey block fields below**)

Required PRF sample volume (ℓ): 1,000 **Fuel temperature (°C):** 20,0

	Iso-octane	n-Heptane	Toluene	Totals
Required PRF volume percentages:	85,00	10,00	5,00	100
resulting volume (ℓ):	0,850	0,100	0,050	1
resulting masses (g):	590,6	68,4	43,5	702,5
resulting mass percentages:	84,08	9,73	6,19	100

Figure 65: PRF blending steps 1 and 2

The third step in the process is to connect the digital scale to the PC through a specified communication port. With the scale in “print” mode, real time measurements are processed by the PC after pressing the “Read” button in the GUI. The user can then zero the scale with an empty flask.

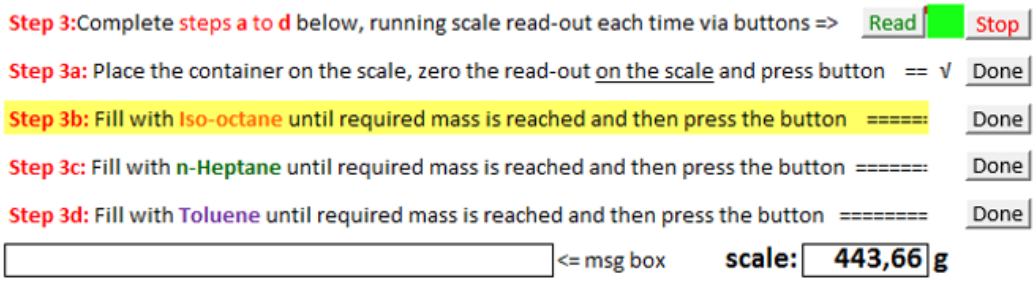

Figure 66: PRF blending Steps 3-5

With the scale zeroed, the user proceeds by adding the first component of the PRF to the empty flask. The mass of liquid added to flask is tracked in real time as illustrated by Figure 66. The orange bar graph is used to compare the required amount of the liquid component with the amount being added to the flask. It should be noted that the process shown in Figures 67 to 69 are for illustrative purposes only and the measured mass in these Figures do not necessarily relate to the blending requirements shown in Figure 65.

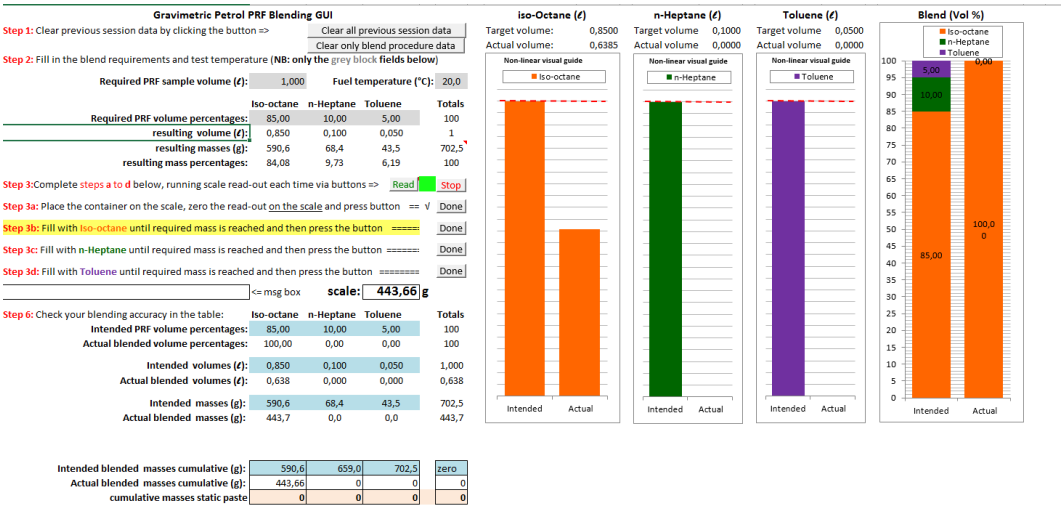

Figure 67: GUI - component 1 added

Figure 68 shows the GUI during step 3c (see Figure 63). It can be seen that the mass added by the first component (orange bars) remains constant, and the second component (green bars) is now being tracked in real time.

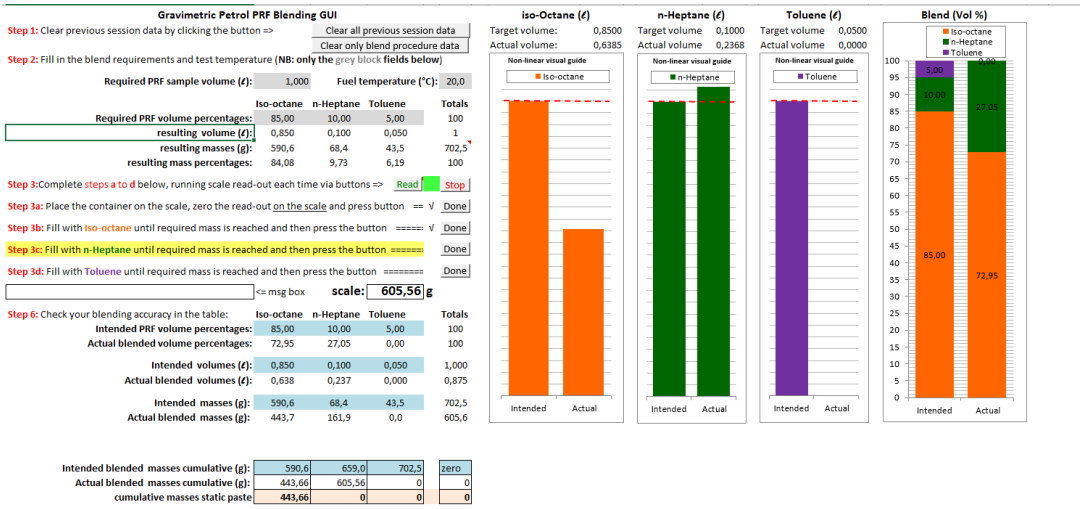

Figure 68: GUI - component 2 added

Figure 69 shows step 3d, where the third component is added (purple bars). The total blend, and blending ratio can be seen on the right, and compared to the

required blending ratio as specified in step 2. This demonstration shows that too little of the first component (orange), and too much of the second and third components (green and purple) was added. This blend will therefore not have the intended knock resistance capabilities.

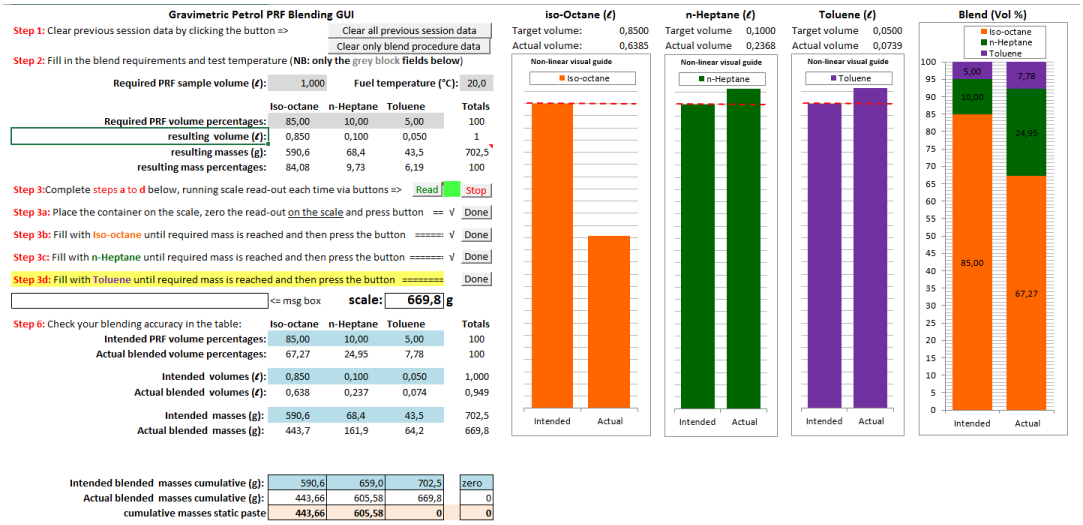

Figure 69: GUI - component 3 added

Step 6, shown in Figure 70, is a summary of the blending process, and compares the intended PRF to the actual blend. This can be used to track test samples, and adds credibility to the test results obtained from the CFR engine.

Step 6: Check your blending accuracy in the table:	Iso-octane	n-Heptane	Toluene	Totals
Intended PRF volume percentages:	85,00	10,00	5,00	100
Actual blended volume percentages:	67,27	24,95	7,78	100
Intended volumes (ℓ):	0,850	0,100	0,050	1,000
Actual blended volumes (ℓ):	0,638	0,237	0,074	0,949
Intended masses (g):	590,6	68,4	43,5	702,5
Actual blended masses (g):	443,7	161,9	64,2	669,8

Intended blended masses cumulative (g):	590,6	659,0	702,5	zero
Actual blended masses cumulative (g):	443,66	605,58	669,81	0
cumulative masses static paste	**443,66**	**605,58**	**669,81**	**0**

Figure 70: Blending accuracy

APPENDIX B – Carbon chains vs. Octane properties

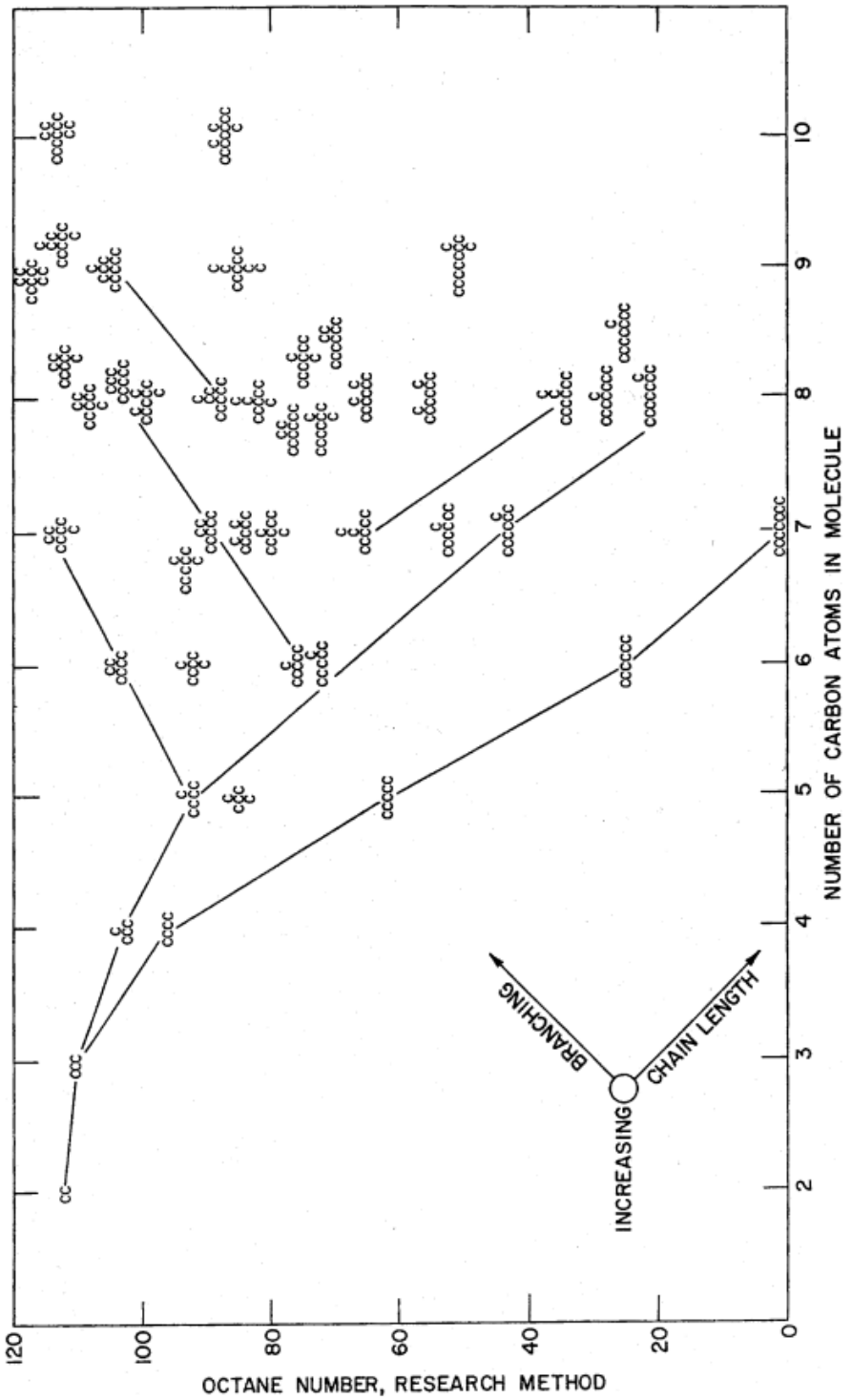

Figure 71: Octane rating vs Fuel structure (Ghosh *et al*., 2006)

APPENDIX C – Calibration data

C1 - Compression tester calibration

A compression tester was purchased in order to verify the improvement in compression of the CFR engine proceeding the upgrades and modification phase. The compression tester was calibrated using a similar methodology to calibrating a pressure transducer. A Fluke P5514-70M Hydraulic compression test pump (serial number: 71343) and Fluke 2700G reference pressure gauge (serial number: 2965022) were used to produce an actual pressure reading. The calibration setup is shown in Figure 72.

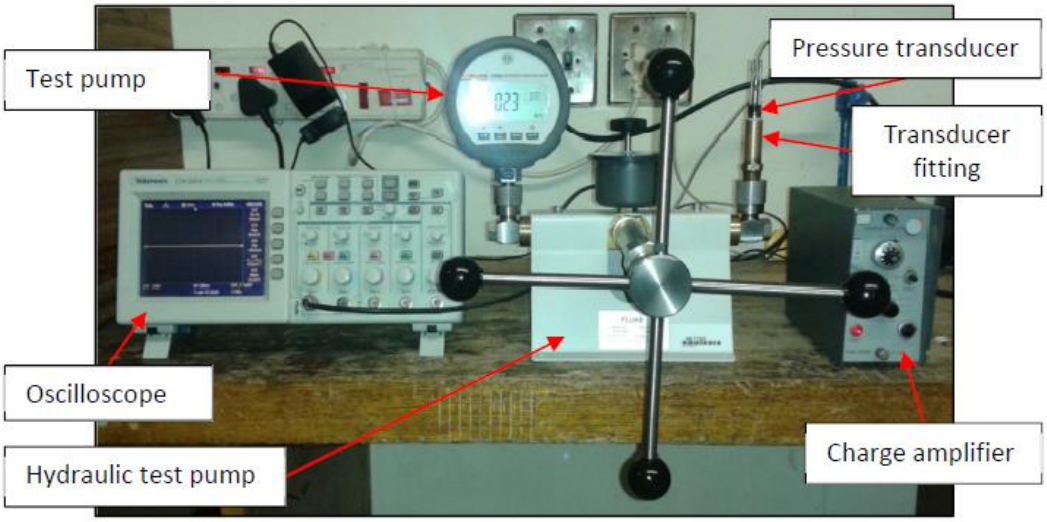

Figure 72: Pressure transducer calibration setup (Reproduced from Jooste (2016))

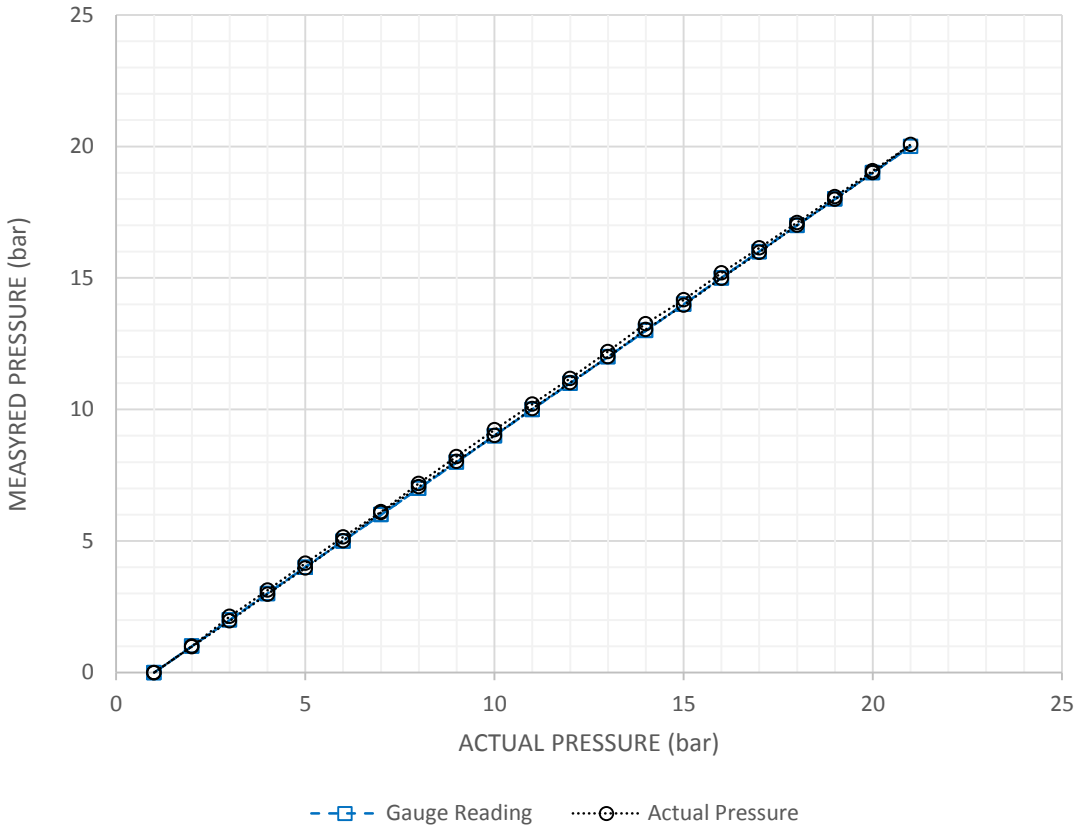

Figure 73: Compression tester calibration

C2 – Thermocouple calibration

Various temperatures of the CFR engine setup are monitored during octane testing to ensure credible testing conditions, and healthy operation of the engine is maintained. Temperatures are measured by J-type and K-type thermocouples, and an Allen Bradley PLC. A LabView programme on a PC converts the PLC data into usable information for the operator. The thermocouples, and LabView temperature readings were calibrated using a Fluke 9142 Field Metrology Well (serial number: B29291). Reference temperatures, in the expected operating range for each thermocouple, were set on the Fluke calibrator, and the LabView temperature readings were adjusted to minimize the measurement error for each thermocouple individually.

C3 – KI / Dial gauge reading calibration

The KI meter of the CFR engine was originally calibrated using pure iso-octane, and octane / KI relationship data from literature. This relationship was continuously checked during the testing phase of this project. Table 22 shows iso-octane / KI calibration test data through the six week testing phase.

Table 21: Iso-octane KI / Dial gauge reading calibration check

Iso-octane calibration check				
Date	**Dial (inch)**	**A/F (λ)**	**CCR**	**Measured O.N**
11-Aug	0.454	0.94	7.7702	100.000
16-Aug	0.455	0.95	7.7601	99.926
23-Aug	0.454	0.94	7.7702	100.000
29-Aug	0.453	0.94	7.7804	100.070
04-Sep	0.454	0.94	7.7702	100.000
14-Sep	0.455	0.93	7.7601	99.926
17-Sep	0.454	0.94	7.7702	100.000
21-Sep	0.454	0.94	7.7702	100.000
02-Oct	0.452	0.94	7.7702	100.150

APPENDIX D – Technical drawings

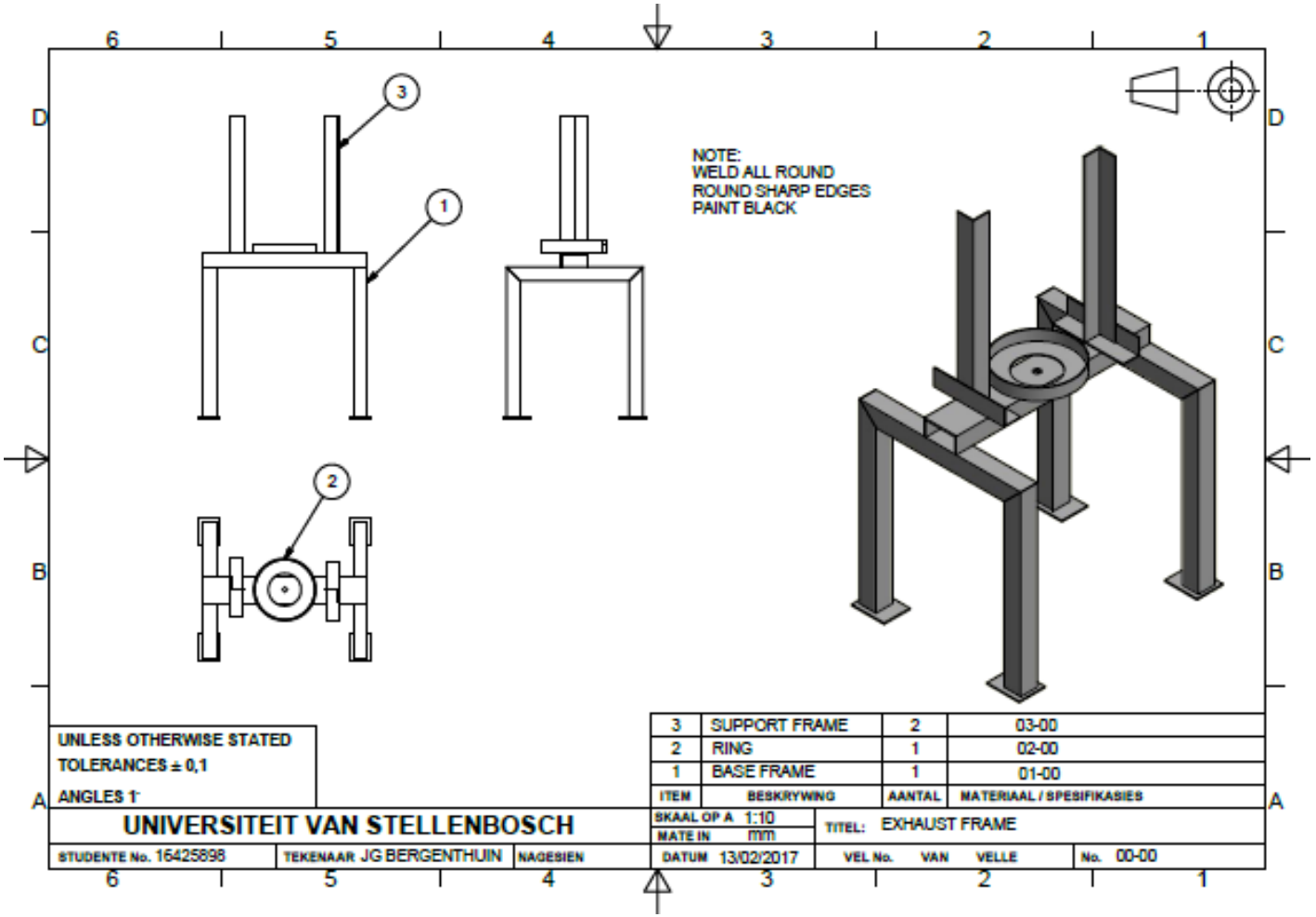

Figure 74: Exhaust frame

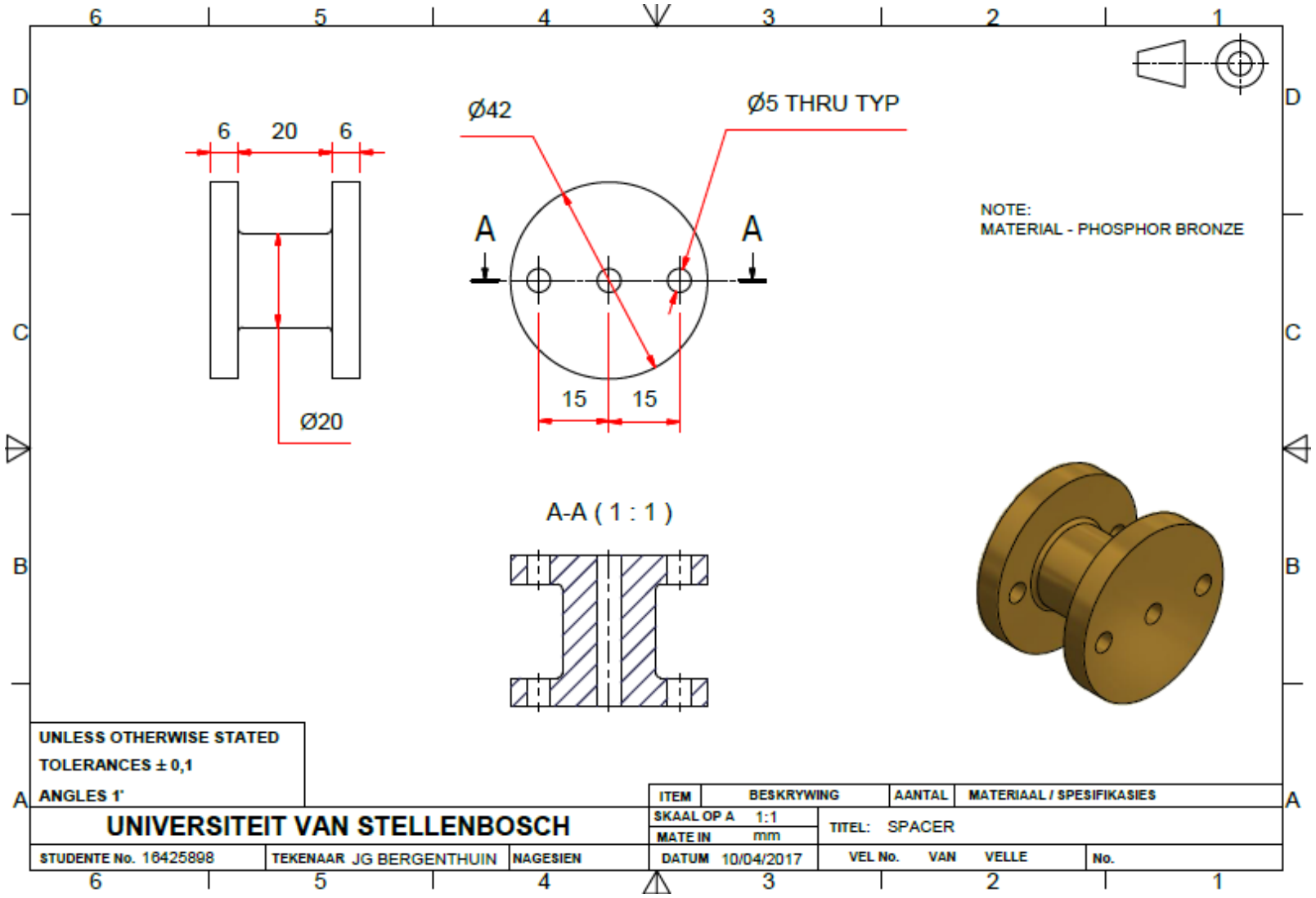

Figure 75: Fuel sight glass spacer

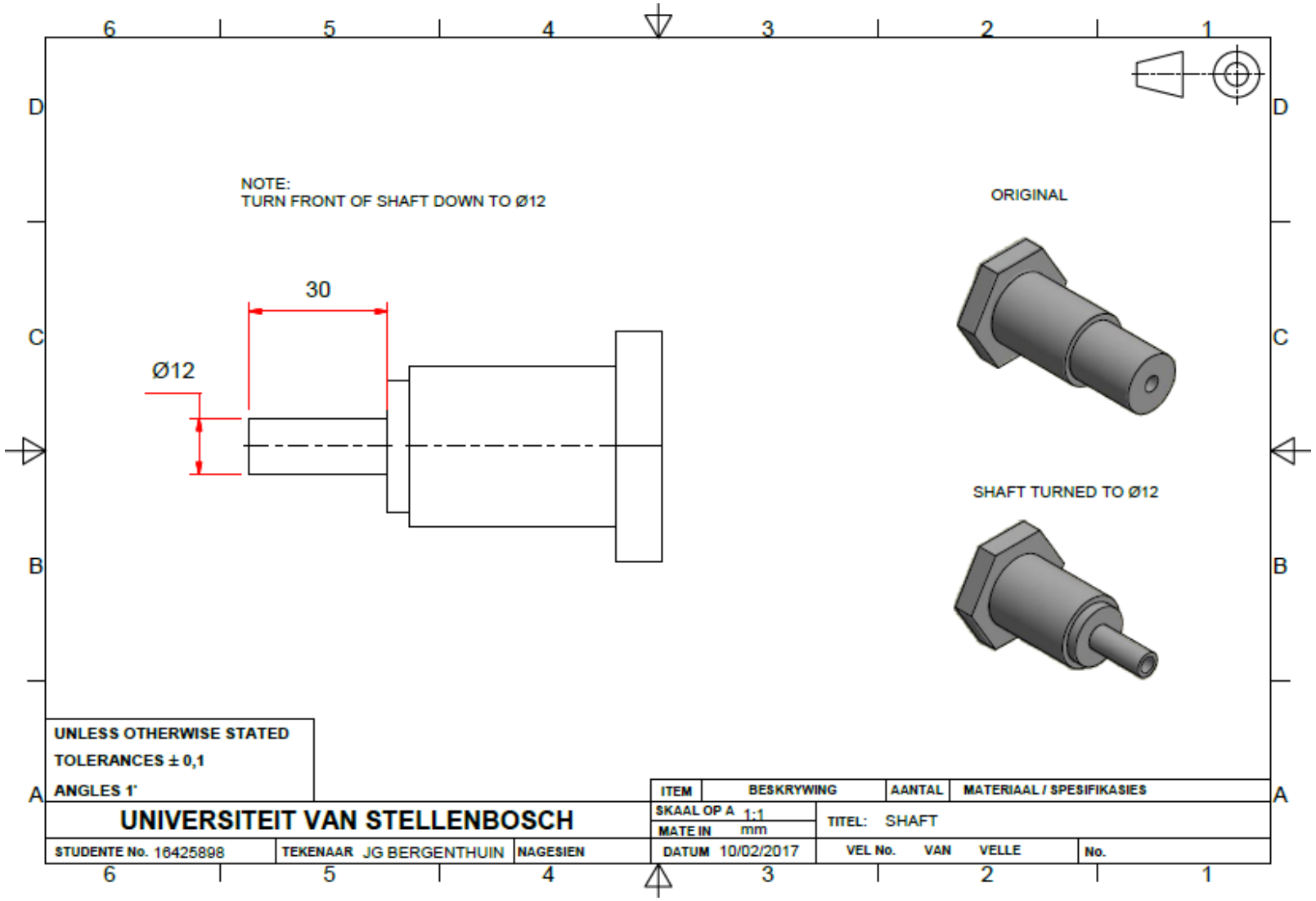

Figure 76: Modified shaft

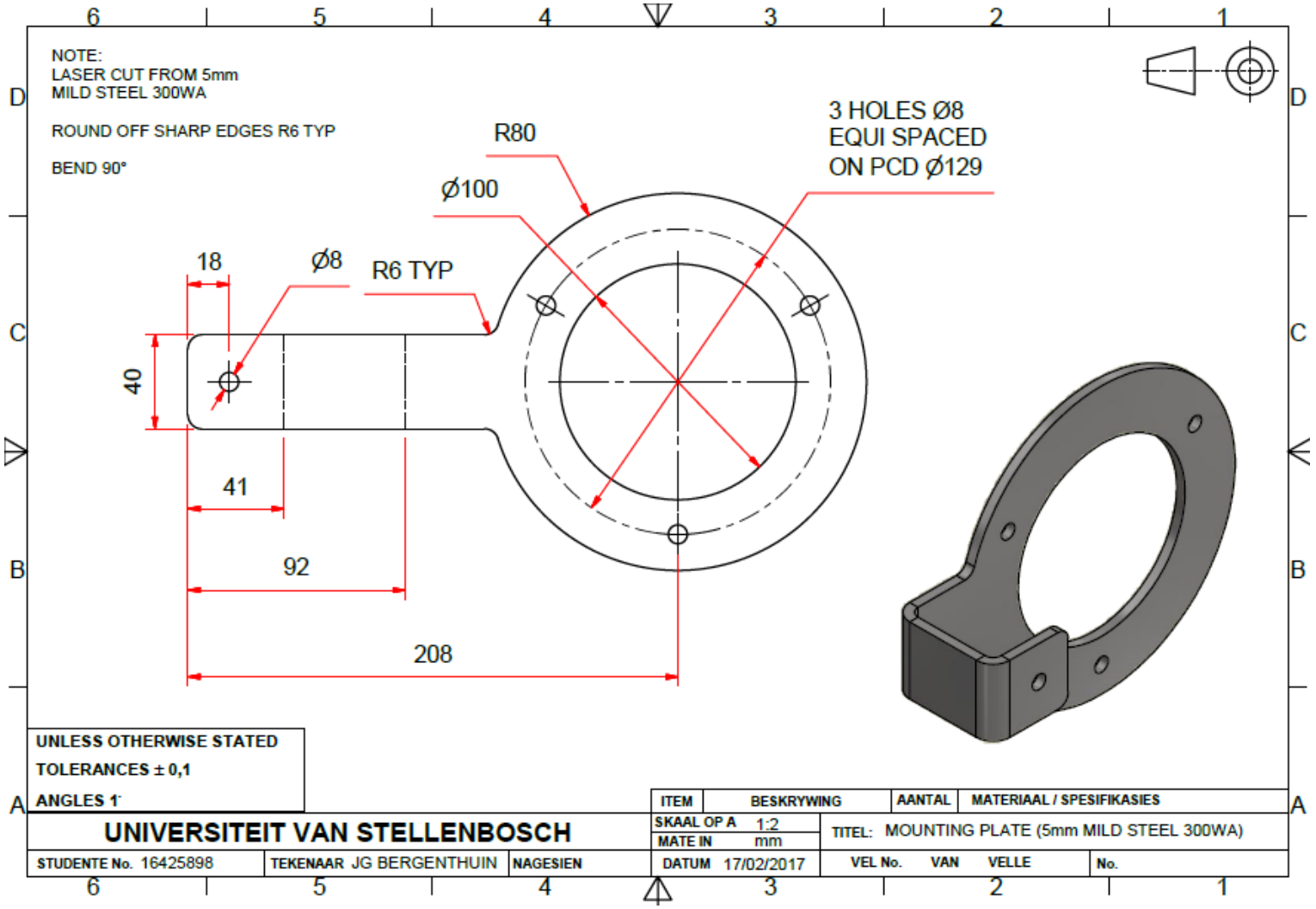

Figure 77: Shaft encoder mounting plate

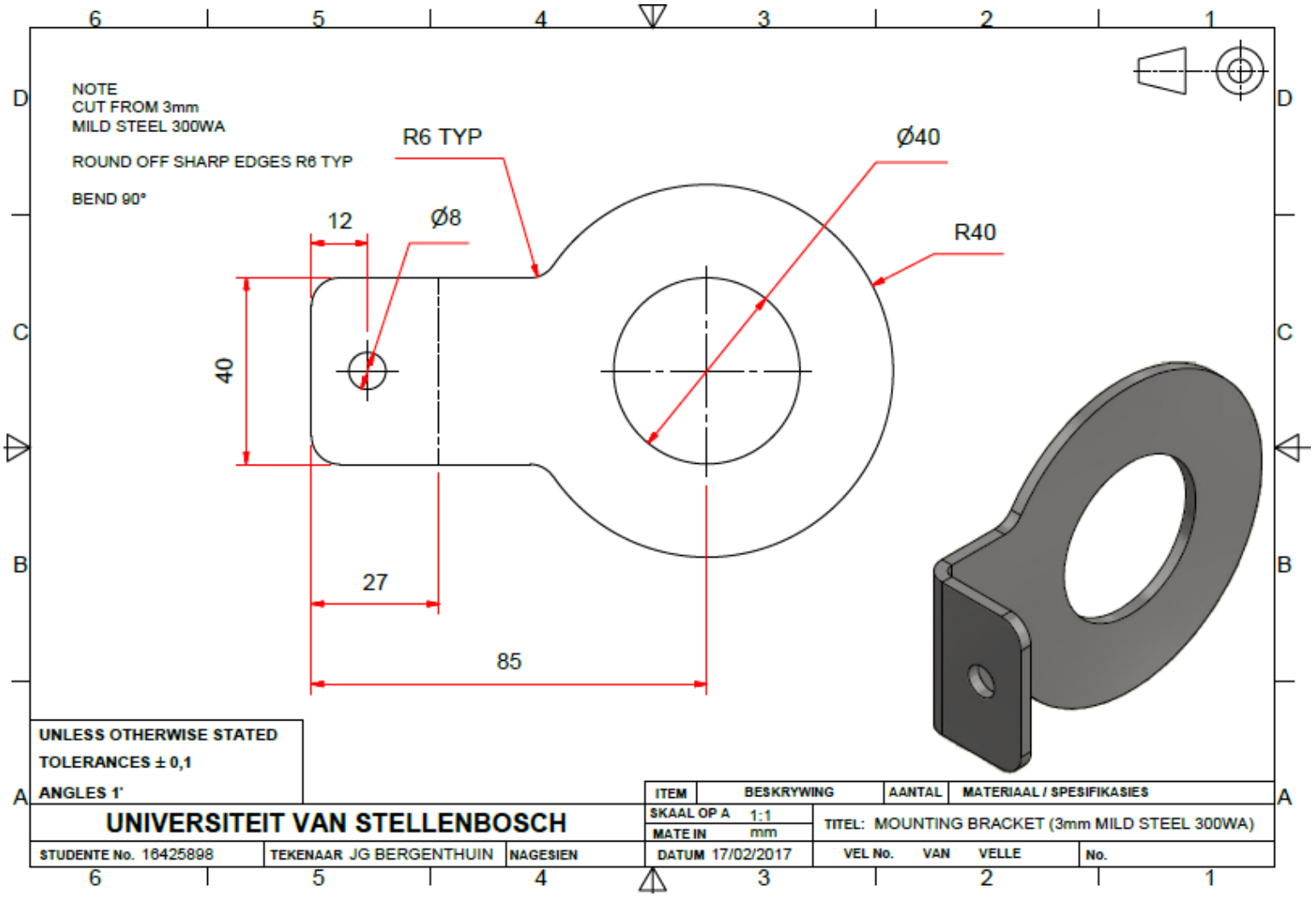

Figure 78: Shaft encoder mounting bracket

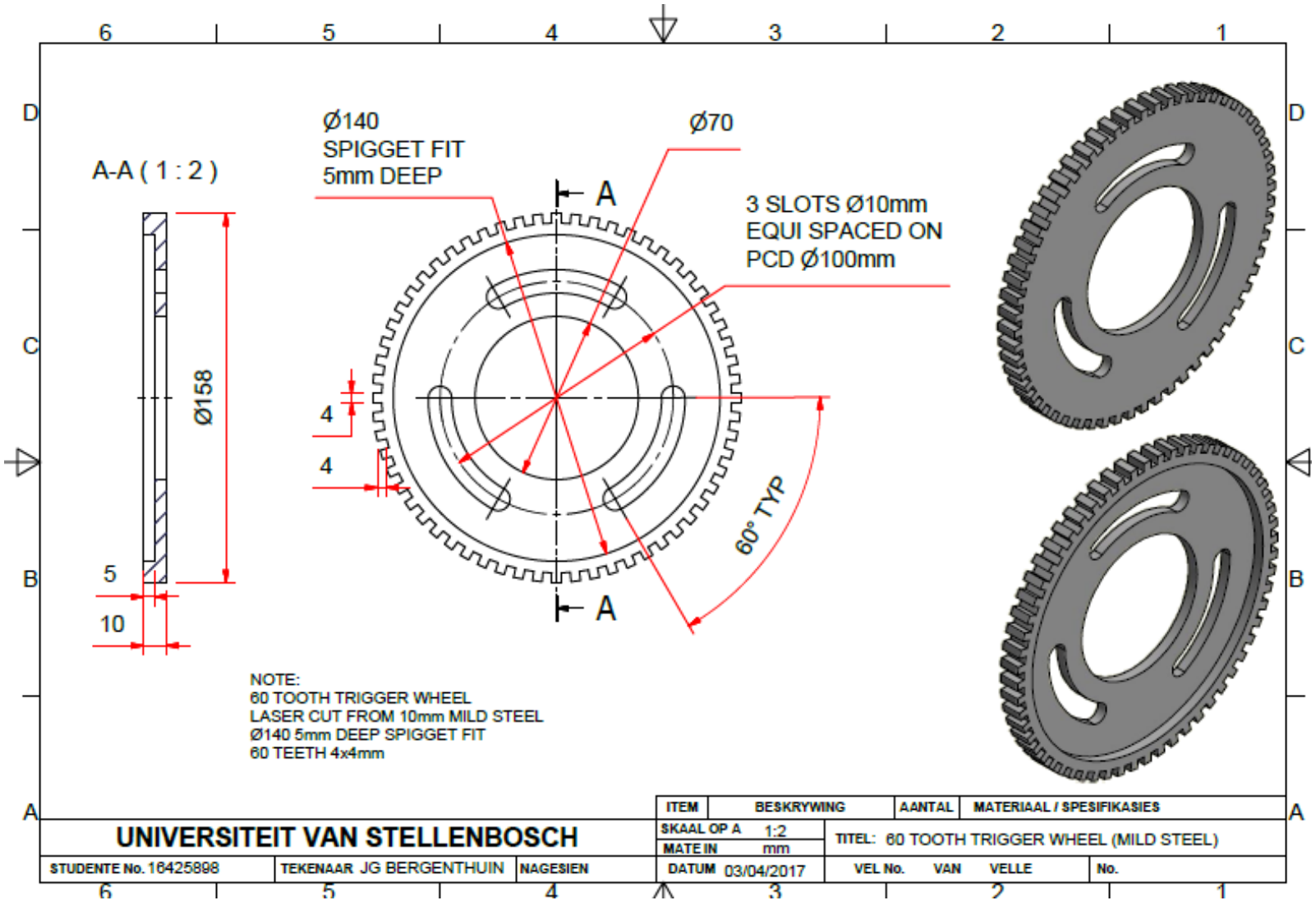

Figure 79: 60-2 Tooth trigger wheel

APPENDIX E – Preliminary testing results

The performance of all three heating elements, working in conjunction, were tested. The CFR engine was run by the electric motor and drive system. The CFR engine was therefore not firing, but acting as an air compressor, pumping air through the series of heater elements. Figure 80 shows the indicated mixture temperature achieved when running all three heater elements in conjunction. The PID controllers were set to 170°C, significantly higher than the required 149°C, and it can be seen that this figure is easily reached, and maintained, with air as the working fluid.

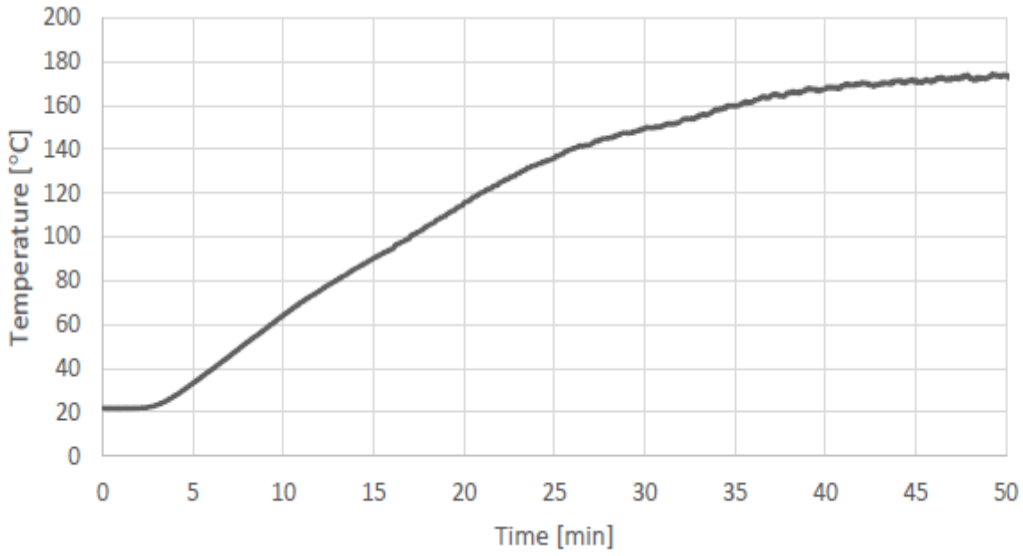

Figure 80: Heating elements performance tests (Reproduced from Jooste (2016))

The effect of the high latent heat of vaporization of ethanol on the mixture temperature was investigated. The CFR engine was run with the electrical drive system, and the fuel line shut off. Only the inlet air temperature was controlled to a constant 54°C, the mixture temperature (downstream of the carburettor) was monitored. Once the steady state was reached, and a constant mixture temperature was measured, the fuel line was opened, allowing the CFR engine to fire. The latent heat of vaporization of the fuel reduced the measured mixture temperature. Figure 81 shows the difference between the cooling effects measured by ethanol, and conventional 95 ULP. It is shown that the mixture

temperature is reduced to ~22°C with the evaporation of ethanol, compared to ~40°C with ULP.

	Initial mixture temperature	Steady mixture temperature	Temperature drop
Ethanol	52.5 °C	22.5 °C	30 °C
95 Petrol	54 °C	40 °C	14 °C

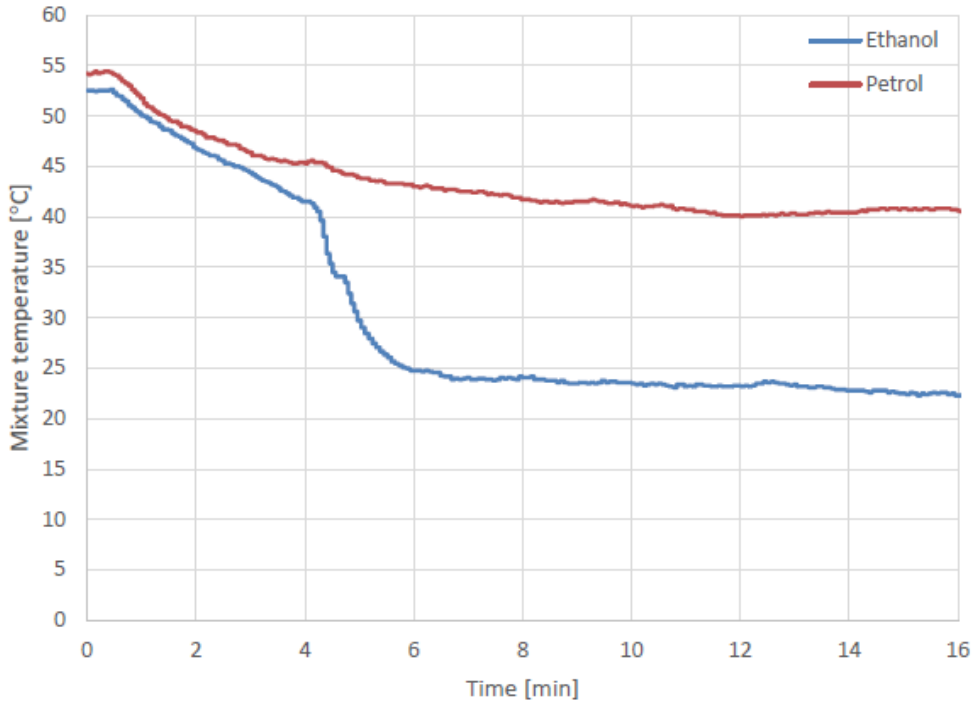

Figure 81: Oxygenated effect on mixture temperature (Reproduced from Jooste (2016))

The difference in the cooling effect of the latent heat of vaporization of ethanol, compared to conventional petrol validates the commissioning of a third heating element to maintain a mixture temperature of 149°C, as specified by the ASTM 2700 standard test procedure. The CFR engine was run using pure ethanol, and all three heating elements were set to work in conjunction to maintain a mixture temperature of 149°C. Figure 82 shows the mixture temperature achieved.

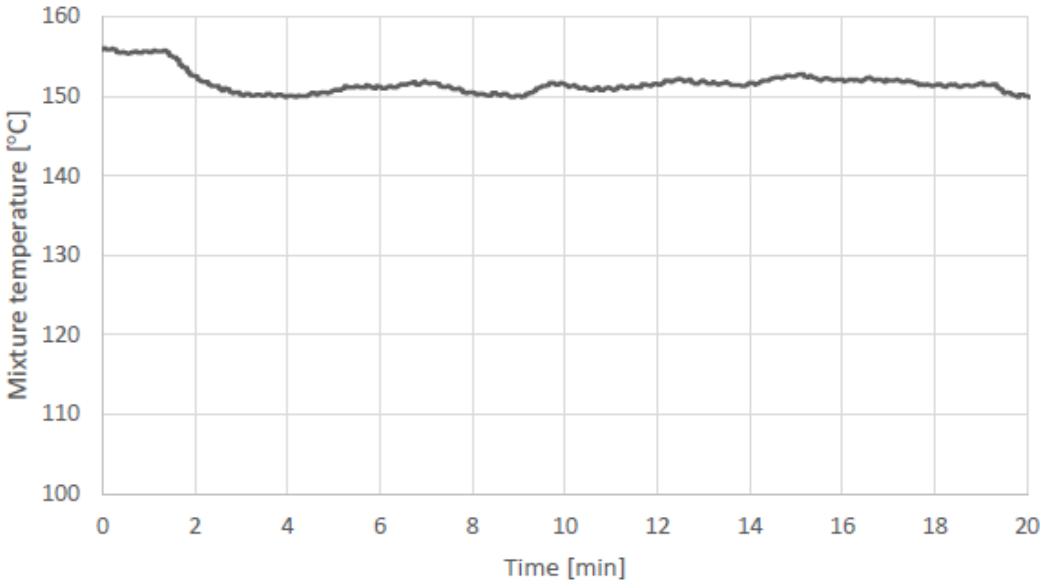

Figure 82: Mixture temperature control (Reproduced from Jooste (2016))

It can be seen from Figure 82 that the three heating elements managed to maintain a mixture temperature higher than 149°C. The adjustable fuel metering system was tested by recording the micrometre reading through an A/F ratio sweep from ~0.8 to ~1.2 lambda. This was repeated on three different CR settings for the CFR engine. Figure 83 shows the A/F ratio control with the needle valve modification.

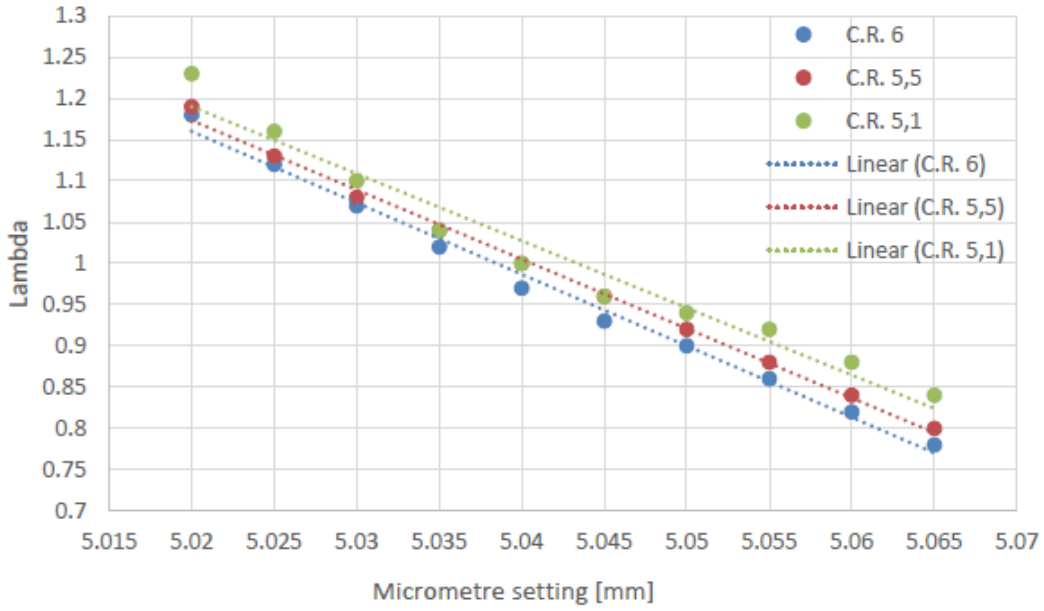

Figure 83: A/F ratio control (Reproduced from Jooste (2016))

It is shown in Figure 83 that the adjustable needle provides good control over the AF ratio of the CFR engine.

It was noted during the testing phase of Mr. Jooste's project that the lamda scanner struggled to maintain a constant reading. It was suspected that this was a result of the electric drive system not maintaining a constant speed. The drive system was originally set up to receive the armature voltage of the electric motor as feedback for speed control. This resulted in a 2.5 % error in speed fluctuation within each firing cycle of the CFR engine. It was also found that the average speed fluctuation through a firing cycle drifted upwards with time. This was due to the build-up of heat in the electric motor, which influenced the armature voltage. Figure 84 shows the speed control of the drive system in its original configuration. It can be seen that the drive requires more accurate feedback, and general tuning.

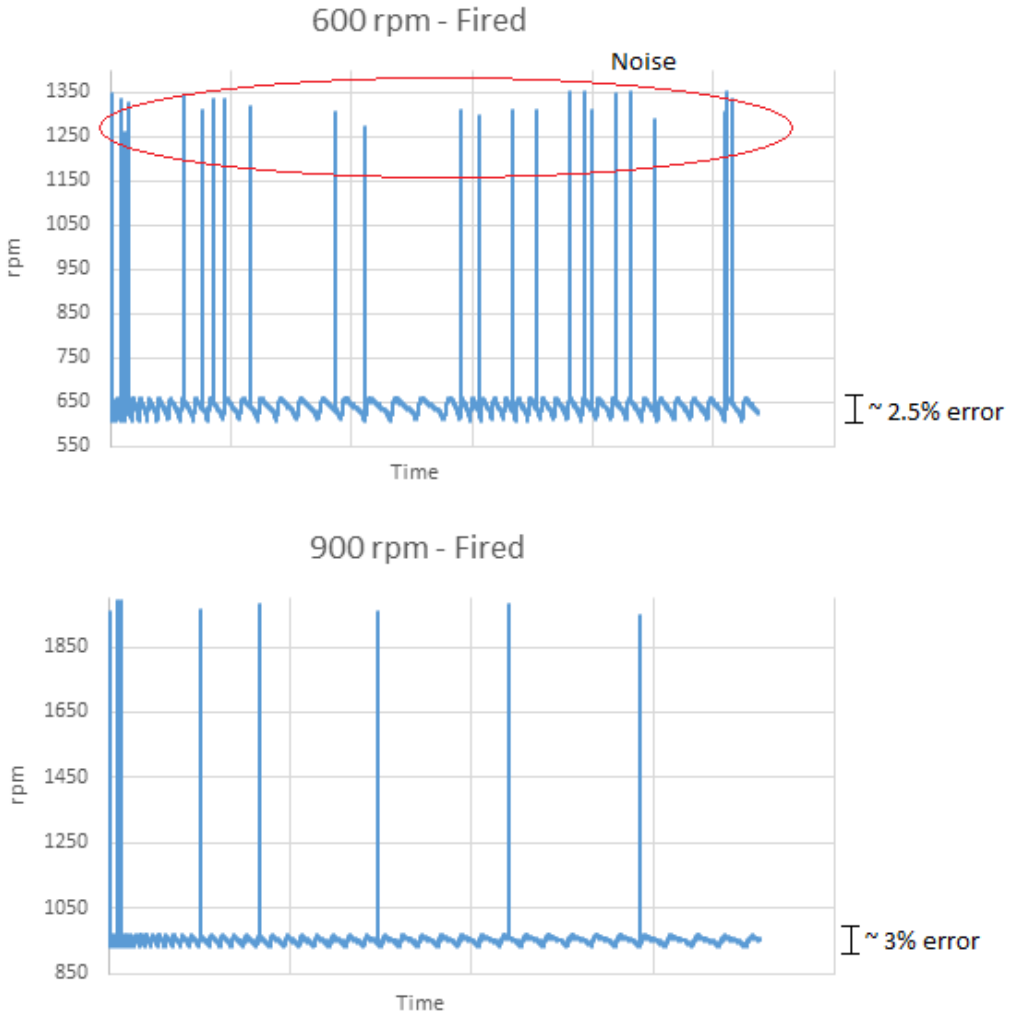

Figure 84: Engine speed control

Adapting the drive system to receive feedback from a tachometer, mounted on the shaft of the electric motor, would significantly improve the accuracy of the feedback. The error in rotational velocity within a firing cycle was expected to decrease to 0.1 % according to the Phantom VIII single phase four quadrant convertor setup document. This will also solve the problem of drift when the electric motor heats up, as a change in armature voltage will not affect the feedback system.

The electrical drive system of the CFR engine is set up to receive an AC signal from a tacho generator, while a DC tacho is fitted to the shaft of the electric motor. Despite the efforts of Mr. Reynaldo Rodrigues to transform the tacho generator signal to AC, it could not be successfully converted to work in conjunction with the existing drive system. It was decided to leave the drive system in its original configuration (with armature voltage feedback), and test the effect of the speed fluctuations on the test results of the CFR engine after modifications and re-assembly. A new drive system and tacho generator would be purchased, if the final testing could justify the additional cost.

APPENDIX F – Test data

F1 – Verification of CR curve

Table 22: Characteristic curve calibration

CR curve calibration					
RON	n-Heptane (Vol %)	Iso-Octane (Vol %)	Dial	A/F (λ)	CCR
50	50	50	0.859	0.94	5.202
60	40	60	0.819	0.93	5.370
70	30	70	0.769	0.93	5.593
80	20	80	0.698	0.94	5.952
85.5	16	84	0.652	0.94	6.216
90	10	90	0.605	0.94	6.516
92	8	92	0.576	0.93	6.720
94	6	94	0.548	0.93	6.931
95	5	95	0.532	0.94	7.059
96	4	96	0.523	0.93	7.133
98	2	98	0.482	0.94	7.496
100	0	100	0.454	0.94	7.770
108.5	100 % Ethanol		0.344	0.95	9.112
120	100 % Toluene		0.275	0.94	10.26

F2 – Toluene test

Table 23: Toluene test RON results

RON						
ON	Tolerance (±)	Dial	A/F (λ)	CCR	Measured ON	Error
65.2	0.9	0.792	0.94	5.498	65.277	0.077
75.5	0.8	0.731	0.94	5.778	75.163	-0.336
85	0.7	0.658	0.94	6.180	84.749	-0.250
89.3	0.6	0.617	0.94	6.436	88.802	-0.497
93.4	0.5	0.568	0.93	6.778	92.568	-0.831
96.9	0.5	0.516	0.94	7.192	96.325	-0.574
99.9	0.8	0.466	0.95	7.650	99.122	-0.777
103.3	1.2	0.419	0.97	8.146	102.380	-0.920
108	1.7	0.355	1.02	8.955	107.000	-1.00
113.7	2.2	0.295	0.97	9.811	117.030	3.330

Table 24: Toluene test MON results

MON						
ON	Tolerance (±)	Dial	A/F (ʎ)	CCR	Measured ON	Error
57.8	0.6	0.826	0.94	5.340	58.240	0.440
66.5	0.3	0.782	0.95	5.533	67.304	0.804
74.4	0.3	0.733	0.96	5.768	74.883	0.483
78	0.3	0.71	0.97	5.887	78.199	0.199
81.6	0.3	0.684	0.97	6.029	81.615	0.015
85.3	0.3	0.653	0.97	6.210	85.374	0.074
88.8	0.3	0.616	0.98	6.443	88.901	0.101
92.6	0.3	0.568	0.97	6.778	92.556	-0.044
96.8	0.4	0.508	0.97	7.261	96.705	-0.095
99.8	0.4	0.455	0.97	7.760	99.926	0.126
100.8	0.4	0.442	0.97	7.894	100.790	-0.010

F3 – Pump fuel tests

Table 25: Sensitivity to inlet air temperature

95 ULP (3 weeks old)				
Intake temp (°C)	Dial	RON	CCR	A/F
65	0.545	94.185	6.954	0.95
60	0.545	94.185	6.954	0.95
55	0.544	94.247	6.962	0.95
50	0.543	94.308	6.970	0.95
45	0.543	94.308	6.970	0.95
40	0.542	94.370	6.978	0.95
35	0.541	94.432	6.986	0.94

F4 – Oxygenated samples

Table 26: Ethanol / iso-octane RON results

Volume %					
Ethanol	Iso-octane	Dial	ON	CCR	A/F (ʎ)
0	100	0.458	100.00	7.770	0.94
10	90	0.350	107.95	9.025	0.95
20	80	0.327	110.12	9.369	0.95
40	60	0.322	110.62	9.447	0.95
60	40	0.329	109.92	9.338	0.95
80	20	0.340	108.87	9.112	0.96
100	0	0.348	108.13	9.054	0.96

Table 27: Ethanol / n-heptane RON results

Volume %					
Ethanol	n-Heptane	Dial	ON	CCR	A/F (λ)
40	60	0.771	68.750	5.565	0.94
50	50	0.672	83.038	6.098	0.94
60	40	0.554	93.560	6.884	0.95
70	30	0.453	100.700	7.780	0.95
80	20	0.398	104.820	8.466	0.96
90	10	0.368	106.970	8.776	0.93
100	0	3.510	108.600	9.011	0.96

Table 28: Ethanol / toluene RON results

Volume %					
Ethanol	Toluene	Dial	ON	CCR	A/F (λ)
0	100	0.277	119.62	10.228	0.93
10	90	0.295	116.34	9.899	0.97
20	80	0.315	112.93	9.560	0.96
40	60	3.390	109.30	9.186	0.96
60	40	0.345	108.41	9.098	0.96
80	20	0.350	107.95	9.025	0.96
100	0	0.349	108.4	9.040	0.95

Table 29: Ethanol / iso-octane MON results

Volume %					
Ethanol	Iso-octane	Dial	ON	CCR	A/F (λ)
0	100	0.454	100.00	7.770	0.94
10	90	0.462	99.411	7.689	0.96
20	80	0.471	98.765	7.601	0.96
40	60	0.522	96.112	7.141	0.96
60	40	0.537	94.683	7.018	0.94
80	20	0.574	92.138	6.734	0.93
100	0	0.590	91.014	6.620	0.95

Table 30: Ethanol / n-heptane MON results

Volume %					
Ethanol	n-Heptane	Dial	ON	CCR	A/F (λ)
40	60	0.766	62.3367	5.607	0.97
60	40	0.656	85.000	6.192	0.97
80	20	0.611	89.395	6.476	0.96
100	0	0.591	90.947	6.130	0.97

Table 31: Ethanol / toluene MON results

Volume %					
Ethanol	Toluene	Dial	ON	CCR	A/F (λ)
0	100	0.373	105.950	8.709	0.94
10	90	0.440	100.920	7.915	0.93
20	80	0.504	96.899	7.296	0.95
40	60	0.540	93.560	6.884	0.95
60	40	0.575	92.072	6.727	0.96
80	20	0.586	91.294	6.648	0.94
100	0	0.590	91.014	6.620	0.95

F5 - Round robin set of fuels

Table 32: RON - CCR Method

Sample	Dial	Measured ON	CCR	A/F (λ)
U-PRF-R1	0.476	98.415	7.553	0.93
U-PRF-R2	0.488	97.693	7.440	0.92
U-PRF-R3	0.532	95	7.059	0.93
U-PRF-R4	0.583	91.504	6.669	0.93
U-PRF-R5	0.588	91.154	6.634	0.93
U-PRF-R6	0.644	86.232	6.265	0.93
U-PRF-R7	0.696	80.229	5.963	0.92
U-PRF-R8	0.7	79.694	5.941	0.93

Table 33: RON - Bracket Method

RON - Bracket Method						
Sample	CCR	Bracket 1		Bracket 2		Interpolated ON
		ON	KI	ON	KI	
U-PRF-R1	7.553	98	53	99	25	98.142
U-PRF-R2	7.446	97	70	98	46	97.833
U-PRF-R3	7.059	94.5	53	95.5	26	95.037
U-PRF-R4	6.669	91	62	92	41	91.571
U-PRF-R5	6.634	91	54	92	27	91.148
U-PRF-R6	6.265	86	72	87	48	86.916
U-PRF-R7	5.963	80	53	81	26	80.111
U-PRF-R8	5.942	79	72	80	47	79.880

Table 34: MON - CCR Method

MON - CCR Method					
Sample	Dial	ON	CCR	Timing	A/F (λ)
U-PRF-M1	0.444	98.167	7.873	18	0.96
U-PRF-M2	0.445	98.039	7.863	18	0.96
U-PRF-M3	0.456	96.653	7.749	19	0.97
U-PRF-M4	0.591	92.530	7.413	20	0.96
U-PRF-M5	0.485	93.209	7.468	20	0.95
U-PRF-M6	0.510	90.459	7.243	21	0.96
U-PRF-M7	0.612	80.232	6.469	23	0.97
U-PRF-M8	0.600	81.319	6.550	23	0.96

Table 35: MON - Bracket Method

MON - Bracket Method						
Sample	CCR	Bracket 1		Bracket 2		Interpolated ON
		ON	KI	ON	KI	
U-PRF-M1	7.873	97	62	100	42	98.50
U-PRF-M2	7.863	97	63	100	41	98.09
U-PRF-M3	7.749	94	58	97	31	94.88
U-PRF-M4	7.413	90	61	94	28	91.33
U-PRF-M5	7.468	90	53	94	26	90.83
U-PRF-M6	7.243	85	65	89	40	86.92
U-PRF-M7	6.469	80	74	81	41	80.80
U-PRF-M8	6.550	81	63	82	53	82.32

APPENDIX G – Round robin octane data

Table 36: Measured RON data

sample	RON actual	correlation	Lower R margin	Upper R margin	Lab A	Lab B	Lab C	Lab D	Stellenbosch University
PRF-R1	99.1	99.1	98.4	99.8	99.45	99.2	99.15	100.3	98.1
PRF-R2	98.8	98.8	98.1	99.5	98.7	98.55	98.65	99	97.8
PRF-R3	96.1	96.1	95.4	96.8	96.4	96.2	96.5	97.8	95.0
PRF-R4	92.3	92.3	91.6	93	92.4	92.8	92.8	94.4	91.6
PRF-R5	92	92	91.3	92.7	92.1	92.05	92.05	93.9	91.1
PRF-R6	86.87	86.87	86.17	87.57	87.65	87.7	87.35	88.8	86.9
PRF-R7	81.2	81.2	80.5	81.9	79.85	81.05	81.5	82.8	80.1
PRF-R8	80.9	80.9	80.2	81.6	81.05	80.95	80.65	82.4	79.9

Table 37: Measured MON data

sample	MON actual	correlation	Lower R margin	Upper R margin	Lab A	Lab B	Lab C	Lab D	Stellenbosch University
PRF-M1	99.2	99.2	98.3	100.1	99.9	99.8	97.9	99.7	98.5
PRF-M2	98.9	98.9	98	99.8	98.75	98.4	98.25	97.8	98.1
PRF-M3	95.9	95.9	95	96.8	96.3	97.05	95.3	96.3	94.9
PRF-M4	92.2	92.2	91.3	93.1	92.1	92.3	92.1	93.6	91.3
PRF-M5	91.9	91.9	91	92.8	91.95	92.1	91.55	90.6	90.8
PRF-M6	87.2	87.2	86.3	88.1	86.45	86.35	86.4	87.8	86.9
PRF-M7	81.1	81.1	80.2	82	79.4	80.2	84	83.2	80.8
PRF-M8	80.8	80.8	79.9	81.7	81.05	81.1	80.05	80.6	82.3

APPENDIX H – n-Heptane chemical analysis report

Dept Process Engineering, US Library Search Report

Data Path : D:\Hanlie\
Data File : N-HEPTANE 28-09-2017
INJ2.D Acq On : 28 Sep 2017 16:08
Operator : manager
Sample : JG Bergenthuin Misc :
ALS Vial : 1 Sample Multiplier: 1

Search Libraries: C:\Database\NIST11.L

Minimum Quality: 0 Unknown

Spectrum: Apex minus start of peak
Integration Events: ChemStation Integrator - autoint1.e

Pk#	RT	Area %	Library/ID	Ref#	CAS#	Qual
1	6.615	9.51	C:\Database\NIST11.L			
			Hexane, 2-methyl-	3976	000591-76-4	90
			Hexane, 2-methyl-	3978	000591-76-4	78
			2H-Pyran, tetrahydro-2-methyl-	3944	010141-72-7	59
2	6.709	3.59	C:\Database\NIST11.L			
			Ethane, isocyanato-	596	000109-90-0	56
			2(3H)-Furanone, dihydro-3,3-dimethyl-	7301	003709-08-8	53
			1-Hexene, 5-methyl-	3321	003524-73-0	50
3	6.780	15.66	C:\Database\NIST11.L			
			Hexane, 3-methyl-	3977	000589-34-4	87
			Hexane, 3-methyl-	3980	000589-34-4	80
			Hexane, 3-methyl-	3974	000589-34-4	68
4	6.902	1.31	C:\Database\NIST11.L			
			2-Hexene, 5-methyl-, (E)-	3380	007385-82-2	43
			3-Hexene, 2-methyl-, (Z)-	3379	015840-60-5	38
			1-Pentyn-1-ol, 4-methyl-	3215	053778-57-7	38
5	7.045	4.80	C:\Database\NIST11.L			
			Cyclopentane, 1,3-dimethyl-, cis-	3405	002532-58-3	94
			Cyclopentane, 1,3-dimethyl-	3392	002453-00-1	93
			Cyclopentane, 1,3-dimethyl-, cis-	3410	002532-58-3	90
6	7.111	3.22	C:\Database\NIST11.L			
			Cyclopentane, 1,3-dimethyl-, cis-	3405	002532-58-3	91

		Cyclopentane, 1,3-dimethyl-	3392	002453-00-1	91
		Cyclopentane, 1,2-dimethyl-, cis-	3406	001192-18-3	87
7	7.205	33.77 C:\Database\NIST11.L			
		Heptane	3970	000142-82-5	91
		Heptane	3971	000142-82-5	91
		Heptane	3972	000142-82-5	90
8	7.811	0.71 C:\Database\NIST11.L			
		Cyclopentane, 1,1,3-trimethyl-	6786	004516-69-2	74
		4,4-Dimethylpent-2-enal	6508	1000195-01-6	52
		2-Heptenal, (Z)-	6480	057266-86-1	50
9	7.910	25.89 C:\Database\NIST11.L			
		Cyclohexane, methyl-	3340	000108-87-2	95
		Cyclohexane, methyl-	3342	000108-87-2	91
		Cyclohexane, methyl-	3338	000108-87-2	87
10	8.147	1.54 C:\Database\NIST11.L			
		Cyclopentane, ethyl-	3341	001640-89-7	70
		Cyclopentane, ethyl-	3337	001640-89-7	62
		3-Hexene, 2-methyl-, (E)-	3378	000692-24-0	46

DN2016 PHEN...DONE FINAL.M Fri Sep 29 10:17:20 2017

APPENDIX I – Safety document

Description of workspace

Figure 85 shows a schematic layout of Room 171, test cell 1 of the internal combustion laboratory at Stellenbosch University.

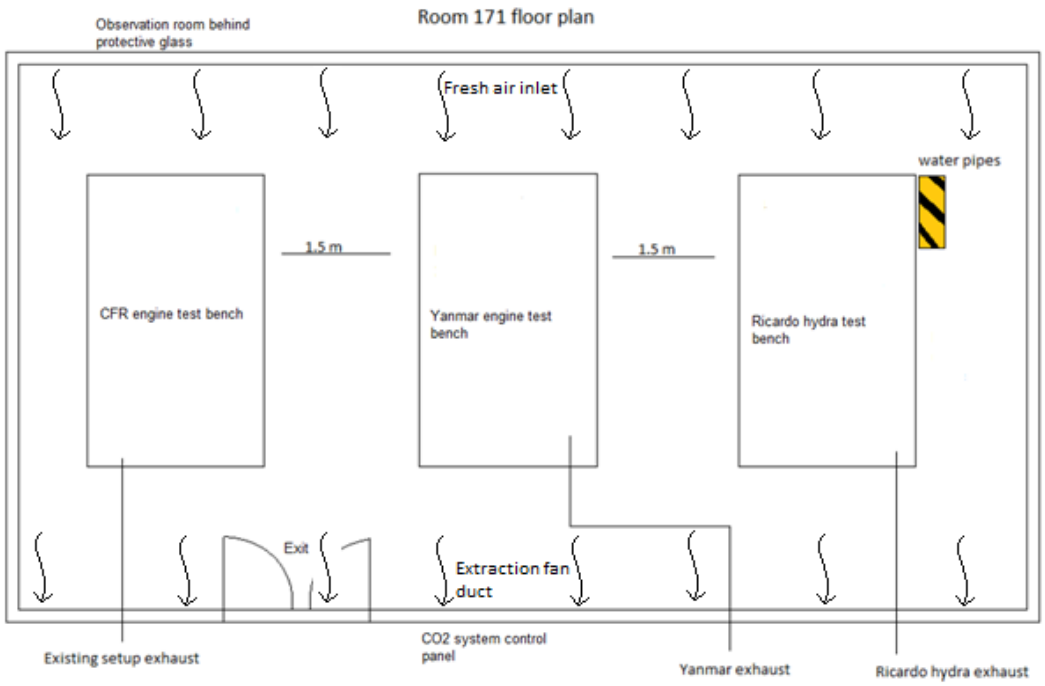

Figure 85: IC test cell 1

Test cell 1 consists of a room with three IC engine test benches. Each engine has an overhead exhaust system, bolted to the ceiling, guiding exhaust gasses out of the building. The room has one main entrance, a double dour leading to a passage way. A safety warning, Figure 86, on the outside of the entrance warns authorised users to always wear safety shoes, and ear and eye protection. The test cell is well ventilated with a fresh air supply fan, and air extraction fan. This ensures that the test cell is constantly replenished with fresh air, and fumes and gasses are extracted out of the test cell.

Figure 86: Entrance warning

All four IC test cells are monitored by an automatic CO_2 fire extinguisher system. The system can be activated and deactivated individually for each test cell via a key operated control panel mounted on the wall by the entrance. When the test cell is **NOT IN USE**, the system is set to “Automatic” by turning the key, and is indicated by two orange LED lights, Figure 87. When **WORKING IN THE TEST CELL**, the CO_2 system should be set to “Manual” mode, as indicated by two green LED lights, shown in Figure 88.

Figure 87: CO_2 system - Automatic

Figure 88: CO_2 system – Manual

The control panel for the CO_2 system is located on the second floor, above the IC test cells. If the system is triggered, it can be deactivated on the control panel shown in Figure 89 by following the instructions as indicated, shown in Figure 90.

Figure 89: CO_2 system control panel

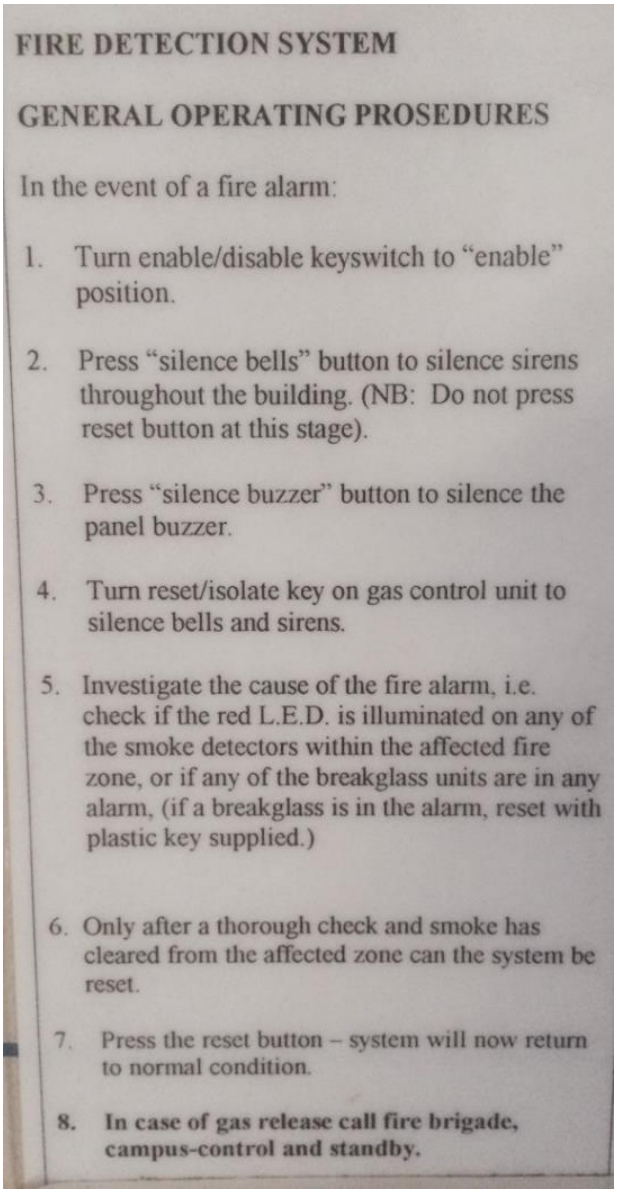

FIRE DETECTION SYSTEM

GENERAL OPERATING PROSEDURES

In the event of a fire alarm:

1. Turn enable/disable keyswitch to "enable" position.
2. Press "silence bells" button to silence sirens throughout the building. (NB: Do not press reset button at this stage).
3. Press "silence buzzer" button to silence the panel buzzer.
4. Turn reset/isolate key on gas control unit to silence bells and sirens.
5. Investigate the cause of the fire alarm, i.e. check if the red L.E.D. is illuminated on any of the smoke detectors within the affected fire zone, or if any of the breakglass units are in any alarm, (if a breakglass is in the alarm, reset with plastic key supplied.)
6. Only after a thorough check and smoke has cleared from the affected zone can the system be reset.
7. Press the reset button – system will now return to normal condition.
8. **In case of gas release call fire brigade, campus-control and standby.**

Figure 90: CO_2 Instructions

Safety equipment, including fire extinguishers, ear and eye protection, respirator and an emergency respirator for the CO_2 system provided in the test cell, see Figure 91.

Figure 91: Emergency respirator and fire extinguisher

Potential risks

The following risks are involved with testing high octane and oxygenated fuels on the CFR engine test setup in the IC laboratory.

Risks to the health and safety of the people who are going to use the setup:

- Moving/rotating equipment.
- Heavy equipment and tools.
- Flammable liquids and gasses.
- High pressure gasses and liquids.
- Toxic gasses.
- High noise levels.
- High temperature surfaces.
- Electric wires and equipment.
- CO_2 fire extinguisher system.

Risks to the health and safety of the people who are in close proximity to the setup:

- Flammable liquids and gasses.
- High pressure gasses and liquids.
- Toxic gasses.
- High noise levels.
- CO_2 fire extinguisher system.

Risks to the equipment itself, the environment and surrounding buildings:

- Flammable liquids and gasses.
- CO_2 fire extinguisher system.
- Electricity, and electrical equipment in close proximity to cooling water.

Minimizing potential risks

The following steps and guidelines should be followed to minimize the potential risks identified above.

- Report, as soon as is practicable, all safety incidents to Mr Haines, the Laboratory Technician or the Laboratory Manager.
- Take all practicable measures to avoid the occurrence of safety incidents.
- Ensure that, when someone is working on a machine, all power sources to the machine are disconnected (not simply turned off).
- Ensure that all power sources to low voltage (less than 24 V) electrical devices and computers (other than machines) are turned off whenever someone is changing the devices'/computers' physical configuration.
- Take particular care when connecting electrical power and/or signal lines to a device, and ensure that the voltages of the connections are appropriate (e.g. not connecting 380V AC where 24V DC is supposed to go).
- Ensure that, before working on the wiring of any setup, the wiring instructions accompanying this document (Test Cells Wiring and Electrical Guidelines) have been studied. These instructions must be adhered to when changing wiring.
- Ensure that, before power is (re)connected to a machine:

  All power connections (note that this includes electrical, pneumatic and hydraulic connections) are firm and secure; Everybody in the laboratory is a safe distance away from the machine; and, if practicable, that the area around the machine is clear of other physical objects. Take into account that a machine may not react as expected upon powering up and could cause damage or injury.

- Ensure that, before power sources are connected to a new (or substantially altered) laboratory setup, a set of safety instructions for the setup has been compiled and approved by the supervising lecturer (if a student is performing the work), the Laboratory Technician and the Laboratory Manager.
- Ensure that, before a laboratory setup is operated, the person operating the setup has studied the setup's safety instructions. The person operating the setup must ensure that these instructions are available at the setup at all times.
- Ensure that, before operating machinery or switching electrical power on, the machine (particularly moving parts and electrical conductors not covered by an electrical insulation material) is as safe as if the area around the machine has been cordoned off. If access to the machine is not physically restricted (e.g. by covers, guards or fences), an area including the machine and, if applicable, its whole range of motion shall be cordoned off and a notice put up alerting people of the danger and instructing them to remain outside the cordoned off area.
- Never leave the laboratory while any power sources that are connected to the machine/setup that he/she was working with are switched on unless (a) the parts of the machine connected to the power were designed to be normally left unattended while on, and (b) an area containing the device's whole range of motion has been cordoned off, and the cordoned off area has been signposted as a dangerous area. Appliances such as soldering irons and space heaters shall not be left on.
- Should the building’s power go out while your machine/experiment is running, switch off all power sources, since it will be uncertain at what time the power will be restored and when power is restored, it may be associated with power spikes that can damage the equipment or can cause unexpected machine movements.
- Ensure that, when he/she is the last one to leave the laboratory, the ventilation fans are shut down, and all lights and electrical appliances (e.g. fan and power supplies) are turned off.
- Ensure that no visitors are allowed to enter the laboratory unless they are accompanied by a lab member. The lab member accompanying the visitors shall take all reasonable steps to ensure the safety of the visitors that he/she is accompanying and shall ensure that the visitors adhere to the laboratory's safety procedures.
- Ensure that no one works alone in the laboratory after hours, unless the work entails what would normally be done in an office or does not involve the use of any power sources or any other potential source of injury.
- Before doing any work in the laboratory, ensure that he/she is aware of the location of all of the following in the laboratory:
    - The fire extinguishers;

  - The emergency exit(s);
  - The 3-phase power sockets mounted on the walls;
  - The pneumatic shut-off valves in the walls;
  - The dangerous zones around test setups.
- Ensure that areas where people normally move are kept clear and the floor clean at all times. Particular care shall be taken to avoid tripping hazards (e.g. cables or tubes lying on the floor).
- Ensure that the area of the laboratory where he/she has worked (including the floor) is tidy and clean at the end of each day. An area of the laboratory must never reach a state where it is dangerous to walk around in it because of cables, components, tools, etc. laying on the floor.
- Ask the Laboratory Technician for training if not absolutely sure how to safely use a tool (especially power tools), device (e.g. power supplies, motor drives, etc.) or machine, before using it.
- Do not give the laboratory keys to anybody without the express permission of Mr Haines, the Laboratory Technician or the Laboratory Manager.
- Always lock the door when leaving the lab.

Test procedures

On Entering the Test Cell

- The test cell is equipped with an automatic fire extinguishing system that expels CO_2 gas to choke fires. Before entering the test cell the system should be isolated to prevent the system triggering before the test cell has been evacuated. The system should again be activated upon exiting the test cell. Ensure that all personnel have exited the test cell before doing so.
- Good Housekeeping: Always ensure that the test cell is kept free of debris and that no obstacles are blocking the entrances to exits out of or pathways inside the test cell.
- Ensure that the test cell is adequately lit.
- The test facility should be well ventilated to prevent the buildup of fumes.
- Fuel should be stored in an approved fuel store. If fuel is to be stored inside the test cell it should at all times be kept as far as possible from any heat or ignition sources and be kept in sealed containers. No slop fuel – fuel used for cleaning purposes – should be kept in open containers inside the test cell. The amount of fuel to be kept in the test cell must at all times be limited to the quantity required for a test.
- Using your senses of smell and sight, check the test cell for any leaks or protruding and exposed electrical cables.

- Examine the test bed itself. Check that all connections are tight and that there are no cracks or leaks.
- Ensure that the battery, if present, is not kept in close proximity to the engine fuel system. Batteries should at all times be kept away from any possible fuel leaks.

Pre Test

- Engine checks:
- Ensure that there is enough coolant in the engine and that the cooling system is functioning correctly. On air cooled engines, ensure that there is sufficient air flow over the engine heat sink.
- Check engine fuel supply and fuel level.
- Check engine lubricant.
- In case of electrical start, check battery charge.
- Dynamometer checks:
- Check that water supply and drainage is functioning correctly.
- Ensure that all measurements are calibrated and all readouts zeroed.
- Turn on ventilation system and check that it is functioning properly.
- Check that all fire extinguishers are certified and check the date of service. Familiarize yourself with where they are located. A fire extinguisher should be kept in close proximity to the activity area.
- Ensure that all personnel that will be present during the test are wearing the correct safety equipment.
- Ensure that the test chamber is clearly marked with the appropriate warning notices.
- Check that both the emergency stops in the control room as well as the one in the test chamber are functional.
- Ensure that shaft guards are in place.

During Test

- At least one other person should at all times be present during testing.
- Ensure ventilation system is switched on. Ensure user and bystanders are wearing safety equipment.
- The test should be preceded by an idle warm up. During the warm up check for the following:
- Look, listen and feel for any unusual vibrations.
- Look for any signs of smoke.
- Check the chamber for any fuel or exhaust gas leaks.

- Do not enter the test chamber while the engine is running. If required to do so make sure a colleague is observing and ready the initiate emergency stop in case of an incident.
- If any work close to a rotating shaft is absolutely necessary, be sure to:
- Not wear any loose clothing (e.g. a tie), jewellery (incl. watches), long sleeves or gloves.
- Tie back long hair.

Post Test

- Wait for test bed to cool down.
- Ensure that all equipment is switched off.
- The test cell should again be cleared of any obstacles and all equipment stored correctly.
- Deactivate the ventilation system.
- Reactivate the automatic fire fighting system once all personnel have exited the test cell.

APPENDIX J – Equipment information

Table 38: Equipment and manufacturer information

Equipment	Manufacturer Information
Knock meter (Analogue dial)	Weston Model 271
Detonation meter	Weston Model 501T
PLC	Allen-Bradley Micro 830 PLC
Lambda Scanner	ETAS LA2 Nr.:2662
DAQ	National Instuments, NI USB625
Thermocouples	K-type (Thermon)
Scale	Scales Inc. Precision balance 5200

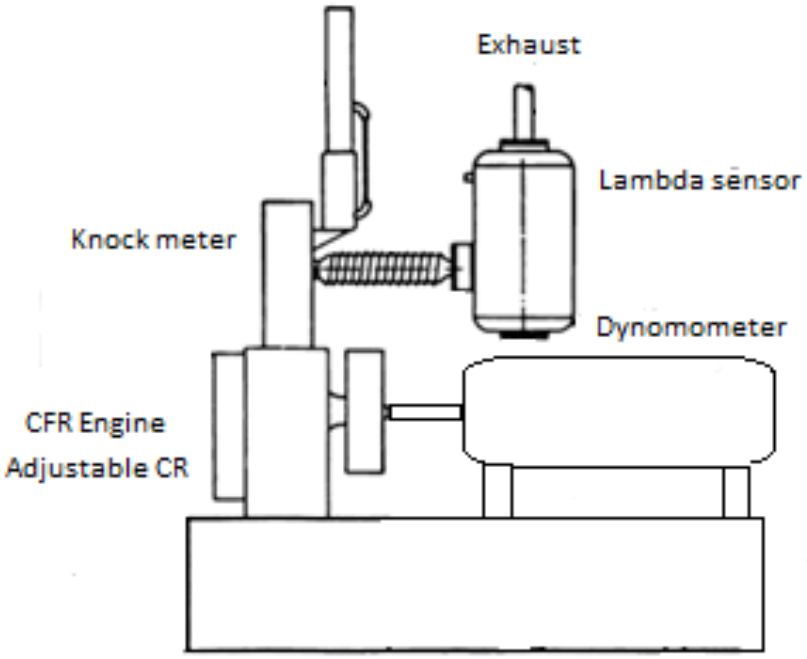

Figure 92: Schematic layout of CFR setup